

DISS. ETH NO. 19997

**C-6 Pyrimidine Analogs for the PET Imaging of HSV1-Thymidine  
Kinase Expression**

A dissertation submitted to

**ETH ZURICH**

for the degree of

**DOCTOR OF SCIENCES**

presented by

**URSINA MÜLLER**

MSc ETH Pharm. Sci.

Born 16.02.1980

Citizen of Wiliberg AG, Switzerland

accepted on the recommendation of

Prof. Dr. Simon M. Ametamey, examiner

Prof. Dr. Roger Schibli, co-examiner

2011



## Acknowledgments

First of all I would like to thank Prof. Simon Ametamey, Prof. Roger Schibli and Prof. P. August Schubiger for giving me the opportunity to perform a PhD in their research group. I would like to thank Roger for kind support and especially Simon for his time that he sacrificed at the end of the thesis. I am grateful for discussions with August Schubiger, bringing optimism and new directions into the unique TK-project and also for trusting a pharmacist to finally successfully produce a radiotracer that found its way into small animal PET. I thank Dr. Miljen Martić for help and for introducing me to the TK-project, and Prof. Dr. Tobias Ross for his optimism, supervision and ability to stay in the B-lab forever. I am very grateful for the lucky collaboration with Dr. Charlene Ranadheera, her enthusiasm about research, her addictive humor and sharing the love for dancing and pink hippos and furthermore for her great friendship. I would like to thank PD Dr. Stefanie Krämer for her immense energy for research and to teach me a lot about scientific writing! In this regard I am very grateful for perfect English and lovely comments by Dr. Jason Holland, for inspiring scientific discussions and especially for efficient corrections, nobody is as fast! I am very grateful for the support and knowledge of Dr. Adrienne Müller, and I will never forget the pleasant working day when the two of us managed a whole animal study! I would like to thank Claudia Keller and Petra Wirth for valuable technical support in the lab.

I would like to thank the semester- and Master's students Mariana Born, Nelly Richina and Evelyn Trauffer for their work, it was a pleasure to supervise you! The unique TK-project would not be so successful without the immense experience and knowledge of lab colleagues and their selfless support! I feel privileged to finish my thesis in a wonderfully relaxed, friendly, supportive and competition free working environment. I am very grateful for endless technical support by Cindy Fischer and her enthusiasm not to finish until a problem is solved. I would like to thank Dr. Aris Chiotellis and Lukas Dialer for the best lab ever! Sharing immense experience in organic chemistry and saving many critical situations (especially during synthesis...), your friendship, sophisticated jokes and your love for seafood with feta (and fresh mensa seafood) are irreplaceable to me. Dr. Linjing Mu has become a very inspiring colleague and I am very grateful for many discussions about radiochemistry and especially about life, for her valuable advice in

any situation and for her believe in me. I appreciate the exclusive ability of Dr. Selena Milicevic to read unreadable NMR-spectra and I would like to thank her for fruitful inputs in organic chemistry. I would like to thank Dr. Svetlana Selivanova for creating a great working atmosphere, for inspiring discussions and sharing supportive advice in the B-lab and for perfect guidance in the dark corners of the city center in Amsterdam. I am very grateful for a huge range of skills from Dr. Thomas Betzel such as saving the day as a very creative baking chief, running immediately when help is needed in the lab (Dr. in first aid), incredible time management not to miss raclette events and not to forget great experience in radiochemistry and analytical methods!

I would like to thank Sabina Hiltbrunner and Sara Wyss for relaxing lunch breaks, Bruno Mancosu, Roger Slavik, Malte Alf and Daniel Bieri for making the time at the lab interesting, Martina Dragic and Christoph Smuda for reliable radiation safety, Kurt Hauenstein for technical support and the most pure precursor ever, Matze Nobst for running to solve technical issues during production, Dominique Leutwiler for energy supply (sirup) and entertainment during collaboration, Monica Langfritz for her big efforts in solving IT issues, and Regula Bischof for managing the whole administration, always with a smile. I would like to thank the Group of Prof. Dr. S. Raic-Malic (University of Zagreb, Croatia) for their collaboration.

No words can do justice towards my gratefulness for the unlimited support, believe in me and encouragement by my family and friends: my parents Gertrud and Guido, my sisters Valeria and Seraina with Ricky and Daniel, Urs, Katrin, Sophia, Gioia, Steffi, Brigitte, Sue and my personal hero Lukas; thanks for keeping my mind off science!

# Contents

<b>Summary</b>	1
<b>Zusammenfassung</b>	5
<b>Abbreviations</b>	9
<b>1 Introduction</b> .....	15
1.1 Imaging of Gene Expression <i>in vivo</i> .....	17
1.2 Herpes Simplex Virus Type 1 Thymidine Kinase .....	25
1.3 Tracer Transport into Cells and Tissues .....	31
1.4 Aim of Thesis .....	35
<b>2 Synthesis and evaluation of a C-6 alkylated pyrimidine derivative for the <i>in vivo</i> imaging of HSV1-TK gene expression</b> .....	39
2.1 Introduction .....	41
2.2 Materials and Methods .....	43
2.3 Results .....	52
2.4 Discussion .....	61
2.5 Conclusion .....	64
<b>3 Synthesis and preclinical evaluation of a new C-6 alkylated pyrimidine derivative as a PET imaging agent for HSV1-<i>tk</i> gene expression</b> .....	67
3.1 Introduction .....	69
3.2 Materials and Methods .....	71
3.3 Results .....	83
3.4 Discussion .....	93
3.5 Conclusion .....	96

<b>4 Conclusion and Future Perspectives</b> .....	99
4.1 Conclusion and Future Perspectives.....	101
<b>References</b>	102
<b>Curriculum Vitae</b>	113
<b>Publications and Presentations</b>	114







## Summary

Gene therapy is a relatively recent therapeutic strategy consisting of the delivery of genetic material into cells for the treatment of life-threatening and chronic diseases. To date, improvements in gene therapy strategies have been hampered by difficulties in monitoring and measuring transgene expression *in vivo* on a whole-body scale. One of the most promising approaches in imaging gene expression uses the gene of the viral herpes simplex type 1 thymidine kinase (HSV1-*tk*) as a reporter gene in combination with an appropriate reporter probe. Positron emission tomography (PET) is a powerful, non-invasive imaging technique which allows for repetitive and quantitative determination of the location, time variation and magnitude of the expression of a gene of interest, and can be used to monitor gene and cell therapies as well as various intracellular events. Two main classes of probes for imaging HSV1-*tk* gene expression have been investigated labeled with fluorine-18 or iodine-124: pyrimidine nucleoside analogs and purine nucleoside analogs. These PET reporter probes are selectively phosphorylated by HSV1-TK enzyme to their monophosphates and metabolically trapped inside transfected cells.

Our investigations were prompted by the need to develop PET imaging agents that lack the major shortcomings of the already existing reporter probes such as unfavorable pharmacokinetics, high cytotoxicity and non-specific cell/tissue accumulation. In order to define the *in vivo* performance for each reporter probe, studies using the same xenograft model and under the same level of HSV1-*tk* expression have been performed and compared to the established reporter probe, 9-(4-[<sup>18</sup>F]-fluoro-3-hydroxymethylbutyl)guanine ([<sup>18</sup>F]FHBG).

Chapter Two in this thesis describes the *in vitro* and *in vivo* evaluation of (6-(3-[<sup>18</sup>F]fluoro-2-(hydroxymethyl)propyl)-1,5-dimethylpyrimidin-2,4(1*H*,3*H*)-dione (*N*-Me-[<sup>18</sup>F]FHBT), a previously synthesized but not pharmacologically characterized C-6 substituted N-1 methylated pyrimidine derivative. In a phosphorylation assay, the non-radioactive reference compound, *N*-Me-FHBT, was observed to be phosphorylated by the HSV1-TK enzyme but not by the human thymidine kinase enzyme. The radiosynthesis of *N*-Me-[<sup>18</sup>F]FHBT was accomplished in a two-step reaction sequence in a moderate radiochemical yield of 5% and radiochemical purity greater than 96 %, and *N*-Me-[<sup>18</sup>F]FHBT showed high plasma stability. The *in vitro* cell uptake of *N*-Me-[<sup>18</sup>F]FHBT was performed using our newly established stably expressing HSV1-TK HEK293 cell

line (HEK293TK+). The ratios of HEK293TK+ to HEK293 control cells were 14.5 and 55 at 30 min and 240 min, respectively and are similar to the most commonly used [<sup>18</sup>F]FHBG. The corresponding ratios for [<sup>18</sup>F]FHBG at 30 min and 240 min were 5.2 and 81.5, respectively. In mice, *N*-Me-[<sup>18</sup>F]FHBT accumulated in the HEK293TK+ xenografts and exhibited similar radioactivity levels in the HEK293TK+ xenografts compared to [<sup>18</sup>F]FHBG. However, a general higher non-specific retention of *N*-Me-[<sup>18</sup>F]FHBT in background tissues resulted in lower standardized uptake value (SUV) ratios of HEK293TK+/HEK293 control. SUV value for *N*-Me-[<sup>18</sup>F]FHBT in HEK293TK+ xenograft was 0.36±0.05 and in HEK293 control xenograft 0.17±0.01. The corresponding SUV values for [<sup>18</sup>F]FHBG were 0.26±0.04 and 0.027±0.011 for HEK293TK+ and control xenografts, respectively. Both, *N*-Me-[<sup>18</sup>F]FHBT and [<sup>18</sup>F]FHBG exhibited high gall bladder and abdominal activity, however, *N*-Me-[<sup>18</sup>F]FHBT showed a lower radioactivity accumulation in the intestines, which could be an advantage for *N*-Me-[<sup>18</sup>F]FHBT.

The rather not promising *in vivo* results with *N*-Me-[<sup>18</sup>F]FHBT prompted us to focus our attention on the development of 6-((1-[<sup>18</sup>F]-fluoro-3-hydroxypropan-2-yloxy)methyl)-5-methylpyrimidine-2,4(1*H*,3*H*)-dione ([<sup>18</sup>F]FHOMP), another pyrimidine nucleoside analog bearing a promising C-6 side chain in analogy to the potent antiviral drug ganciclovir. The synthesis and the pharmacological characterization of [<sup>18</sup>F]FHOMP and its non-radioactive counterpart, FHOMP are described in Chapter Three. FHOMP, the synthesis of which was accomplished in an 8-step reaction sequence in an overall yield of 7%, was observed to be specifically phosphorylated by HSV1-TK but not by the human thymidine kinase. The corresponding precursor for the radiosynthesis of [<sup>18</sup>F]FHOMP was prepared in 9 steps and incorporated N-1 and N-3 methoxymethyl (MOM) protection in order to prevent intramolecular cyclization during radiosynthesis. The MOM-protected precursor allowed for an efficient two-step radiolabeling strategy which was accomplished via nucleophilic substitution using [<sup>18</sup>F]tetrabutylammonium fluoride ([<sup>18</sup>F]TBAF) and subsequent cleavage of the protecting groups with conc. hydrochloric acid. [<sup>18</sup>F]FHOMP was obtained in a radiochemical yield of 25% and a radiochemical purity greater than 95% after semi-preparative HPLC purification. [<sup>18</sup>F]FHOMP displayed high stability in mouse and human liver microsomes and same hydrophilicity as [<sup>18</sup>F]FHBG ( $\log D_{\text{pH}7.4} = -0.87$ ). *In vitro* cell uptake studies revealed statistically significant ( $P < 0.02$ ) higher uptake ratios of [<sup>18</sup>F]FHOMP in HEK293TK+ cells over control HEK293 cells compared to [<sup>18</sup>F]FHBG. The

accumulation ratios for [ $^{18}\text{F}$ ]FHOMP were 9.9-fold (at 30 min), 7.1-fold (at 60 min) and 3.6-fold (at 120 min) higher than [ $^{18}\text{F}$ ]FHBG. Subsequent PET imaging studies performed on mice bearing HEK293TK+ and HEK293 control-xenografts showed accumulation of [ $^{18}\text{F}$ ]FHOMP in the TK-positive xenograft and low accumulation in the control xenograft, which was similar to background activity. Compared to [ $^{18}\text{F}$ ]FHBG, [ $^{18}\text{F}$ ]FHOMP revealed very similar imaging characteristics with higher activity in HEK29TK+ xenograft, slightly higher general background activities, but less intense abdominal activity. *Ex vivo* biodistribution studies confirmed the distribution pattern observed in the PET images for [ $^{18}\text{F}$ ]FHOMP and [ $^{18}\text{F}$ ]FHBG. The reduced abdominal background activity is an advantage for [ $^{18}\text{F}$ ]FHOMP because it may allow HSV1-TK imaging in the abdominal region. To determine whether probe transport via equilibrative nucleoside transporter 1 (ENT1) is the reason for the general background activity observed for [ $^{18}\text{F}$ ]FHOMP in mice, an ENT1 inhibition study was performed. *In vivo* PET studies in normal mice with the ENT1 inhibitor NBMPR-P (15 mg/kg) resulted in reduced uptake of [ $^{18}\text{F}$ ]FHOMP in the brain, stomach, spleen, intestines and pancreas, indicating that ENT1 is likely one of the possible nucleoside transporters involved in [ $^{18}\text{F}$ ]FHOMP cell uptake and partly responsible for [ $^{18}\text{F}$ ]FHOMP accumulation in these organs.

[ $^{18}\text{F}$ ]FHOMP outperformed *N*-Me-[ $^{18}\text{F}$ ]FHBT with higher radiochemical yields and [ $^{18}\text{F}$ ]FHBG with 3.6- to 9.9-fold higher cell uptake *in vitro*. Although [ $^{18}\text{F}$ ]FHOMP and *N*-Me-[ $^{18}\text{F}$ ]FHBT are not superior to [ $^{18}\text{F}$ ]FHBG in their *in vivo* performance, the feasibility of using both C-6 substituted pyrimidine derivatives as PET probes to monitor HSV1-*tk* gene expression *in vivo* has successfully been demonstrated. HSV1-*tk* gene expression imaging in the abdominal region could be a potential application of these two new tracers in the clinic. A shortcoming of both tracers is the general higher background radioactivity and it needs to be determined in future studies what the possible reasons are. Transportocytes prepared from transporter-cRNA injected oocytes could be used to measure transporter-mediated uptake of test tracers. In the search for the optimal HSV1-TK PET tracer, this assay could give answers about the blood clearance of the tracers in the liver into the bile and resulting tissue/blood ratios.



## Zusammenfassung

Die Gentherapie ist eine relativ neue Behandlungsmethode, bei der genetisches Material in Zellen eingeschleust wird, um eine Vielzahl von lebensbedrohlichen und chronischen Krankheiten zu therapieren. Bis heute ist der Fortschritt der Gentherapie und die Optimierung durch fehlende Systeme zur Überwachung und Messung der Expression eines therapeutischen Gens im Organismus erschwert. Ein vielversprechender Ansatz für die bildliche Darstellung der Genexpression ist die Nutzung des Gens für die Thymidinkinase des Herpes Simplex Virus (*HSV1-tk*) als Reporter gen in Kombination mit einer geeigneten Reportersubstanz. Positronen-Emissions-Tomographie (PET) ist ein nicht-invasives, bildgebendes Verfahren der Nuklearmedizin, die es erlaubt den Ort, die Dauer und das Ausmass der Expression eines eingeschleusten Gens quantitativ zu bestimmen. PET kann somit zur Überwachung von Gen- und Zelltherapien, als auch verschiedener intrazellulärer Ereignisse verwendet werden. Diverse mit Fluor-18 oder Iod-124 markierte Pyrimidin- und Purin-Analoga wurden bereits synthetisiert und als potentielle Radiodiagnostika für die Expression des Enzyms HSV1-TK *in vivo* getestet. Diese zwei Substratklassen werden selektiv durch HSV-TK zu Monophosphaten phosphoryliert und dadurch in den transfizierten Zellen metabolisch angereichert.

Die Motivation unserer Untersuchungen ist PET-Reportersubstanzen zu finden, die eine günstigere Pharmakokinetik zeigen als die bisher entwickelten Reportersubstanzen mit tiefer Zytotoxizität und keine nicht-spezifische Zell- und Gewebeaufnahme aufweisen. In dieser Studie sind die neuen Substrate *in vivo* mit der bereits bekannten Reportersubstanz 9-(4-[<sup>18</sup>F]-fluoro-3-hydroxymethylbutyl)guanine ([<sup>18</sup>F]FHBG) verglichen worden durch die Verwendung desselben Tumormodels und Expressionsniveaus von HSV1-*tk*.

Kapitel 2 dieser Arbeit beschreibt die *in vitro* und *in vivo* Evaluierung von (6-(3-[<sup>18</sup>F]fluoro-2-(hydroxymethyl)propyl)-1,5-dimethylpyrimidin-2,4(1*H*,3*H*)-dione (*N*-Me-[<sup>18</sup>F]FHBT). *N*-Me-[<sup>18</sup>F]FHBT, ein C-6 substituiertes N-1 methyliertes Pyrimidin Derivat, wurde in einer früheren Arbeit synthetisiert aber nicht pharmakologisch charakterisiert. Durch Etablierung eines Phosphorylierungsassays konnte nachgewiesen werden, dass die nicht-radioaktive Referenzsubstanz *N*-Me-FHBT durch das HSV1-TK Enzym, aber nicht durch die humane

Thymidinkinase, phosphoryliert wird. *N*-Me-[<sup>18</sup>F]FHBT konnte in einer 2-Schritt Radiosynthese in einer moderaten radiochemischen Ausbeute von 5% und einer radiochemischen Reinheit von über 96% hergestellt werden. *N*-Me-[<sup>18</sup>F]FHBT wies eine hohe Plasmastabilität auf. Die *in vitro* Zellaufnahmen von *N*-Me-[<sup>18</sup>F]FHBT wurden durch Verwendung der neu etablierten, HSV1-TK exprimierenden HEK293 Zelllinie (HEK293TK+) durchgeführt. Das Verhältnis der Zellaufnahme in HEK293TK+ Zellen und HEK293 Kontrollzellen betrug 14.5 nach 30 min und 55 nach 240 min und war ähnlich wie bei [<sup>18</sup>F]FHBG, welches ein Verhältnis von 5.2 bei 30 min und 81.5 bei 240 min aufwies. *N*-Me-[<sup>18</sup>F]FHBT akkumulierte in HEK293+ Tumorzellen in Mäusen in ähnlichem Ausmass wie [<sup>18</sup>F]FHBG. Eine allgemein höhere, nicht-spezifische Retention von *N*-Me-[<sup>18</sup>F]FHBT in Geweben führte jedoch zu tieferen Standardized Uptake Values (SUV) für das Verhältnis von HEK293TK+/HEK293. Die SUV Werte für *N*-Me-[<sup>18</sup>F]FHBT in HEK293TK+ Tumorzellen betrugen 0.36±0.05 und in HEK293 Tumorzellen als Kontrolle 0.17±0.01. Die entsprechenden Werte für [<sup>18</sup>F]FHBG waren 0.26±0.04 in HEK293TK+ Tumorzellen und 0.027±0.011 in Kontrolltumorzellen. Beide Radiotracer, *N*-Me-[<sup>18</sup>F]FHBT und [<sup>18</sup>F]FHBG, wiesen hohe Aktivitäten in der Gallenblase und im Abdomen auf, wobei *N*-Me-[<sup>18</sup>F]FHBT jedoch weniger im Darm akkumulierte als [<sup>18</sup>F]FHBG. Die tiefere Aktivität von *N*-Me-[<sup>18</sup>F]FHBT im Darm könnte ein Vorteil für HSV1-TK Imaging im abdominalen Bereich sein.

Da die *in vivo* Resultate von *N*-Me-[<sup>18</sup>F]FHBT nicht sehr vielversprechend waren, wurde der Fokus auf die Entwicklung von 6-((1-[<sup>18</sup>F]-fluoro-3-hydroxypropan-2-yloxy)methyl)-5-methylpyrimidine-2,4(1*H*,3*H*)-dione ([<sup>18</sup>F]FHOMP) gelegt. Dabei handelt es sich um ein neues, C-6 substituiertes Pyrimidinnukleosidanalogon mit einer vielversprechenden Seitenkette in Analogie zum antiviralen Wirkstoff Ganciclovir. Kapitel 3 beschreibt die Synthese und die pharmakologische Charakterisierung von [<sup>18</sup>F]FHOMP und der nicht-radioaktiven Referenzsubstanz FHOMP. FHOMP wurde mit einer Gesamtausbeute von 7% in 8 Schritten synthetisiert und zeigte eine spezifische Phosphorylierung durch HSV1-TK, jedoch nicht durch die humane TK. Die entsprechende Vorstufe (Precursor) zur Radiosynthese von [<sup>18</sup>F]FHOMP wurde in 9 Schritten hergestellt und wies eine N-1 und N-3 MOM Schutzgruppe auf, um eine intramolekulare Zyklisierung während der Radiosynthese zu verhindern. Durch den MOM-geschützten Precursor war eine effiziente Zwei-Schritt Radiosynthese via nukleophiler Substitution möglich durch die Verwendung von [<sup>18</sup>F]Tetrabutylammoniumfluorid ([<sup>18</sup>F]TBAF)

und nachfolgender Abspaltung der Schutzgruppen mittels konzentrierter Salzsäure. [<sup>18</sup>F]FHOMP wurde nach der semi-präparativen HPLC Reinigung in 25% radiochemischer Ausbeute und einer radiochemischen Reinheit von über 95% erhalten. [<sup>18</sup>F]FHOMP zeigte eine hohe Stabilität in Maus- und Humanlebermikrosomen und wies die gleiche Hydrophilie wie [<sup>18</sup>F]FHBG ( $\log D_{\text{pH}7.4} = -0.87$ ) auf. Die *in vitro* Zellaufnahmen zeigten statistisch signifikant höhere ( $P < 0.02$ ) Aufnahmeleistungen für [<sup>18</sup>F]FHOMP in HEK293+ Zellen gegenüber HEK293 Kontrollzellen im Vergleich zu [<sup>18</sup>F]FHBG. Die Aufnahmeleistungen für [<sup>18</sup>F]FHOMP waren 9.9- (nach 30 min), 7.1- (nach 60 min) und 3.6- (nach 120min) mal höher als für [<sup>18</sup>F]FHBG. Nachfolgende PET Studien in Mäusen mit HEK293TK+- und HEK293 Kontrolltumoren zeigten eine hohe Akkumulation von [<sup>18</sup>F]FHOMP in TK-positiven Tumoren und eine geringe Anreicherung in den Kontrolltumoren (ähnlich der Hintergrundradioaktivität). [<sup>18</sup>F]FHOMP verhielt sich ähnlich wie [<sup>18</sup>F]FHBG, mit leicht erhöhter Hintergrundaktivität aber tieferer Abdomenaktivität. *Ex vivo* Biodistributions Studien bestätigten das gleiche Verteilungsmuster für [<sup>18</sup>F]FHOMP und [<sup>18</sup>F]FHBG wie in den PET Bildern ersichtlich war. Die reduzierte abdominale Aktivität ist ein Vorteil von [<sup>18</sup>F]FHOMP und könnte HSV1-TK Imaging im abdominalen Bereich ermöglichen. Um zu bestimmen, ob der Nucleosid Transporter 1 (ENT1) zur allgemein erhöhten Hintergrundaktivität von [<sup>18</sup>F]FHOMP in Mäusen beiträgt, wurde eine ENT1-Inhibierungsstudie durchgeführt. *In vivo* PET Studien mit dem ENT1-Inhibitor NBMPR-P (15 mg/kg) in normalen Mäusen wiesen eine reduzierte Aufnahme von [<sup>18</sup>F]FHOMP in Hirn, Magen, Milz, Darm und Pankreas auf. Dieses Ergebnis deutet darauf hin, dass ENT1 möglicherweise einer der Nucleosidtransporter für die [<sup>18</sup>F]FHOMP Zellaufnahme ist und teilweise verantwortlich für die [<sup>18</sup>F]FHOMP Akkumulation in den erwähnten Organen ist.

[<sup>18</sup>F]FHOMP übertraf *N*-Me-[<sup>18</sup>F]FHBT mit einer höheren radiochemischen Ausbeute und [<sup>18</sup>F]FHBG mit 3.6- bis 9.9-mal erhöhter *in vitro* Zellaufnahme. *In vivo* verhielten sich [<sup>18</sup>F]FHOMP und *N*-Me-[<sup>18</sup>F]FHBT nicht vorteilhafter als [<sup>18</sup>F]FHBG. Jedoch wurde erfolgreich gezeigt, dass es möglich ist, C-6 substituierte Pyrimidin Derivate als PET Reportersubstanzen zum Überwachen der HSV1-*tk* Genexpression *in vivo* einzusetzen. Eine mögliche klinische Anwendung der zwei neuen Substanzen könnte HSV1-TK Imaging im Abdomen sein. Ein Nachteil der beiden evaluierten Substanzen ist die generell höhere Hintergrundaktivität. Mögliche Gründe dafür sollten in zukünftigen Studien evaluiert werden. Transportozyten, Transporter-

cRNA injizierte Oozyten, könnten zur Messung von einer Transporter-vermittelten Aufnahme von Substraten benutzt werden. Bei der Suche nach dem optimalen HSV1-TK PET Substrat könnte die Transportozyten-Studie Klarheit über die Eliminierung eines Substrates vom Blut in die Galle und die daraus resultierenden Gewebe/Blut Verhältnisse bringen.



## Abbreviations

3D	three dimensional
ACN	acetonitrile
ACV	acyclovir
ADP	adenosine 5'-diphosphate
ATP	adenosine 5'-triphosphate
BLI	bioluminescent imaging
Bn	benzyl
Boc	<i>tert</i> -butoxycarbonyl
Cbz	benzyloxycarbonyl
CCD	charged-couple device
cDNA	complementary DNA, synthesized from a mature mRNA template
CNT	concentrative nucleoside transporter
CNT1-3	concentrative nucleoside transporter 1-3
cRNA	RNA derived from cDNA through standard RNA synthesis
CT	computed tomography
D2R	dopamine 2 receptor
DAST	diethylaminosulfur trifluoride
dCK	deoxycytidine kinase
DCM	dichloromethane
dGK	deoxyguanosine kinase
DHBT	6-(1,3-dihydroxyisobutyl)thymine
DIPEA	N-ethyl-N-isopropylpropan-2-amine
DMAP	4-(dimethylamino)pyridin
DMF	dimethylformamide
DMSO	dimethyl sulfoxide
DNA	deoxyribonucleic acid
dT	deoxythymidine
dT-mP	deoxythymidine monophosphate
EOB	end of bombardment

ENT	equilibrative nucleoside transporter
ENT1-4	equilibrative nucleoside transporter 1-4
ESI	electrospray ionization
Et <sub>3</sub> N	triethylamine
FDA	U S Food and Drug Administration
FDG	fluorodeoxyglucose
FDOPA	3,4-dihydroxy-6-fluoro-L-phenylalanine
FEAU	2'-deoxy-2'-fluoro-5-ethyl-1-β-D-arabinofuranosyluracil
FHBDMP	(1-(4-fluoro-3-(hydroxymethyl)butyl)-5,6-dimethylpyrimidine-2,4(1 <i>H</i> ,3 <i>H</i> )-dione
FHBG	9-(4-fluoro-3-hydroxymethylbutyl)guanine
FHBMP	(6-(4-fluoro-3-(hydroxymethyl)butyl)-5-methylpyrimidine-2,4(1 <i>H</i> ,3 <i>H</i> )-dione
FHBT	6-(3-fluoro-2-(hydroxymethyl)propyl)-5-methylpyrimidine-2,4(1 <i>H</i> ,3 <i>H</i> )-Dione
FHOMDHP	6-(((1-fluoro-3-hydroxypropan-2-yl)oxy)methyl)-5-methyldihydro-pyrimidine-2,4(1 <i>H</i> ,3 <i>H</i> )-dione
FHOMP	6-(((1-fluoro-3-hydroxypropan-2-yloxy)methyl)-5-methylpyrimidine-2,4(1 <i>H</i> ,3 <i>H</i> )-dione
FHPG	9-((3-fluoro-1-hydroxy-2-propoxy)-methyl)guanine
FIAU	2'-fluoro-2'-deoxy-1-β-D-arabinofuranosyl-5-iodouracil
Fluoromethyl-HHT	6-(2-hydroxy-hydroxypropyl)-5-fluoromethyl(1 <i>H</i> ,3 <i>H</i> )-pyrimidine-2,4-dione
FLT	3'-fluoro-3'-deoxy-L-thymidine
FMAU	1-(2'-deoxy-2'-fluoro-β-d-arabinofuranosyl)thymine
G418	geneticine
GCV	ganciclovir
GFP	green fluorescent protein
hCNT1-3	human concentrative nucleoside transporter 1-3
hENT1-4	human equilibrative nucleoside transporter 1-4
HEK293	human embryonic kidney 293 cells

HEK293TK+	HEK293 cell line stably expressing HSV1-TK
HEPES	4-(2-hydroxyethyl)piperazine-1-ethanesulfonic acid
HMTT	( <i>R,R</i> )-6-(6-hydroxymethyl-5-methyl-2,4-dioxo-hexahydro-pyrimidin-5-ylmethyl)-5-methyl-1H-pyrimidin-2,4-dione
HPLC	high-performance liquid chromatography
HRMS	high-resolution mass spectra
HSV1- <i>tk</i>	herpes simplex virus type 1 thymidine kinase gene
HSV1-TK	herpes simplex virus type 1 thymidine kinase protein
HSV1-sr39 <i>tk</i>	a mutant herpes simplex virus type 1 thymidine kinase gene
HSV1-sr39TK	a mutant herpes simplex virus type 1 thymidine kinase protein
LC	liquid chromatography
IC <sub>50</sub>	half maximal (50%) inhibitory concentration of a substance
ID	injected dose
K2.2.2	4,7,13,16,21,24-hexaoxa-1,10-diazabicyclo[8.8.8]-hexacosane
$K_i$	inhibition constant
LOR	line of response
LRMS	low-resolution mass spectra
MIP	maximum intensity projection
MRI	magnetic resonance imaging
MOM	methoxy methyl
mRNA	messenger ribonucleic acid
MS	mass spectroscopy
MTr	4-methoxytrityl
NADPH-RS	NADPH regenerating system
NBMPr	nitrobenzylthioinosine
NBMPr-P	nitrobenzylthioinosine phosphate
NBTI	nitrobenzylthioinosine
nca	no-carrier-added
NIS	Na/I symporter
<i>N</i> -Me-FHBT	6-(3-fluoro-2-(hydroxymethyl)propyl)-1,5-dimethylpyrimidin-2,4(1 <i>H</i> ,3 <i>H</i> )-Dione

NMR	nuclear magnetic resonance
NT	nucleoside transporter
PBS	phosphate buffered saline
PCV	penciclovir
PEG	polyethyleneglycol
PET	positron emission tomography
PMB	<i>p</i> -methoxybenzyl
POCl <sub>3</sub>	phosphorous oxychloride
ppm	parts per million
RCP	radiochemical purity
RCY	radiochemical yield
RP	reversed phase
RFP	red fluorescent protein
RNA	ribonucleic acid
ROI	region of interest
RT-PCR	real-time polymerase chain reaction
SDS	sodium dodecyl sulfate
SLC	solute linked carrier
SLC28	concentrative nucleoside transporters
SLC29	equilibrative nucleoside transporters
S <sub>N</sub> 2	bimolecular nucleophilic substitution
SPECT	single photon emission computed tomography
SUV	standardized uptake value
TBAF	tetrabutylammonium fluoride
TBS-T	tris-buffered saline-Tween-20
THF	tetrahydrofurane
<i>tk</i>	thymidine kinase gene
TK1	thymidine kinase 1 protein
TK2	thymidine kinase 2 protein
TLC	thin layer chromatography
TMSCl	trimethylsilyl chloride

TPase	thymidine phosphorylase
Tris	tris(hydroxymethyl)aminomethane
Ts	tosyl
UPLC	ultra performance liquid chromatography
UV	ultra violet
VOI	volume of interest



# **Introduction**





## 1.1 Imaging of Gene Expression *in vivo*

Molecular imaging allows the visualization of normal and abnormal cellular processes in living subjects at the molecular level rather than at the anatomic level [1]. For many years invasive methods such as biopsy or post-mortem tissue sampling and tissue processing were required for quantitative analysis and visualization of cellular processes. However, in the past decade the technologies of medical imaging in living organisms made remarkable progress. In particular, non-invasive imaging technologies have become an important field with exceptional growth. Their rapid and feasible translation into clinical settings offered the possibility to launch new standards of medical practice. Perhaps the most exciting novel imaging paradigm being developed is the approach of imaging molecular and cellular processes, as it is of great interest to monitor these processes in animal models of human disease. This approach towards a specific imaging can now provide the potential for understanding integrative biology, earlier detection and characterization of disease, and evaluation of treatment such as gene therapy. Gene therapy is a relatively recent therapeutic strategy consisting of the delivery of genetic material into cells for a therapeutic purpose such as treatment of cystic fibrosis or chronic pain [2, 3]. To date, improvements in gene therapy strategies have been hampered by difficulties in the monitoring and measuring transgene expression *in vivo* on a whole-body scale. The traditional methods for evaluating gene transfer such as analysis of biopsy samples can only provide limited information regarding the biodistribution, magnitude and persistence of transgene expression over time. Therefore, non-invasive techniques capable of repeated sampling are required to determine transgene expression in living subjects.

The main goal of molecular imaging is to develop non-invasive *in vivo* imaging methods that reflect specific cellular processes, such as gene expression, protein-protein interactions; to follow trafficking and targeting of cells, e.g. immune cells, stem cells, cancer cells; to optimize drug and gene therapy; to image drug effects at a molecular and cellular level; and to achieve all these imaging goals in a rapid, reproducible and quantitative manner. Magnetic resonance imaging (MRI), computed tomography (CT), nuclear imaging modalities such as positron emission

tomography (PET) and single photon emission computed tomography (SPECT), ultrasound and optical imaging are today's major non-invasive *in vivo* imaging modalities. Although MRI is a widely utilized modality in clinical settings, its general applicability is limited by its inferior sensitivity relative to PET or SPECT nuclear techniques. These latter techniques are some of the most important to the field of imaging of gene expression *in vivo* as they are also potentially quantitative and readily translatable from the laboratory to the patient.

### 1.1.1 Nuclear Imaging

Molecular imaging using SPECT requires a probe that is labeled with a radionuclide such as  $^{123}\text{I}$  or  $^{99\text{m}}\text{Tc}$  that results in the emission of gamma-ray or high-energy X-ray photons. In contrast to PET, only one photon is emitted making the determination of LORs (line of response) and photon quantification in SPECT more difficult than in PET.

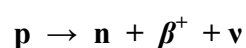
The principle of PET is further described in Section 1.1.2. Both imaging modalities provide molecular and functional information with a high sensitivity (Table 1.), whereas PET provides even higher sensitivity than SPECT. Nuclear imaging permits monitoring of functional processes in the intact organism at physiological concentrations and delivers three-dimensional images. PET as a medical imaging technique offers a range of advantages, including high spatial resolution of 3-5 mm for clinical PET and ~1.0 mm for preclinical PET as well as full quantitative capability [4, 5]. This means, that dynamic and kinetic modeling studies can be easily performed. Furthermore, the possibility of combining PET with high resolution imaging devices such as MRI or CT paves the way for a new perspective in molecular imaging for early detection, characterization, and "real-time" monitoring of disease as well as investigating the efficacy of drugs [6]. Applied to gene therapy, PET can provide critical information regarding transduction efficiency, as well as the duration and distribution of gene expression. This information is essential for the improvement of gene delivery vectors [7, 8]. In addition, only tracer doses of imaging probes are required, thus limiting undesired side-effects for the patient and by using low activity limiting radiation protection issues for members of staff and the patient. Consequently, PET scanning has been used for a host of applications in biomedical research, including gene therapy, and currently offers great potential for translation to clinical use [5, 9].

**Table 1** Comparison of nuclear and optical imaging parameters [10]

Parameter	Optical imaging	Nuclear medicine imaging
Spatial resolution	3-5 mm	1-2 mm
Temporal resolution	Seconds to minutes	10 s to minutes
3D tomography	Not yet available	Yes
Tissue penetration	1 cm (variable)	No limit
Sensitivity	10 <sup>-15</sup> -10 <sup>-17</sup> mol/L (bioluminescence)	10 <sup>-11</sup> -10 <sup>-12</sup> mol/L (PET)
	10 <sup>-9</sup> -10 <sup>-12</sup> mol/L (fluorescence)	10 <sup>-10</sup> -10 <sup>-11</sup> mol/L (SPECT)
Background	Low (bioluminescence)	Moderate to high
	Moderate (fluorescence)	
Reporter gene transfer	Yes	Yes
Probes	Yes (bioluminescence)	Radiolabeled tracers
	No (fluorescence)	
Chemical synthesis or labeling labor	No	Yes
Radiation hazard	No	Yes
Costs	Low	High (PET)
Potential for clinical use	Very low	Yes

### 1.1.2 Principle of PET

Proton rich nuclei are unstable and can decay by  $\beta^+$ -particle emission (positron decay) accompanied by the emission of a neutrino  $\nu$ , which is an opposite entity of an antineutrino:



The positron is the antiparticle or the antimatter counterpart of the electron with the same mass as an electron, an electric charge of +1 and a spin of 1/2. With the conversion of a proton into a neutron, a positron and a neutrino, the daughter nuclide has an atomic number that is 1 less than the parent nuclide. During positron decay the energy released is shared between the positron and the neutrino and maximum energies are different for each nuclide (Table 2). Since a neutron is equivalent to one proton plus an electron, a mass equivalent of two electrons (2 x 511 keV) are created by the conversion of a proton to a neutron in positron decay. Therefore, positron emission takes place only when the energy difference between the parent and daughter nuclides is equal to or greater than 1.02 MeV. The range of positrons is short in matter. At the end of the path of  $\beta^+$ -

particles, positrons combine with electrons and are thus annihilated, each event giving rise to two gamma ray photons of 511 keV that are emitted in opposite directions. These photons are referred to as annihilation radiations in order to conserve for energy and momentum. The energies of the emitted positrons determine the path length before annihilation. The larger the positron energy, the larger the average distance the positron travels before annihilating and the lower the spatial resolution for PET. Gamma rays are electromagnetic radiation with very short wavelengths and high energy. Therefore, relatively few gamma rays are absorbed in tissue which allows for external detection. The two photons are emitted simultaneously in opposite direction and are detected by two detectors in coincidence. Along a virtual line (line of response, LOR) connecting those two detectors, positron annihilation must have occurred. A large number of coincident events are collected over many angles around the object axis and these data are used to reconstruct the image of the activity distribution in the region of interest (Fig. 1.) [11-13].

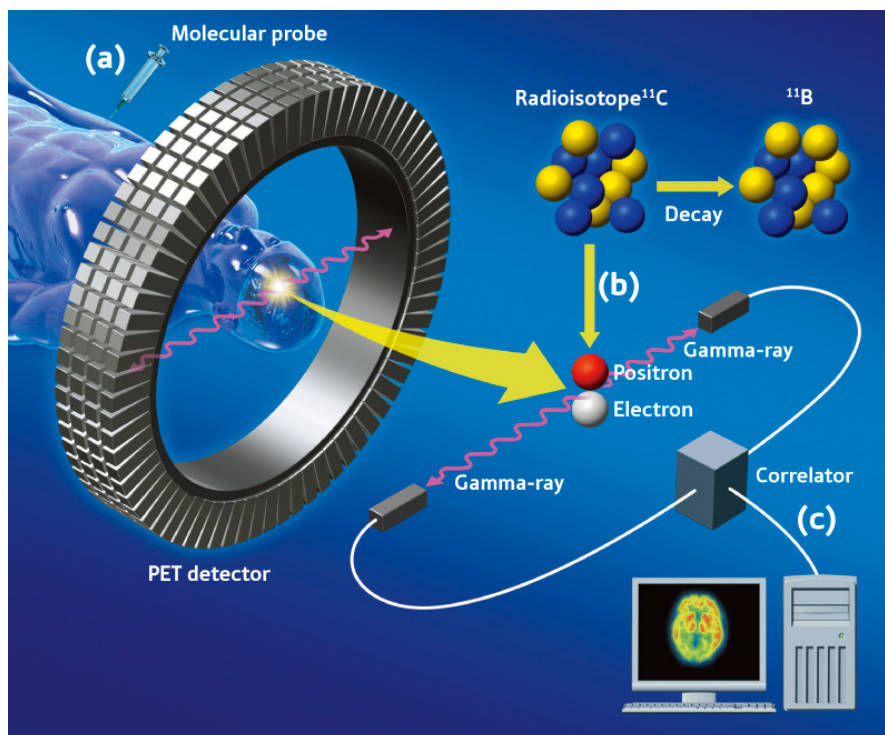


**Figure 1.** Setup for [ $^{11}\text{C}$ ]-tracer evaluation with PET [14]. (a) Injection of a radiolabeled probe which accumulates at a region of interest (e.g. brain). (b) Emission of positron from radionuclide and annihilation with electron in tissue producing two gamma rays with 511 keV each in opposite direction. (c) Detection and data acquisition to reconstruct an image of region of interest

### 1.1.3 PET Nuclides

Several PET nuclides exist for incorporation into biomolecules (Table 2.), but the most common used ones are  $^{18}\text{F}$  and  $^{11}\text{C}$ . The choice of a nuclide for PET imaging is made depending on the different physical properties of the nuclides such as physical half-life and maximum energy according to its application. Fluorine-18 with the low positron energy has the best imaging physical characteristics because it allows for good spatial resolution and a low radiation dose for the patient. A further advantage of fluorine-18 is the physical half-life of 110 min. It allows for longer *in vivo* investigation and complex radiosyntheses. Furthermore, the tracer can be transported to clinical PET centers that lack radiochemistry facilities. Even though the fluorine atom is not a part of organic biomolecules, the substitution of a hydroxyl group or a hydrogen atom by fluorine is a very common applied bioisosteric replacement. Steric parameters of a biomolecule remain similar by fluoride introduction, but the strong electron-withdrawing properties of fluoride have an effect on the electronic properties, lipophilicity and the biological characteristics of the biomolecule. Carbon is naturally a part of biomolecules and thus allows the syntheses of radiopharmaceuticals that are chemically indistinguishable from their non-radioactive counterparts. Carbon-11 has a very short half-life of 20.3 min and is suited for compounds with short biological half-lives. It allows for repeated investigations in the same subject within short time intervals but it also requires fast radiosyntheses and on-site cyclotrons. Positron-emitting radionuclides with longer half-lives such as  $^{124}\text{I}$  are useful to study processes with slow pharmacokinetics and they can easily be distributed to clinical centers [11].

**Table 2.** Physical properties of some PET radionuclides

Nuclide	Half-life (min)	Maximum energy (MeV)	$\beta^+$ decay (%)
$^{18}\text{F}$	109.8	0.64	97
$^{11}\text{C}$	20.3	0.96	99
$^{13}\text{N}$	9.96	1.20	100
$^{15}\text{O}$	2	1.74	100
$^{68}\text{Ga}$	68.1	1.83	90
$^{124}\text{I}$	6019	4.10	25

### 1.1.4 Strategies for $^{18}\text{F}$ -labeling

The half-life of fluorine-18 requires a convenient radiosynthesis strategy which aims to introduce the radionuclide into the molecule as late as possible using nucleophilic or electrophilic substitution.

#### **Nucleophilic Radiofluorination**

Sufficiently high specific activities can be obtained with the no-carrier-added (nca) nucleophile substitution using nca  $^{18}\text{F}$ fluoride ion and nucleophile substitution is, therefore, the method of choice for PET tracers.  $^{18}\text{O}(\text{p},\text{n})^{18}\text{F}$  reaction by cyclotron-accelerated proton bombardment of  $^{18}\text{O}$ -enriched  $\text{H}_2\text{O}$  yields  $^{18}\text{F}$ fluoride as a water solution.  $^{18}\text{F}$ fluoride in water is non-nucleophilic. Therefore, the water must be removed typically by trapping  $^{18}\text{F}$ fluoride on an ion-exchange column and subsequent elution with kryptand in combination with alkali salts ( $\text{K}^+$ ,  $\text{Cs}^+$ ,  $\text{Rb}^+$ ) or tetra-*n*-butylammonium cation followed by repeated azeotropic evaporation of solvents. Mainly dipolar aprotic solvents such as acetonitrile, DMF or DMSO are used for nucleophilic substitution. Addition of protic *tert*-butanol to acetonitrile can dramatically improve the radiochemical yields [15].

Nucleophilic substitution reactions with  $^{18}\text{F}$ fluoride have been largely developed for aromatic and aliphatic systems. In aliphatic systems, a leaving group (e.g. tosylate, mesylate nosylate, triflate, iodide or bromide) is substituted with  $^{18}\text{F}$ fluoride via an  $\text{S}_{\text{N}}2$  reaction. Nucleophilic substitution can be applied directly on a suitable precursor, or for more complex molecules in a multistep synthesis via a prosthetic group which is then chemoselectively coupled to e.g. a peptide or an antibody.  $^{18}\text{F}$ fluoride allows for synthesis of a large variety of fluorine-18 labeled compounds.

#### **Electrophilic Radiofluorination**

Highly reactive  $^{18}\text{F}\text{F}_2$  or its secondary derived precursors are used as fluorinating reagents for electrophilic reactions.  $^{18}\text{F}\text{F}_2$  can be produced either by  $^{20}\text{Ne}(\text{d},\alpha)^{18}\text{F}$  reaction or by  $^{18}\text{O}(\text{p},\text{n})^{18}\text{F}$  reaction. Having generally poor capacity for fluorine, only a limited range of adequately resistant solvents (e.g. freon, dichloromethane, anhydrous hydrogen fluoride, trifluoroacetic acid, glacial acetic acid and water) may be employed for  $^{18}\text{F}\text{F}_2$  fluorination.  $^{18}\text{F}\text{F}_2$  is generally converted into less reactive and more selective  $^{18}\text{F}$ -labeled fluorination agents such as acetyl hypofluorite,

perchloryl fluoride, halogen fluorides, xenon fluoride and fluorosulfonamides. Since only one of the fluorine atoms in  $[^{18}\text{F}]\text{F}_2$  carries the  $[^{18}\text{F}]$ fluorine, low specific radioactivities of the final  $^{18}\text{F}$ -labeled products and maximum 50% radiochemical yields will be obtained. Despite the possibility of only moderately high production using electrophilic fluorination agents, they have found some application (mainly  $^{18}\text{F}$ -labeled acetyl hypofluorite and  $[^{18}\text{F}]\text{F}_2$ ) in the radiosynthesis of different tracers such as  $[^{18}\text{F}]\text{FDOPA}$  [16-18]. Nevertheless, electrophilic radiofluorination is not the method of choice for PET studies requiring high specific radioactivities.

### 1.1.5 Reporter Gene Imaging

Currently, the most commonly used molecular-genetic imaging modalities are ‘indirect’. Meaning that a “reporter gene” is coupled with a complimentary “reporter probe” resulting in a selective interaction among them and an accumulation of their products in the transfected cells. This general paradigm for non-invasive reporter gene imaging using radiolabeled probes was initially described in 1995 [19].

The alternative to ‘indirect’ imaging is ‘direct’ imaging. Radiolabeled antisense oligonucleotide probes have been used to directly image endogenous gene expression at the transcription level [10]. However, this technique has been hindered by formidable biologic barriers and by low concentrations of target mRNA or DNA, and the direct imaging technology is less extensively used compared to the indirect one [20].

To date, three types of PET reporter genes have been developed: those encoding following proteins [21]:

- Enzymes (e.g. herpes simplex virus type 1 thymidine kinase gene (*HSV1-tk*))
- Receptors (e.g. dopamine 2 receptor (D2R))
- Transporters (e.g. Na/I symporter (NIS))

*HSV1-tk* is one of the most commonly used reporter genes. It is an attractive approach as it can be used both as a reporter gene and a suicide gene therapy and indeed has been used for some decades in clinical trials in which this suicide gene is transferred into tumors [22]. The major advantages of its intracellular protein expression are the relatively uncomplicated expression strategy and lack of recognition of the expression product by the immune system. Furthermore,

an additional advantage is the potential for signal amplification if the reporter protein can act on a reporter probe and is then free to continue to act on other reporter probes [21].

### 1.1.6 Principle of Imaging HSV1-TK Reporter Gene Expression

The general concept of a reporter gene is simple. A defined nucleotide sequence is introduced into a cell by using common transfer protocols. Once in the target cell, the DNA will be transcribed to the corresponding mRNA, adequately processed, and translated into the subsequent proteins. HSV1-TK is an extensively studied PET reporter protein that selectively phosphorylates the complementary radiolabeled PET reporter probe and as a result of the negative charge the products are trapped inside the transfected cells (Fig. 2.). The radioactive accumulation is detected using PET imaging. Simultaneous expression of the reporter gene and a therapeutic gene indirectly demonstrate whether a gene of interest is expressed as well as the duration and localization of its expression. Therefore, PET, as a non-invasive, clinically applicable imaging method, would be of considerable value for monitoring and evaluating gene therapy in human subjects.

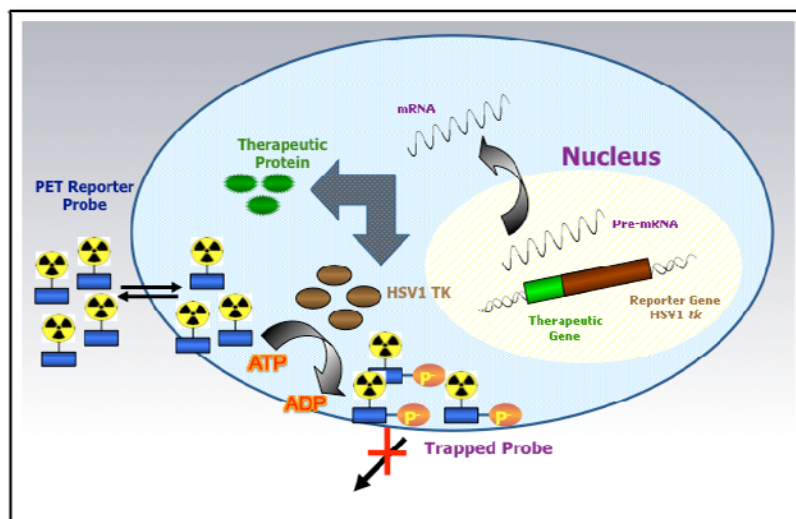


**Figure 2.** Principle of gene monitoring using HSV1-TK substrate as PET reporter probe



## 1.2 Herpes Simplex Virus Type 1 Thymidine Kinase

### 1.2.1 Human and Viral Thymidine Kinase

Thymidine kinase is an enzyme having key function in the synthesis of DNA by recovering nucleosides and thereby in cell proliferation. In mammalian cells, the first step in the salvage of deoxynucleosides is a phosphorylation step carried out by thymidine kinase 1 (TK1) and deoxycytidine kinase (dCK) in the cytosol (highly expressed in S phase and therefore in proliferating cells) and thymidine kinase 2 (TK2) and deoxyguanosine kinase (dGK) in the mitochondria (low expression) [23]. In addition to the salvage pathway, cells can synthesize phosphorylated nucleotides via *de novo* synthetic pathway.

**HSV1-*tk* reporter gene:** Of considerable importance in clinical medicine and in several research fields is the herpes simplex virus type 1 thymidine kinase (HSV1-TK). This enzyme phosphorylates thymidine to thymidine monophosphate, as eukaryotic TKs do. In contrast to mammalian TK1s, which phosphorylate only thymidine and a few close derivatives, HSV1-TK phosphorylates a wide range of thymidine analogs whereby some of them are modified to a high extent. The substrate variety includes pyrimidine derivatives such as 2'-fluoro-2'-deoxy-1- $\beta$ -D-arabinofuranosyl-5-iodouracil (FIAU) as well as guanosine derivatives such as 9-(4-fluoro-3-hydroxymethylbutyl)guanine (FHBG) and ganciclovir (GCV). This difference in terms of substrate selectivity permits the development and use of radiolabeled probes which are selectively phosphorylated only by the HSV1-TK. Currently, wild-type HSV1-*tk* and the mutated HSV1-sr39*tk* which provides a further increase in sensitivity for acycloguanosines, are the reporter genes most widely used in current molecular imaging studies using radiolabeled probes and PET imaging [24, 25].

Since human thymidine kinase 1 is expressed in the cytoplasm of rapidly proliferating cells and shows high substrate specificity accepting only close analogs of thymidine, thymidine analogs such as 3'-[<sup>18</sup>F]fluoro-3'-deoxy-L-thymidine [<sup>18</sup>F]FLT or 1-(2'-deoxy-2'-[<sup>18</sup>F]fluoro- $\beta$ -D-arabinofuranosyl)thymine [<sup>18</sup>F]FMAU can be used to image cell proliferation [26-28].

**HSV1-*tk* therapeutic gene:** Furthermore HSV1-*tk* can be used as a therapeutic suicide gene in cancer gene therapy. By infection with e.g. recombinant viruses, HSV1-*tk* is transferred into tumors leading to expression of the enzyme within tumor tissues [22]. Due to the relaxed substrate specificity, a systemically administered prodrug (usually an acycloguanosine, such as ganciclovir) in a patient is phosphorylated by the HSV1-*tk* transgene and only poorly by the endogenous thymidine kinase. This phosphorylation converts the membrane-permeable prodrug into a polar product, which is trapped in the cell and acts as chain terminator when incorporated into the DNA and finally leads to death of the transduced cancer cells.

Following the prodrug principle, guanosines such as acyclovir can be used as antiviral medication for the treatment of herpes simplex infections [29].

The combination of therapeutic and reporter gene allows a direct imaging of the therapeutic gene product without the need for an extra reporter gene. Jacobs *et al.* published the first clinical trial with HSV1-*tk* as a reporter gene system in 2001 [30]. They assessed the intratumoral infusion of liposome-gene complexes, followed by ganciclovir treatment, in patients with glioblastoma lesions. Using PET imaging, the authors were able to image the specific accumulation of the [<sup>124</sup>I]FIAU tracer in a patient, providing proof of principle that the extent of vector-mediated gene expression may predict the therapeutic response.

### 1.2.2 HSV1-TK Substrates for PET

During the past two decades, many radiolabeled probes have been developed for imaging HSV1-*tk* reporter gene expression with PET (Fig. 3.) [31]. There are two classes of probes: pyrimidine nucleoside analogs and purine (acycloguanosine) analogs. The pyrimidine analogs are 2'-[<sup>18</sup>F]fluoro-arabinofuranisyluracil derivatives and a few other C-5 substituted uracil derivatives. The purine analogs are fluorinated derivatives of guanosine with open chains substituted for the sugar moiety.

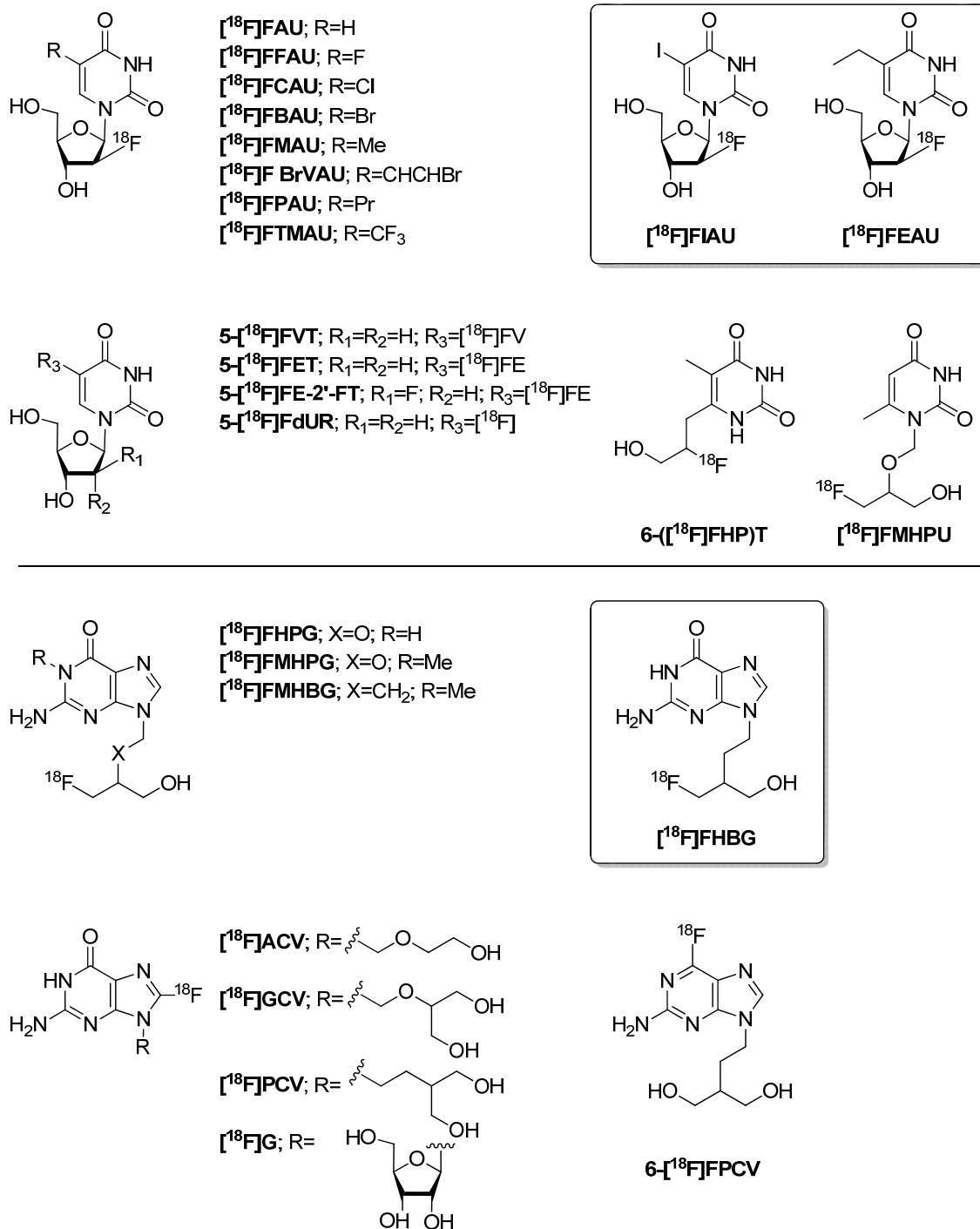


**Figure 3.** Structures of <sup>18</sup>F-labeled pyrimidine and purine probes for imaging HSV1-TK with PET [31]

The most successful candidates among them are pyrimidine analogs FIAU and FEAU and acycloguanosine analog FHBG. Well known and extensively studied they differ in terms of efficacy for imaging HSV1-*tk* gene expression.

**Pyrimidines FIAU, FEAU:** [ $^{18}\text{F}$ ]FIAU and [ $^{18}\text{F}$ ]FEAU were investigated in animals bearing xenografts implanted with transduced HT-29 cells, and their accumulation (%ID/g) was  $15.48 \pm 3.94$  and  $9.98 \pm 1.99$ , respectively [32]. The ratio of tumor uptake between the transduced and wild-type cells for [ $^{18}\text{F}$ ]FIAU was higher than that of [ $^{18}\text{F}$ ]FEAU, however, FIAU had also some accumulation in wild-type tumor due to non-specific phosphorylation by host thymidine kinase 1, and therefore, suffers from lower specificity towards HSV1-TK. Furthermore, [ $^{18}\text{F}$ ]FEAU has been shown to have the highest uptake ratio between HSV1-TK positive cells and wild-type cells compared with FHPG, FHBG, FIAU, FMAU, and [ $^{18}\text{F}$ ]FLT [33]. The HSV1-TK activity in tumors could be monitored non-invasively after systemic viral vector treatments using [ $^{18}\text{F}$ ]FEAU-PET as a basis for determining the levels and tissue distribution of vector noninvasively in living animals and for optimizing *in vivo* transfection rates [34]. *In vitro* and *in vivo* results showed in a different study that [ $^{124}\text{I}$ ]FIAU is a substantially more efficient probe than [ $^{18}\text{F}$ ]FHBG or [ $^{18}\text{F}$ ]FHPG for imaging HSV1-TK expression, with greater sensitivity and contrast [35]. The only pyrimidine analog used in the clinic is [ $^{124}\text{I}$ ]FIAU as shown by Jacobs *et al.* [30].

**Guanosine FHBG:** Much attention has been given to the penciclovir (PCV) analog [ $^{18}\text{F}$ ]FHBG because the efficacy of PCV as an antiviral drug is better than that of ganciclovir (GCV) [36, 37]. In human pharmacokinetic studies, [ $^{18}\text{F}$ ]FHBG has been shown to be a safe tracer with highly desirable pharmacokinetic properties [38]. Its rapid clearance and low background activity make it suitable for imaging HSV1-*tk* gene expression in all regions except the brain and the lower abdomen. [ $^{18}\text{F}$ ]FHBG has been shown to detect HSV1-*tk* transgene expression in liver tumors of patients [39]. The first study of reporter-gene-based imaging of therapeutic cells in a human patient with glioma was performed by Yaghoubi *et al.* in 2009 [40]. It illustrates that [ $^{18}\text{F}$ ]FHBG, which normally cannot cross the blood-brain barrier, can accumulate within glioma tumors after intratumoral infusion of a vector expressing HSV1-*tk*. Furthermore, [ $^{18}\text{F}$ ]FHBG has been shown to be more sensitive to HSV1-sr39TK and to be phosphorylated at higher rates by HSV1-sr39TK, which is derived from the mutated HSV1-TK [41]. [ $^{18}\text{F}$ ]FHBG has been approved by the U.S. Food and Drug Administration (FDA) as an investigational new drug (imaging agent), and is in human use (IND #61,880) at UCLA and Stanford University nuclear medicine clinics.

However, these studies demonstrated that even the most successful tracers still bear disadvantages such as low specificity towards HSV1-TK due to some substrate acceptance by host TK1 (FIAU), and therefore non-specific cell uptake, low sensitivity for HSV1-TK (FEAU) or unfavorable *in vivo* kinetics due to high abdominal background (FHBG) [32, 38]. Furthermore mitochondria cytotoxicity has been observed in long term use for FIAU [42].

It can be concluded that pyrimidine derivatives have two advantages over guanosine derivatives [31]. First, pyrimidines show higher sensitivity towards wild type HSV1-TK. Pyrimidine analogs are excellent substrates for HSV1-TK; however, some of them e.g. FIAU are also substrates for cellular TK1, so their specificity towards HSV1-TK is lower than that of other analogs [32]. Second, pyrimidine analogs profit from a negligible background activity due to renal clearance. [<sup>18</sup>F]FHBG is cleared through the hepatobiliary pathway, such that radioactivity is retained in the intestine and other organs which makes HSV1-TK imaging in the abdominal region difficult [38, 43].

### 1.2.3 Requirements for Ideal HSV1-TK Reporter Probe

To be considered a suitable HSV1-TK substrate for PET imaging, a compound has to fulfill several requirements:

- High sensitivity towards HSV1-TK (wild type or a mutant version)
- High specificity towards HSV1-TK favored by low sensitivity towards host TK1
- Possibility to enter a cell
- Accumulate only where the reporter gene is expressed
- Low cytotoxicity of probe and possible metabolites
- Suitable structure for radiolabeling and an efficient and convenient radiosynthesis
- High *in vivo* stability
- Favorable pharmacokinetics: high target/non-target ratio

As discussed in 1.2.2 the optimal PET tracer for HSV1-TK imaging fulfilling all the above requirements has not been found yet.

### 1.2.4 C-6 Substituted Pyrimidine Derivatives

One drawback of the N-1 substituted pyrimidine analogs is cleavage of the glycosilic bond between the sugar and the base by thymidine phosphorylase (TPase). In the search for novel derivatives for HSV1-*tk* gene expression imaging, C-6 substituted 6-(1,3-dihydroxyisobutyl)thymine (DHBT) (Fig. 4.) with high sensitivity towards HSV1-TK and low cytotoxicity was found in a serendipitous reaction between thymine and several alcohols induced by gamma irradiation [44]. With two free hydroxyl groups DHBT offered the possibility for phosphorylation by HSV1-TK [44, 45]. Bioisosteric replacement of one hydrogen atom of the methyl group at the C-5 position with  $^{18}\text{F}$  resulted in 6-(2-hydroxy-hydroxypropyl)-5- $^{18}\text{F}$ fluoromethyl(1*H*,3*H*)-pyrimidine-2,4-dione ( $^{18}\text{F}$ fluoromethyl-HHT). High *in vivo* defluorination of the substrate was observed during PET studies [46]. Therefore, the position of label was changed to the C-6 position, which resulted in the development of 6-(3- $^{18}\text{F}$ -fluoro-2-(hydroxymethyl)propyl)-5-methylpyrimidine-2,4(1*H*,3*H*)-dione ( $^{18}\text{F}$ FHBT) [46]. Unfortunately, intramolecular cyclization occurred during radiosynthesis for  $^{18}\text{F}$ FHBT between N-1 and C-6 of the acyclic moiety [47]. In order to prevent intramolecular cyclization, N-1 protected 6-(3- $^{18}\text{F}$ -fluoro-2-(hydroxymethyl)propyl)-1,5-dimethylpyrimidin-2,4(1*H*,3*H*)-dione (*N*-Me- $^{18}\text{F}$ FHBT) was developed [47].

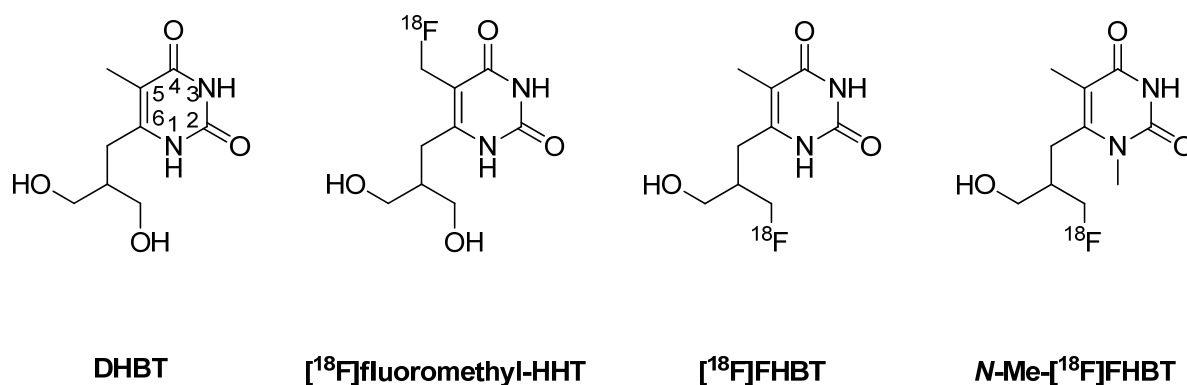


**Figure 4.** Chemical structures of C-6 substituted pyrimidine derivatives DHBT,  $^{18}\text{F}$ fluoromethyl-HHT,  $^{18}\text{F}$ FHBT and *N*-Me- $^{18}\text{F}$ FHBT

### 1.3 Tracer Transport into Cells and Tissues

Pharmacokinetics of a HSV1-TK PET tracer are not only determined by phosphorylation but also by transport of the drug from plasma into the cell. Little is known about transport of HSV1-TK tracers across cell membrane. It is crucial to investigate on probe transport across cell and tissue membranes. HSV1-TK tracers, like nucleosides, are relatively hydrophilic molecules and their uptake into cells depends upon specific transport proteins in the plasma membrane [48]. Nucleoside transporters (NTs) are membrane proteins that play a key role in the nucleoside salvage pathway for nucleotide synthesis and are responsible for mediating cellular uptake of nucleosides and nucleobases, and consequently of a variety of nucleoside-derived drugs. NTs are classified into equilibrative nucleoside transporters (ENT) and concentrative nucleoside transporters (CNT). Nucleoside flux is driven by the concentration gradient for ENT, whereas for CNT the driving force is a  $\text{Na}^+$  gradient such that the electrochemical gradient can drive cellular uptake of nucleosides against their concentration gradient. ENT (gene family SLC29) as a bidirectional carrier consists of four isoforms ENT1-4 and unidirectional CNT (SLC28) consists of three isoforms CNT1-3 (Table 3) [49, 50].

**Table 3.** Substrate Selectivity of Nucleoside Transporters [51]

Substrates	Ado	Guo	Urd	Cyd	Thy	Nucleobases
<b>hENT1</b>	S (40 $\mu\text{M}$ )	S (140 $\mu\text{M}$ )	S (260 $\mu\text{M}$ )	S (580 $\mu\text{M}$ )	S (300 $\mu\text{M}$ )	nt
<b>hENT2</b>	S (100 $\mu\text{M}$ )	S	S (250 $\mu\text{M}$ )	S (5610 $\mu\text{M}$ )	S (710 $\mu\text{M}$ )	S
<b>hENT3</b>	S (1860 $\mu\text{M}$ )	S	S (2020 $\mu\text{M}$ )	S	S	S (Adenine)
<b>hENT4</b>	S (7800 $\mu\text{M}$ )	nt	nt	nt	nt	nt
<b>hCNT1</b>	nt	nt	S (40-60 $\mu\text{M}$ )	S (40 $\mu\text{M}$ )	S (6 $\mu\text{M}$ )	nt
<b>hCNT2</b>	S (8 $\mu\text{M}$ )	S (21 $\mu\text{M}$ )	S (80 $\mu\text{M}$ )	nt	nt	nt
<b>hCNT3</b>	S (15 $\mu\text{M}$ )	S (43 $\mu\text{M}$ )	S (22 $\mu\text{M}$ )	S (15 $\mu\text{M}$ )	S (21 $\mu\text{M}$ )	nt

S: substrate (when known, apparent  $K_m$  value is given); nt: not transported

### 1.3.1 Equilibrative Nucleoside Transporters

ENT proteins contain 11 hydrophobic transmembrane  $\alpha$ -helices, with an intracellular amino and an extracellular carboxy terminus [52]. Human equilibrative nucleoside transporters 1 and 2 (hENT1 and hENT2) each contain 456 residues and are 50% identical in sequence. They exhibit broad substrate specificities accepting most pyrimidines and purines, however, they have lower affinities for natural nucleosides than CNTs (100-800  $\mu$ M) (Table 3.). hENT1 is a ubiquitous transporter with significant variability in tissue abundance. hENT1 mRNA is expressed in many tissues, including erythrocytes, vascular endothelium, placenta,, heart, liver, lung and colon [53]. The wide distribution of ENT1 and ENT2 systems in human, rat and mice brain has been verified [54-56]. hENT2, with highest level occurring in skeletal muscle, has also been detected in many tissues such as vascular endothelium, heart, placenta, thymus, pancreas, prostate and kidney [57, 58]. hENT3 is a 475 amino acid protein 29% identical in sequence to hENT1, has a broad substrate selectivity and is widely expressed in human tissues with particular abundance in placenta [59, 60]. hENT4 is a protein of 530 residues which presents some capability of transporting adenosine at acidic pH. hENT4 is particularly abundant in heart, but it is likely to be ubiquitously expressed in human tissues [61]. hENT1-4 differ in their sensitivity to inhibitors such as nitrobenzylthioinosine (NBTI or NBMPR), dipyridamole and dilazep (Table 4., Fig. 5.).

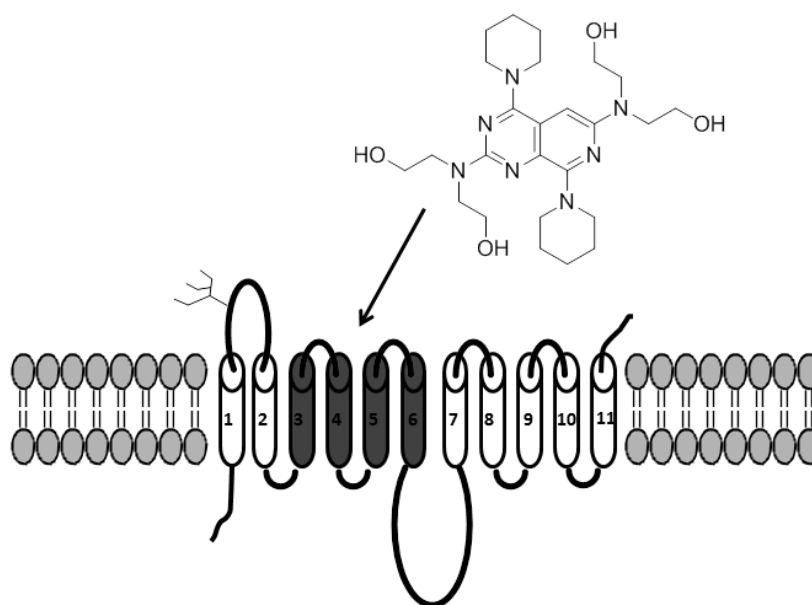


**Figure 5.** Predicted transmembrane topology of hENT1 and the region responsible for binding dipyridamole [62]



**Table 4.** Inhibitors of Nucleoside Transporters [51]

<b>Inhibitors*</b>	<b>NBTI</b>	<b>Dipyridamole</b>	<b>Dilazep</b>
<b>hENT1</b>	0.005 $\mu$ M	0.05 $\mu$ M	0.02 $\mu$ M
<b>hENT2</b>	>1 $\mu$ M	5 $\mu$ M	120 $\mu$ M
<b>hENT3</b>	>10 $\mu$ M	>10 $\mu$ M	>10 $\mu$ M
<b>hENT4</b>	>1 $\mu$ M	>1 $\mu$ M	>1 $\mu$ M

\*K<sub>i</sub> values of ENT transporters

### 1.3.2 Concentrative Nucleoside Transporters

CNT share a probable topology of 13 transmembrane proteins, with an extracellular carboxy terminus including the cation and substrate recognition sites [63]. CNTs are more selective for their substrates than ENTs with higher affinities (Table 3.) [50]. hCNT1 is the pyrimidine preferring transporter, hCNT2 prefers purines and hCNT3 translocates both nucleoside types. Mammalian CNT1 proteins (~650 residues) exhibit >64% sequence identity to the CNT2 proteins (~660 residues). CNTs are broadly present in the body and active transport is found particularly in specialized epithelial cells such as small intestine, kidney and liver [53]. CNT1 is particularly abundant in liver but virtually absent in most of the immune system cells. CNT2 expression in immune system cells is ubiquitous but highly variable. CNT3 is low in lymphoid cells but high in monocytes and macrophages. CNT1 and CNT3 have been detected in some brain regions and CNT2 is widespread in brain [64-66].

### 1.3.3 Cellular Localization of Nucleoside Transporters

Tissue distribution of NTs shows that mammalian cells express more than one type, often combining CNTs and ENTs in a single cell type. In general, there are large differences in the functional expression of NT depending on cell type. In addition, NT activities within the same cell type vary with changes in growth state and differentiation. The liver has the capacity of modulating its nucleoside transport and salvage pathway by bile acids which are capable of increasing CNT2 transport activity by increasing CNT2 translocation to the plasma membrane [67]. The presence of CNT on apical membranes and ENTs on basolateral membranes of polarized cells provide a plausible model for the vectorial flow of physiologically relevant

## Introduction

molecules in tissue absorptive epithelia such as the intestines and kidney [68]. As another example, at the blood-brain-barrier NTs are co-expressed but their localization has not been determined [69].

## 1.4 Aim of Thesis

Herpes simplex virus type 1 thymidine kinase (HSV1-TK) is one of the most commonly used reporter genes to visualize gene expression by PET in animals and humans. However, even the most established tracers such as 2'-[<sup>18</sup>F]fluoro-2'-deoxy-1-β-D-arabinofuranosyl-5-iodouracil / 2'-fluoro-2'-deoxy-1-β-D-arabinofuranosyl-5-[<sup>124</sup>I]iodouracil ([<sup>18</sup>F/<sup>124</sup>I]FIAU) and 9-(4-[<sup>18</sup>F]fluoro-3-hydroxymethylbutyl)guanine ([<sup>18</sup>F]FHBG) have some major shortcomings such as unfavorable pharmacokinetics, cytotoxicity and unspecific cell accumulation. In the search for novel tracers, we focus on the development of C-6 substituted pyrimidine nucleoside derivatives labeled with fluorine-18. Recently, our group showed that C-6 substituted pyrimidines are valid candidates for HSV1-TK with high affinity for HSV1-TK and low cytotoxicity. The major advantage of pyrimidines over purines is their higher sensitivity towards wild type HSV1-TK and negligible background activity due to renal clearance. We therefore expect a different and improved pharmacokinetic profile of these new radiotracers, and different cell and tissue transport due to the shift from N-1 substitution to C-6 substitution.

In a previous work, a series of novel C-6 alkylated pyrimidines as HSV1-TK substrates were identified from docking studies. Among them was 6-(3-fluoro-2-(hydroxymethyl)propyl)-5-methylpyrimidine-2,4(1*H*,3*H*)-dione (FHBT). Unfortunately, intramolecular cyclization occurred during its radiosynthesis and thus the target compound, [<sup>18</sup>F]FHBT, could not be synthesized. To prevent intramolecular cyclization, 6-(3-[<sup>18</sup>F]fluoro-2-(hydroxymethyl)propyl)-1,5-dimethylpyrimidin-2,4(1*H*,3*H*)-dione (*N*-Me-[<sup>18</sup>F]FHBT) protected at the N-1 position was proposed. As expected, the radiosynthesis of *N*-Me-[<sup>18</sup>F]FHBT was successfully accomplished without any observable cyclization products. However, the lack of appropriate *in vitro* and *in vivo* assays prevented the pharmacological characterization of *N*-Me-[<sup>18</sup>F]FHBT. Therefore, one goal of this thesis was to establish appropriate *in vitro* and *in vivo* assays which could be used to characterize *N*-Me-[<sup>18</sup>F]FHBT.

A second aim of the thesis was to synthesize the novel radiotracer 6-((1-[<sup>18</sup>F]-fluoro-3-hydroxypropan-2-yloxy)methyl)-5-methylpyrimidine-2,4(1*H*,3*H*)-dione ([<sup>18</sup>F]FHOMP), which was also identified from docking studies (Fig. 6.) and to elucidate its potential as a PET reporter

probe for monitoring HSV1-*tk* gene expression *in vivo*. A further objective was to compare the *in vivo* properties of these C-6 substituted pyrimidine derivatives with [ $^{18}\text{F}$ ]FHBG, the most commonly used reporter probe in an animal model.

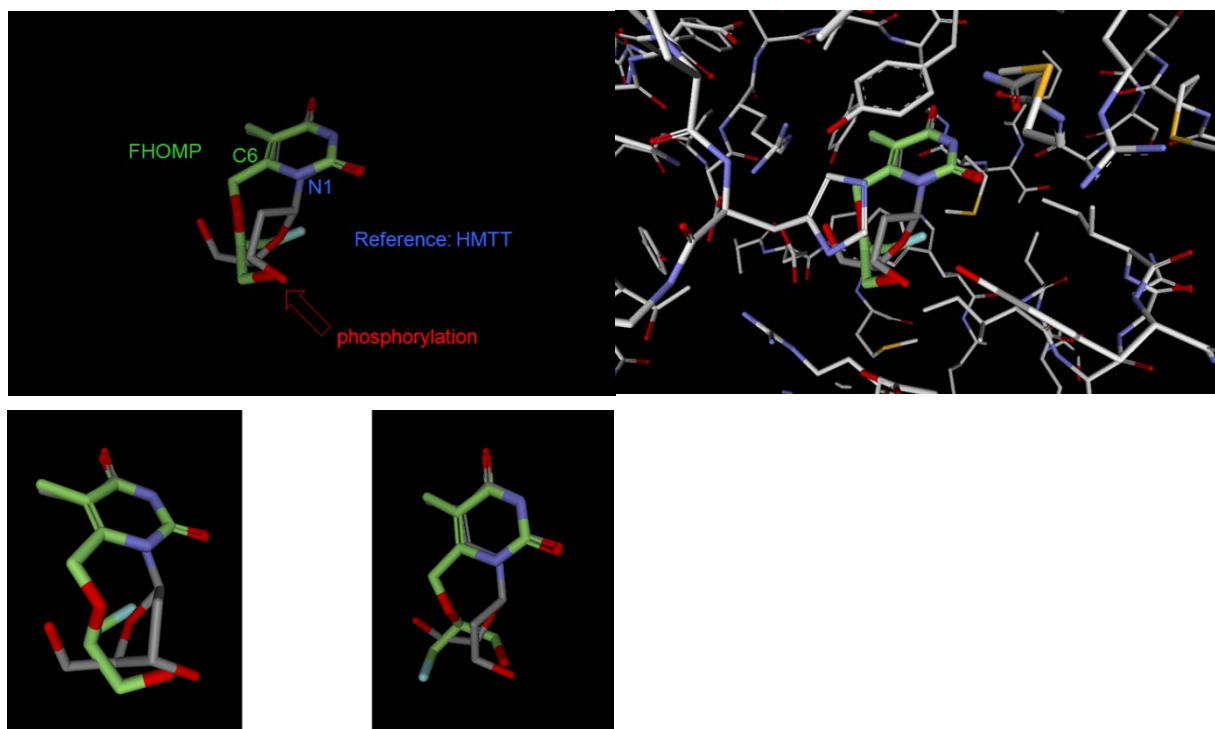


**Figure 6.** Docking of FHOMP in HSV1-TK protein. Top right: looking at the binding site, FHOMP fits well into HSV1-TK in comparison with the reference (*R,R*)-6-(6-hydroxymethyl-5-methyl-2,4-dioxo-hexahydro-pyrimidin-5-ylmethyl)-5-methyl-1H-pyrimidin-2,4-dione (HMTT) [70]. Top left: The pyrimidine ring is at the same position as the reference HMTT and the side chain has enough space and allows for phosphorylation. Bottom: geometric orientation allows phosphorylation of both enantiomers (left: (*R*)-enantiomer; right: (*S*)-enantiomer) of FHOMP





# Synthesis and evaluation of a C-6 alkylated pyrimidine derivative for the *in vivo* imaging of HSV1-TK gene expression

Ursina Müller, Miljen Martić, Tatjana Gazivoda Kraljević, Sjetlana Krištafor, Tobias L. Ross, Charlene Ranadheera, Adrienne Müller, Mariana Born, Stefanie D. Krämer, Silvana Raić-Malić, Simon M. Ametamey

*Nuclear Medicine and Biology*

Author contributions:

Ursina Müller carried out the radiosyntheses, established, organized and carried out *in vitro* and *in vivo* experiments and wrote the paper.

Miljen Martić developed all syntheses.

Tatjana Gazivoda Kraljević and Sjetlana Krištafor performed the upscale of the reference standard and the precursor for radiolabeling.

Charlene Ranadheera and Mariana Born developed the cell line.

Stefanie D. Krämer and Adrienne Müller carried out the *in vivo* studies and evaluated the PET data.





## 2.1 Introduction

The most studied system for the visualization of gene expression *in vivo* uses Herpes Simplex Virus type 1 thymidine kinase (HSV1-TK) as a reporter gene. HSV1-TK has been used in experimental models and clinical trials to evaluate responses to HSV1-TK-mediated suicide gene therapy [71-73], track the migration of HSV1-TK-expressing cells [40, 74, 75], and non-invasively assess the activity of endogenous gene expression [76, 77]. Numerous radiolabeled purine and pyrimidine analogues have been prepared as HSV1-TK substrates and evaluated for their potential to image HSV1-TK expression *in vivo* [21, 78]. PET probes for the visualization of HSV1-TK are designed to be selectively phosphorylated by HSV1-TK in order to achieve metabolic trapping in transfected cells thus providing indirect information about the location, extent and duration of expression of the gene of interest.

Pyrimidine and purine nucleoside analogs differ in their efficacies as substrates for PET imaging of HSV1-TK gene expression. The pyrimidine analog [<sup>124</sup>I]FIAU and the purine analog [<sup>18</sup>F]FHBG (Fig. 1) are typically considered as gold standards in clinical studies for reporter gene imaging with PET [30, 40, 79]. However, [<sup>18</sup>F]FHBG exhibits high abdominal activity due to hepatobiliary elimination [80-82] and, when compared to pyrimidines, [<sup>18</sup>F]FHBG is less sensitive towards the native HSV1-TK [80]. On the other hand, FIAU showed some accumulation in control xenografts in mice due to nonspecific phosphorylation by cellular thymidine kinase 1 and therefore suffers from lower specificity towards HSV1-TK [80]. Recently the pyrimidine substrate [<sup>18</sup>F]FEAU (Fig. 1) has been recognized to be a good candidate for imaging native HSV1-TK gene expression in animals [32, 83]. We reported previously on a number of C-6 alkylated pyrimidine derivatives and showed that these new pyrimidine derivatives have good binding affinities for HSV1-TK and exhibited no cytotoxic effects [45, 84]. Among these series of compounds was DHBT (6-(1,3-dihydroxyisobutyl)thymine) (Fig. 1), which we attempted to develop as a PET tracer for imaging HSV1-TK expression but were unable to radiolabel this compound with fluorine-18 due to intramolecular cyclization. Meanwhile, we reasoned intramolecular cyclization could be circumvented by *N*-methylation of DHBT at the *N*-1 position of the thymine ring. In this manuscript, we report on the synthesis, radiolabeling, *in vitro* and *in vivo* characterization of a fluorinated derivative of DHBT, *N*-Me-

FHBT (6-(3-fluoro-2-(hydroxymethyl)propyl)-1,5-dimethylpyrimidin-2,4-dione), a pyrimidine derivative that bears a methyl substitution at the *N*-1 position of the thymine ring (Fig. 1). Its potential as a PET imaging agent for monitoring HSV1-TK expression was elucidated in TK-positive and control HEK293 (human embryonic kidney) cells and xenografts. The well established PET ligand, [ $^{18}\text{F}$ ]FHBG, was used as a reference in all the biological evaluations.

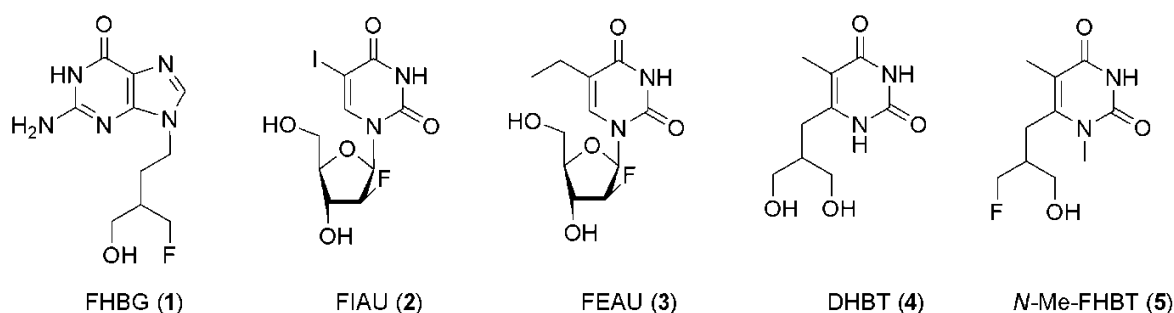


**Figure 1.** Structures of some well established HSV1-TK PET radioligands, DHBT and *N*-Me-FHBT.

## 2.2 Materials and Methods

### 2.2.1 General

Melting points (uncorrected) were determined with Kofler micro hot-stage (Reichert, Wien). Precoated Merck silica gel 60F-254 plates were used for thin layer chromatography and the spots were detected under UV light (254 nm). Column chromatography was performed using silica gel (0.063-0.2 mm) Fluka; glass column was slurry-packed under gravity. Mass spectra were recorded by an *Agilent 6410* instrument equipped with electrospray interface and triple quadrupole analyzer (LC/MS/MS).  $^1\text{H}$  and  $^{13}\text{C}$  NMR spectra were acquired on Bruker 300 MHz NMR spectrometer. All data were recorded in  $\text{DMSO-}d_6$  at 298 K. Chemical shifts were referenced to the residual solvent signal of DMSO at  $\delta$  2.50 ppm for  $^1\text{H}$  and  $\delta$  39.50 ppm for  $^{13}\text{C}$ . Individual resonances were assigned on the basis of their chemical shifts, signal intensities, multiplicity of resonances and H-H coupling constants.

All reagents and solvents were purchased from Sigma-Aldrich Chemie GmbH or VWR International AG. All chemicals were used as supplied unless stated otherwise. The precursor *N*<sup>2</sup>-(*p*-Anisyldiphenylmethyl)-9-[(4-(*p*-toluolsulfonyloxy))-3-(*p*-anisyldiphenylmethoxymethyl)-butyl]guanine (tosyl-FHBG) and the reference compound (9-(4-fluoro-3-[hydroxymethyl]butyl)guanine) were purchased from ABX GmbH, Germany. Production of [ $^{18}\text{F}$ ]fluoride: No-carrier-added aqueous [ $^{18}\text{F}$ ]fluoride ion was produced on an IBA Cyclone 18/9 cyclotron by irradiation of 2.0 mL water target (for a large volume target) or 0.585 mL (for a small volume target), using a 18 MeV proton beam on 98 % enriched [ $^{18}\text{O}$ ]water using the [ $^{18}\text{O}(\text{p},\text{n})^{18}\text{F}$ ] nuclear reaction. [ $^{18}\text{F}$ ]FHBG was prepared as previously reported [85]. Dulbecco's modified Eagle's medium (DMEM+GlutaMAX<sup>TM</sup>-I) with a high glucose concentration (4.5 g/L) and pyruvate, trypsin 0.25 % with EDTA, geneticine (G418) and fetal bovine serum (FBS) were purchased from Gibco.

Analytic radio-high performance liquid chromatography (HPLC) of *N*-Me-[ $^{18}\text{F}$ ]FHBT was performed on an Agilent 1100 series HPLC system equipped with a UV multi-wavelength detector and a Raytest Gabi Star detector using a Gina software. *N*-Me-[ $^{18}\text{F}$ ]FHBT was analyzed on a reversed-phase column, (Gemini C18, 250 x 4.6 mm, particle size: 5  $\mu\text{m}$ , Phenomenex) using a flow rate of 1 mL/min (UV detection at 254 nm) and a gradient as follows: Eluent A was

water, eluent B was acetonitrile and eluent C was methanol. The gradient was from 97 % A and 3 % C to 90 % A, 5 % B and 5 % C at 0-7 min, then to 9 % A, 81 % B and 10 % C from 7-17 min. Semi-preparative radio-HPLC was performed on an HPLC system equipped with a Merck-Hitachi L-6200A intelligent pump, a Knauer variable-wavelength ultraviolet detector and an Eberline radiation monitor. *N*-Me-[<sup>18</sup>F]FHBT was purified on a reversed phase column, (Gemini C18, 250 x 10 mm, particle size: 5 µm, Phenomenex) using a flow rate of 4 mL/min and a gradient as follows: Eluent A was water, eluent B was acetonitrile and eluent C was methanol. The gradient was from 97 % A and 3 % C to 90 % A, 5 % B and 5 % C at 0-12 min, then to 9 % A, 81 % B and 10 % C from 12-25 min.

For the determination of the *in vitro* stability of *N*-Me-[<sup>18</sup>F]FHBT Ultra Performance Liquid Chromatography (UPLC) was performed using a Waters ACQUITY UPLC<sup>®</sup> system equipped with a Berthold FlowStar LB513 radioactivity flow through detector (coincidence detection) and a Waters ACQUITY UPLC<sup>®</sup> BEH 2.1 x 50 mm, 1.7 µm C<sub>18</sub> reversed-phase analytic column. Elution was performed at a flow of 0.5 mL/min and a wavelength of 254 nm with a gradient from 100 % A (water) and 0 % B (acetonitrile) to 90 % A and 10 % B over a 0.6-min period, then a gradient to 10 % A and 90 % B until 2 min followed by a constant flow of 10 % A and 90 % B until 2.5 min, then a gradient to 100 % A and 0 % B to 2.6 min followed by a constant flow of 100 % A until 3 min.

### 2.2.2 Cell lines

HEK293 human embryonic kidney cells (DMSZ, Braunschweig, D) and HEK293 stably transfected with non-mutant *HSV1-tk* (HEK293TK+ cells) (the plasmid containing the *HSV1-tk*, a red fluorescent protein, RFP, and the G418 resistance gene was kindly provided by Prof. Sanjiv Sam Gambhir, Department of Radiology – Nuclear Medicine, University of Stanford, Stanford USA) were cultured in DMEM supplemented with 10 % FBS. Cells were grown in humidified atmosphere with 5 % CO<sub>2</sub> at 37 °C. TK expression in the HEK293TK+ cells was maintained with 0.3 mg/mL G418 in the culture medium and was routinely verified by visualization of the co-transfected RFP with a fluorescence microscope (200x, Zeiss).

### 2.2.3 Animals

Animal studies complied with Swiss and local laws on animal protection and husbandry. After an acclimatization period, subcutaneous xenografts were produced in 6 weeks old female NMRI nude mice (Charles River) by subcutaneous injection in the shoulder region of  $5 \times 10^6$  cells in 100  $\mu$ L phosphate buffered saline, pH 7.4 (PBS) under 2-3 % isoflurane anesthesia. Transfected HEK293TK+ cells were injected on the right side, control HEK293 (HEK293control) cells on the left side. Xenograft growth and body weight were monitored regularly. Experiments were conducted when the xenografts reached a volume between 1 and 2  $\text{cm}^3$ , 4 weeks after subcutaneous inoculation.

### 2.2.4 Syntheses of reference *N*-Me-FHBT(5) and precursor 10

**6-[3-Benzyloxy-2-(benzyloxymethyl)propyl]-4-methoxy-1,5-dimethylpyrimidin-2-one (7).** A mixture of **6** (200 mg, 0.47 mmol) and  $\text{CH}_3\text{I}$  (2.8 mL) was refluxed at 50 °C for 4 days and then evaporated to dryness. The crude product was purified by silica column chromatography ( $\text{CH}_2\text{Cl}_2$  :  $\text{CH}_3\text{OH}$  = 15 : 1) to afford yellow oil **7** (178 mg, 89 %).  $^1\text{H-NMR}$ : ( $\delta$ ) 1.86 (3H, s, H-5), 2.19 (1H, m, H-2'), 2.79 (2H, d,  $J$  = 7.11 Hz, H-1'), 3.36 (3H, s, N- $\text{CH}_3$ ), 3.43 (4H, d,  $J$  = 5.34 Hz, H-3', 3''), 3.78 (3H, s,  $\text{OCH}_3$ ), 4.43 (4H, s, H-4', 4''), 7.24-7.31 (10H, m, Ph) ppm.  $^{13}\text{C-NMR}$ : ( $\delta$ ) 10.87 ( $\text{CH}_3$ -5), 38.73 (N- $\text{CH}_3$ ), 54.19 ( $\text{OCH}_3$ ), 26.71 (C-1'), 26.85 (C-2'), 70.03 (C-3', 3''), 72.68 (C-4', 4''), 101.81 (C-5), 127.84 (CH-Ph), 127.89 (CH-Ph), 128.71 (CH-Ph), 138.71 ( $\text{C}_{\text{quat}}$ -Ph), 156.18 (C-6), 156.54 (C-2), 169.37 (C-4) ppm. MS  $m/z$ : 424.1 ( $M+\text{H}^+$ )

**6-[3-Hydroxy-2-(hydroxymethyl)propyl]-1,5-dimethylpyrimidin-2,4-dione (8).** A mixture of **7** (1.5 g, 3.54 mmol) in dry  $\text{CH}_2\text{Cl}_2$  (40 mL) was cooled to -78 °C and  $\text{BCl}_3$  (1 M in  $\text{CH}_2\text{Cl}_2$ , 14.13 mL, 14.13 mmol) was added under argon atmosphere. The mixture was stirred at -78 °C for 4 h, and then mixture was stirred at -40 °C for 4 h, and then at -20 °C for 14 h. The mixture of  $\text{CH}_2\text{Cl}_2/\text{CH}_3\text{OH}$  (1/1, 100 mL) was added and cooling bath was removed. The solvent was removed under reduced pressure and then purified by column chromatography ( $\text{CH}_2\text{Cl}_2$ :  $\text{CH}_3\text{OH}$  = 10 :1) to give a white powder of **8** (714 mg, 88 %, m.p. = 192-194 °C).  $^1\text{H-NMR}$ : ( $\delta$ ) 1.66 (1H, m, H-2'), 1.72 (3H, s, H-5), 2.52 (2H, d,  $J$  = 6.99 Hz, H-1'), 3.20 (3H, s, N- $\text{CH}_3$ ), 3.29 (4H, AB,  $J_{AB}$  = 5.23, 10.36 Hz, H-3', 3''), 4.52 (2H, t,  $J$  = 4.94 Hz, OH), 11.08 (1H, s, NH) ppm.  $^{13}\text{C-NMR}$ :

( $\delta$ ) 11.60 (CH<sub>3</sub>-5), 28.17 (C-1'), 31.40 (N-CH<sub>3</sub>), 43.31 (C-2'), 61.23 (C-3', 3''), 107.71 (C-5), 151.83 (C-6), 152.31 (C-2), 163.73 (C-4) ppm. MS m/z: 230.1 (*M*+H<sup>+</sup>)

**6-[3-Hydroxy-2-(4-methoxytriphenylmethoxymethyl)propyl]-1,5-dimethylpyrimidin-2,4-**

**dione (9).** A solution of **8** (500 mg, 2.18 mmol) and DMAP (5.0 mg) in DMF (7.5 mL) and Et<sub>3</sub>N (1 mL) was stirred at room temperature for 10 min. Mixture was cooled to 0 °C and MTrCl (1.08 g, 4.34 mmol) was added. The mixture obtained was stirred at room temperature for an additional 2 h, before removing the solvent by evaporation. The crude product was purified by column chromatography (initial eluent CH<sub>2</sub>Cl<sub>2</sub> : CH<sub>3</sub>OH = 50 : 1, then CH<sub>2</sub>Cl<sub>2</sub> : CH<sub>3</sub>OH = 10 : 1) afforded colorless oil of **9** (730 mg, 67 %). <sup>1</sup>H-NMR: ( $\delta$ ) 1.66 (3H, s, H-5), 2.28 (1H, m, H-2'), 2.56 (2H, d, *J* = 6.90 Hz, H-1'), 3.26 (3H, s, N-CH<sub>3</sub>), 3.42 (4H, m, H-3', 3''), 3.74 (3H, s, OCH<sub>3</sub>), 4.73 (1H, t, *J* = 4.73 Hz, OH), 6.88 (2H, d, *J* = 8.88 Hz, Ph 7''-Tr-OCH<sub>3</sub>), 7.18 (2H, d, *J* = 8.85 Hz, Ph 6''-Tr), 7.22-7.32 (10H, m, Ph), 11.17 (1H, s, NH) ppm. <sup>13</sup>C-NMR: ( $\delta$ ) 11.66 (CH<sub>3</sub>-5), 29.07 (C-1'), 31.45 (C-2'), 41.56 (N-CH<sub>3</sub>), 55.50 (OCH<sub>3</sub>), 61.64 (C-3''), 64.26 (C-3'), 86.50 (C<sub>quat</sub>MTr, C-4'), 107.70 (C-5), 113.59 (CHMTr, C-7''), 127.31 (CHMTr, C-8'), 128.29-128.32 (CHMTr, C-6'), 130.31 (CHMTr, C-6''), 130.36 (CHMTr, C-7'), 135.63 (C<sub>quat</sub>MTr, C-5''), 144.90-144.73 (C<sub>quat</sub>MTr, C-5'), 151.73 (C-6), 151.77 (C-2), 158.59 (C<sub>quat</sub>MTr, C-8''), 163.62 (C-4) ppm. MS m/z: 501.1 (*M*+H<sup>+</sup>)

**6-[3-Fluoro-2-(hydroxymethyl)propyl]-1,5-dimethylpyrimidine-2,4-dione (N-Me-FHBT, 5).**

A solution of **9** (330 mg, 0.66 mmol) in dry CH<sub>2</sub>Cl<sub>2</sub> (63 mL) was cooled to -78 °C and stirred for 15 min under argon atmosphere. Diethylaminosulfur trifluoride (0.46 mL) was added dropwise and reaction was kept at -78 °C for additional 15 min after which the cooling bath was removed. After 45 min of stirring at room temperature, a saturated aqueous solution of NaHCO<sub>3</sub> (30 mL) was added and reaction was partitioned. The organic layer was separated, dried over MgSO<sub>4</sub> and evaporated to dryness. The crude product was then dissolved in CH<sub>3</sub>OH (5 mL) and 5 % HCl (5 mL) and refluxed for 15 min. Solvent was evaporated and residue was purified by column chromatography (CH<sub>2</sub>Cl<sub>2</sub> : CH<sub>3</sub>OH = 20 : 1) to afford gray powder of **5** (33 mg, 22 %, m.p. = 159-162 °C). <sup>1</sup>H-NMR: ( $\delta$ ) 1.82 (3H, s, H-5), 2.08 (1H, m, H-2'), 2.67 (2H, m, H-1'), 3.29 (3H, s, N-CH<sub>3</sub>), covered with water (H-3'), 4.37 (1H, t, *J* = 5.46 Hz, Ha-3'), 4.53 (1H, t, *J* = 5.39 Hz, Hb-3'), 4.89 (1H, t, *J* = 5.07 Hz, OH), 11.23 (1H, s, NH) ppm. <sup>13</sup>C-NMR: ( $\delta$ ) 11.00 (CH<sub>3</sub>-5),

26.81 (d,  $J_{C-F} = 4.22$  Hz, C-1'), 30.84 (N-CH<sub>3</sub>), 40.61 (d,  $J_{C-F} = 17.79$  Hz, C-2'), 59.55 (d,  $J_{C-F} = 5.69$  Hz, C-3'), 83.05 (d,  $J_{C-F} = 165.24$  Hz, C-3''), 107.58 (C-5), 150.51 (C-6), 151.28 (C-2), 163.22 (C-4) ppm. MS m/z: 231.1 ( $M+H^+$ )

### 6-([2-(4-Methoxytriphenylmethoxymethyl)-3-tosyl]propyl)-1,5-dimethylpyrimidin-2,4-dione

**(10).** A solution of **9** (50 mg, 0.10 mmol) and tosyl chloride (76 mg, 0.40 mmol) in dry pyridine (2.5 mL) was stirred at room temperature for 3 h. To reaction mixture ethyl acetate (70 mL) was added and extracted with water. Separated organic layer was dried over MgSO<sub>4</sub> and evaporated to dryness. Purification of crude product by silica column chromatography (CH<sub>2</sub>Cl<sub>2</sub> : CH<sub>3</sub>OH = 30 : 1) afforded white crystals of **10** (36 mg, 5 %, m.p. = 130-133 °C). <sup>1</sup>H-NMR: (δ) 1.58 (3H, s, H-5), 2.39 (3H, s, CH<sub>3</sub>-Tos), 2.04 (1H, m, H-2'), 2.96 (2H, m, H-1'), 3.11 (3H, s, N-CH<sub>3</sub>), 3.74 (2H, m, H-3''), 3.79 (3H, s, OCH<sub>3</sub>), 4.09 (2H, d,  $J = 4.83$  Hz, H-3'), 6.85 (2H, d,  $J = 8.82$  Hz, Ph 7''-Tr-OCH<sub>3</sub>), 7.07 (2H, d,  $J = 8.85$  Hz, Ph 6''-Tr), 7.17-7.33 (10H, m, Ph), 7.43 (2H, d,  $J = 8.10$  Hz, Ph 7'-Tos), 7.72 (2H, d,  $J = 8.22$  Hz, Ph 6'-Tos), 11.20 (1H, s, NH) ppm. <sup>13</sup>C-NMR: (δ) 11.64 (CH<sub>3</sub>-5), 21.59 (CH<sub>3</sub>-Tos), 28.25 (C-1'), 31.30 (C-2'), 38.20 (N-CH<sub>3</sub>), 55.51 (OCH<sub>3</sub>), 62.62 (C-3''), 63.52 (C-3'), 86.71 (C<sub>quat</sub>Tr), 108.14 (C-5), 113.29 (CH-7'' OCH<sub>3</sub>-Tr), 125.95-130.64 (CH-Ph), 132.24 (C-5'-Tos), 135.37 (C 5''-Tr), 145.62 (Ph<sub>quat</sub>), 149.96 (C<sub>quat</sub> 8'-Tos), 151.57 (C-6), 151.69 (C-2), 158.66 (C<sub>quat</sub>-8'' TrOCH<sub>3</sub>), 163.55 (C-4) ppm. MS m/z: 655.1 ( $M+H^+$ ).

### 2.2.5 Radiosynthesis of 6-(3-[<sup>18</sup>F]fluoro-2-(hydroxymethyl)propyl)-1,5-dimethylpyrimidin-2,4-dione (N-Me-[<sup>18</sup>F]FHBT, <sup>18</sup>F-5)

To a 10-mL Pyrex brand tube with screw cap containing 10 mg Kryptofix 2.2.2 and 13 μL of 1 M K<sub>2</sub>CO<sub>3</sub> was added 80.1 GBq of <sup>18</sup>F-fluoride. Water was azeotropically evaporated from the mixture using dry CH<sub>3</sub>CN (3 x 0.9 mL) at 90 °C under a stream of nitrogen. After the final drying sequence, 2 mg of **10** dissolved in 250 μL dry CH<sub>3</sub>CN were added to the F-18 residue. Reaction was carried out at 90 °C for 30 min to the <sup>18</sup>F-intermediate **11**. The reaction mixture containing **11** was passed through Sep-Pak Silica cartridge and washed with 3.5 mL of CH<sub>3</sub>CN. The solvent was evaporated at 90 °C under a stream of nitrogen. 300 μL of HCl (5 % in CH<sub>3</sub>OH) was added and reaction was kept for 10 min at 90 °C after which it was allowed to cool to room temperature. Water (2 mL) was added and the mixture was passed through Sep Pak C18 cartridge and washed

with ethanol (2 mL). The mixture was purified on semi-preparative radio-HPLC. Typically, 2 GBq of *N*-Me-[<sup>18</sup>F]FHBT in 4.0 mL was collected after 20 min. The product was resolved in sterile saline for injection after removal of the solvent.

### **2.2.6 *In vitro* phosphorylation of *N*-Me-FHBT**

Phosphorylation of *N*-Me-FHBT, penciclovir (PCV) as a well known substrate for HSV1-TK but not the human TK (hTK) and deoxythymidine (dT; positive control to assess the functionality of both HSV1-TK and the hTK) by HSV1-TK and hTK were monitored with a Merck L-7455 HPLC system based on reverse-phase (RP) chromatography (LiChrospher® 100 RP-C18e (5 µm) column (Merck); 0.2 M NaH<sub>2</sub>PO<sub>4</sub>, 25 mM Bu<sub>4</sub>N<sup>+</sup>HSO<sub>4</sub><sup>-</sup>, 3 % MeOH; flow rate 1.0 mL/min; UV detection at 254 nm) according to a previously published protocol [86]. Reactions were carried out in a final volume of 75 µL containing 50 mM Hepes buffer (pH 7.4), 5 mM ATP, 5 mM MgCl<sub>2</sub>, 1-5 mM Substrate, and 3 µg of HSV1-TK or hTK. The recombinant enzymes, HSV1-TK and hTK, were expressed and purified according to a previously published protocol [87]. The reaction was performed at 37 °C, and quenched after 20 min and 60 min by a ten-fold dilution with 2.5 mM EDTA prior to HPLC injection. The formation of adenosine-diphosphate (ADP) and the phosphorylated product was monitored. A blank reaction (without substrate) was run concurrently to account for substrate-independent ATP hydrolysis.

### **2.2.7 Determination of partition coefficient**

The log  $D_{\text{pH}7.4}$  of *N*-Me-[<sup>18</sup>F]FHBT in 1-octanol/PBS was determined by the shake flask method according to Wilson et al. [88]. 5 µL *N*-Me-[<sup>18</sup>F]FHBT in saline was added to vials containing 0.5 mL each of 1-octanol and PBS. The vials were shaken for 20 min at room temperature and the phases were separated by centrifugation. The radioactivity was measured in 50 µL of each phase with a gamma counter (Wizard, Perkin Elmer). Measurements were performed in triplicates and log  $D_{\text{pH}7.4}$  values were calculated as the logarithmic ratio of the counts in the octanol and saline samples.



### 2.2.8 *In vitro* stability

The stability of *N*-Me-[<sup>18</sup>F]FHBT was assessed by measuring the radiochemical purity (RCP) at different time points after the radiosynthesis. To study the stability in PBS and plasma, 10 MBq *N*-Me-[<sup>18</sup>F]FHBT was incubated in 500  $\mu$ L PBS at room temperature or mouse or human plasma at 37 °C. After 30 min, 60 min, 90 min and 120 min, 100  $\mu$ L samples were withdrawn and proteins were precipitated with 200  $\mu$ L acetonitrile. The supernatants were analyzed with a Waters ACQUITY UPLC<sup>®</sup> system [89].

### 2.2.9 *In vitro* cell uptake in HEK293TK+ and HEK293control cells

HEK293TK+ and HEK293control cells were seeded in 12-well culture plates ( $8 \times 10^5$  cells per well) in DMEM supplemented with 10 % FBS. After 24 h when cultures reached 80 % confluence, cells were incubated for 30 to 240 min with 1 mL medium containing 130 kBq *N*-Me-[<sup>18</sup>F]FHBT or [<sup>18</sup>F]FHBG per well. At the end of the incubation, cells were washed twice with PBS and detached with 0.3 mL 0.25 % trypsin. The cells were resuspended in 0.7 mL culture medium, sedimented and lysed in 0.5 mL lysis buffer (0.0625M Tris, 2 % SDS, 7 % glycerol, pH 6.8). The radioactivity of the cell lysate and the combined incubation medium and washing solutions were measured in a gamma counter (Wizard, Perkin Elmer). Radioactivity of the cell lysates was normalized to total protein determined in 50  $\mu$ L cell lysate with the DC<sup>™</sup> Protein Assay Kit I (Bio Rad, Hercules CA). Data were expressed as percent accumulated activity/ $\mu$ g protein ( $(\text{dpm cells} \times 100 \% / (\text{dpm cells} + \text{dpm medium})) / \mu\text{g protein}$ ) and uptake ratios ( $\text{dpm HEK293TK+} / \text{dpm HEK293control}$ ), respectively [90].

### 2.2.10 Small-animal PET

Xenograft bearing animals (23-29 g) were administered 9-10 MBq *N*-Me-[<sup>18</sup>F]FHBT or 11-15 MBq [<sup>18</sup>F]FHBG in 100  $\mu$ L saline containing  $\leq 5$  % ethanol via tail vein injection. Anesthesia was induced with 2-3 % isoflurane (Abbott) in air-oxygen 5 min prior to PET/CT acquisition. Depth of anesthesia and temperature were controlled as described in [91]. PET/CT scans were performed with a GE VISTA eXplore PET/CT tomograph with an axial field of view of 4.8 cm [92]. Dynamic (one bed position, list mode) ( $n=2$ ) and static (two bed positions, 15 min upper

body followed by 15 min lower body) (n=3) scans were acquired over 90 and 30 min, respectively. Data were reconstructed by 2D ordered-subset expectation maximization (2D OSEM), dynamic scans were reconstructed into 5 min time frames. Region of interest analysis was conducted with the software PMOD 3.2 (PMOD, Switzerland). The xenograft volumes of interest (VOIs) were drawn according to the CT images. Average background activity was estimated from a sphere with a volume of ca 0.5 cm<sup>3</sup> between the two xenografts. VOIs for abdominal average activity were drawn according to the PET images. Standardized uptake values (SUVs) were calculated from the VOI average activities per cm<sup>3</sup> multiplied with the body weight (with 1 g corresponding to 1 cm<sup>3</sup>) and divided by the injected activity dose (all decay corrected).

### **2.2.11 Biodistribution of *N*-Me-[<sup>18</sup>F]FHBT and [<sup>18</sup>F]FHBG**

To perform *ex vivo* biodistribution studies of *N*-Me-[<sup>18</sup>F]FHBT and [<sup>18</sup>F]FHBG, HEK293control and HEK293TK+ xenograft bearing nude mice (23-29 g) were administered 14-21 MBq *N*-Me-[<sup>18</sup>F]FHBT in 100 μL saline (n=4) or 19-26 MBq [<sup>18</sup>F]FHBG in 100 μL saline containing ≤ 5 % ethanol (n=3) via tail-vein injection. Animals were sacrificed and dissected at the indicated time points after injection, organs and tissue samples were weighed and the radioactivity determined in a gamma counter (Wizard, Perkin Elmer). The time points of dissection (90 and 120 min, respectively) were chosen according to dynamic PET scans when activity ratios between HEK293TK+ and control xenografts were highest. Decay corrected radioactivity was expressed in analogy to the SUV as the ratio between the detected activity per gram tissue and the injected dose per gram body weight (SUV<sub>biodis</sub>).

### **2.2.12 *Ex vivo* metabolite studies**

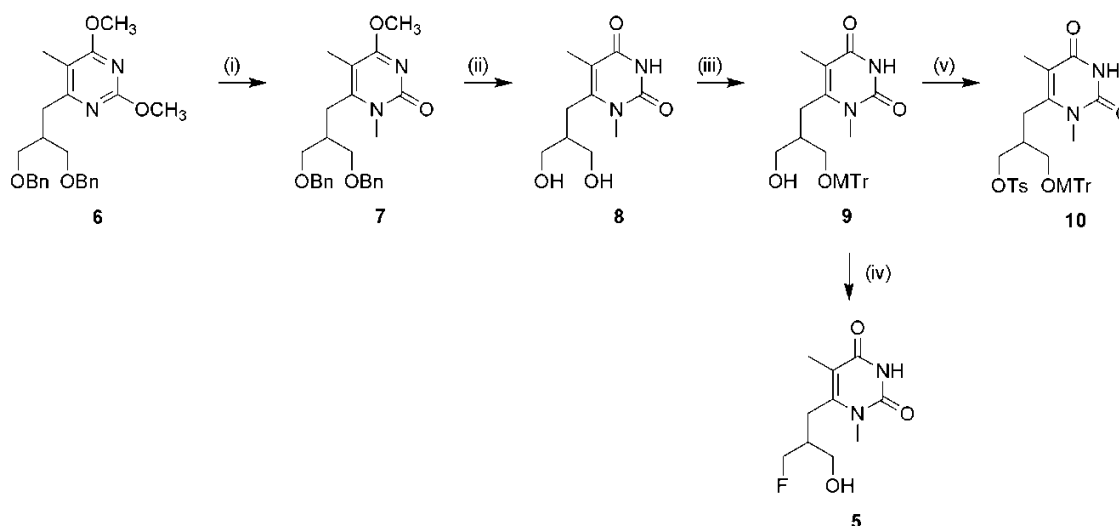
*N*-Me-[<sup>18</sup>F]FHBT (35-41 MBq) in saline was injected into two xenograft bearing mice via a lateral tail vein. Animals were sacrificed by decapitation 30 or 120 min after radiotracer injection. Blood and urine were collected, and xenografts were dissected. Whole blood was separated into plasma and cells by centrifugation (5000 g, 5 min, 4 °C). Xenograft tissue was homogenized in an equal volume of PBS with a PT 1200 C Polytron (Kinematica AG) for about 1 min at speed 4 and centrifuged at 5000 g for 5 min at 4 °C. Proteins in plasma, urine and supernatant of xenograft homogenate were precipitated with an equal volume of acetonitrile and separated by

centrifugation (5000 g, 5 min, 4 °C). The supernatants were passed through a 0.25 µm filter unit and analyzed by radio-UPLC.

## 2.3 Results

### 2.3.1 Syntheses of reference *N*-Me-FHBT (**5**) and precursor **10**

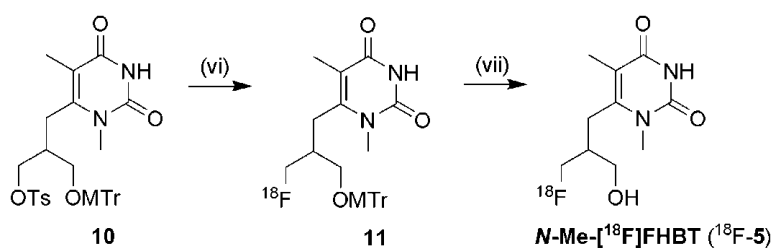
Compound **6** was synthesized as described previously [45] to give a pyrimidine derivative containing 3-benzyloxy-2-(benzyloxymethyl)propyl side chain. To avoid intramolecular cyclization and formation of conformationally constrained carbon-bridged pyrrolido[1,2-*c*]pyrimidines formed by *N*-1 linkage to the acyclic moiety at C-6 position [45], *N*-methylation of **6** was performed with methyl iodide as reagent to give *N*-1 methylated pyrimidine derivative **7** (Scheme 1.). Debenzylation was carried out using boron trichloride to afford *N*-methylpyrimidin-2,4-dione derivative **8** in 88 % chemical yield. Compound **8** was treated with methoxytrityl chloride to afford monotritylated derivative **9** according to the modified procedure [85]. Fluorination of the monotritylated compound **9** with diethylaminosulfur trifluoride (DAST) and subsequent hydrolysis of the trityl group gave target compound **5** in 22 % yield. The tosylate precursor **10** was prepared following a known literature procedure [93].



**Scheme 1.** Reagents and conditions: (i) CH<sub>3</sub>I, 50 °C; (ii) BCl<sub>3</sub>, CH<sub>2</sub>Cl<sub>2</sub>, -78 °C; (iii) MTrCl, DMAP, pyridine, 50 °C; (iv) 1. DAST, CH<sub>2</sub>Cl<sub>2</sub>, -50 °C; 2. CH<sub>3</sub>OH, 5 % HCl; (v) TsCl, pyridine

### 2.3.2 Radiosynthesis of *N*-Me-<sup>18</sup>F]FHBT (<sup>18</sup>F-5)

The strategy for the radiosynthesis of *N*-Me-<sup>18</sup>F]FHBT was based on a commonly employed two step procedure. The first step was nucleophilic substitution on a tosyl leaving group and was accomplished using potassium fluoride and Kryptofix<sup>®</sup> 2.2.2 in acetonitrile at 90 °C (Scheme 2).



**Scheme 2.** Radiosynthesis of *N*-Me-<sup>18</sup>F]FHBT (<sup>18</sup>F-5): (vi) [<sup>18</sup>F]KF-, K2.2.2; CH<sub>3</sub>CN, 90 °C; (vii) 5 % HCl, CH<sub>3</sub>OH, 90 °C

Purification of the <sup>18</sup>F-labeled intermediate **11** was achieved by passing the reaction mixture through a SepPak silica cartridge. The second step was deprotection of methoxytrityl group which was removed by 5 % HCl in methanol during 10 minutes at reflux. <sup>18</sup>F-5 was obtained by passing the reaction mixture first through SepPak C-18 cartridge followed by purification on semi-preparative HPLC. *N*-Me-<sup>18</sup>F]FHBT (<sup>18</sup>F-5) was obtained in maximal 5 % RCY (decay corrected) after semi-preparative radio-HPLC purification and radiochemical purity was > 96 %. Co-injection with the reference compound confirmed the identity of *N*-Me-<sup>18</sup>F]FHBT (Fig. 2).

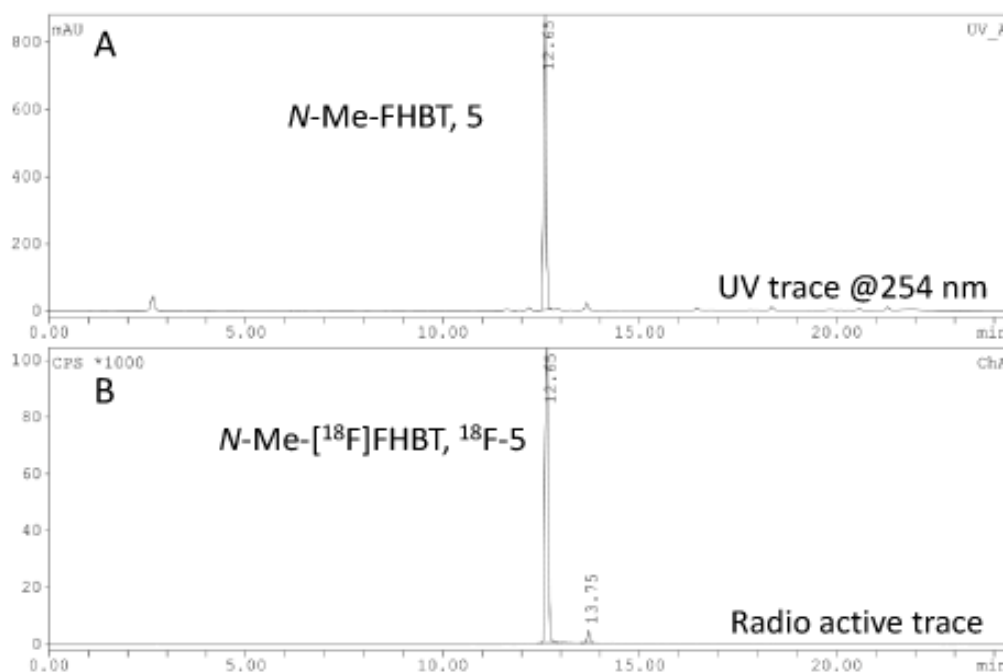


**Figure 2.** HPLC profile of *N*-Me-[<sup>18</sup>F]FHBT (<sup>18</sup>F-5) after semi-preparative HPLC purification. **A:** co-injected non radioactive *N*-Me-FHBT (5). **B:** radioactive trace of *N*-Me-[<sup>18</sup>F]FHBT (<sup>18</sup>F-5).

### 2.3.3 *In vitro* phosphorylation of *N*-Me-FHBT

A qualitative phosphorylation assay was performed *in vitro* to investigate the specificity of the non-radiolabeled *N*-Me-FHBT towards HSV1-TK, compared to human-TK. Incubation of HSV1-TK and hTK, respectively, with the control substrate dT resulted in the formation of ADP and phosphorylated dT (dT-mP), confirming the functionality of both enzymes. Incubation with *N*-Me-FHBT resulted in ADP formation with HSV1-TK but not with hTK. The ADP peak in the incubations with HSV1-TK increased with time. The same behavior was observed with PCV, a well known substrate for HSV1-TK but not hTK. Very small substrate-independent ATP hydrolysis was observed for the blank (no substrate) for both enzymes. The data indicate that *N*-Me-FHBT is indeed a substrate for HSV1-TK, but not for human-TK (Figure S1).

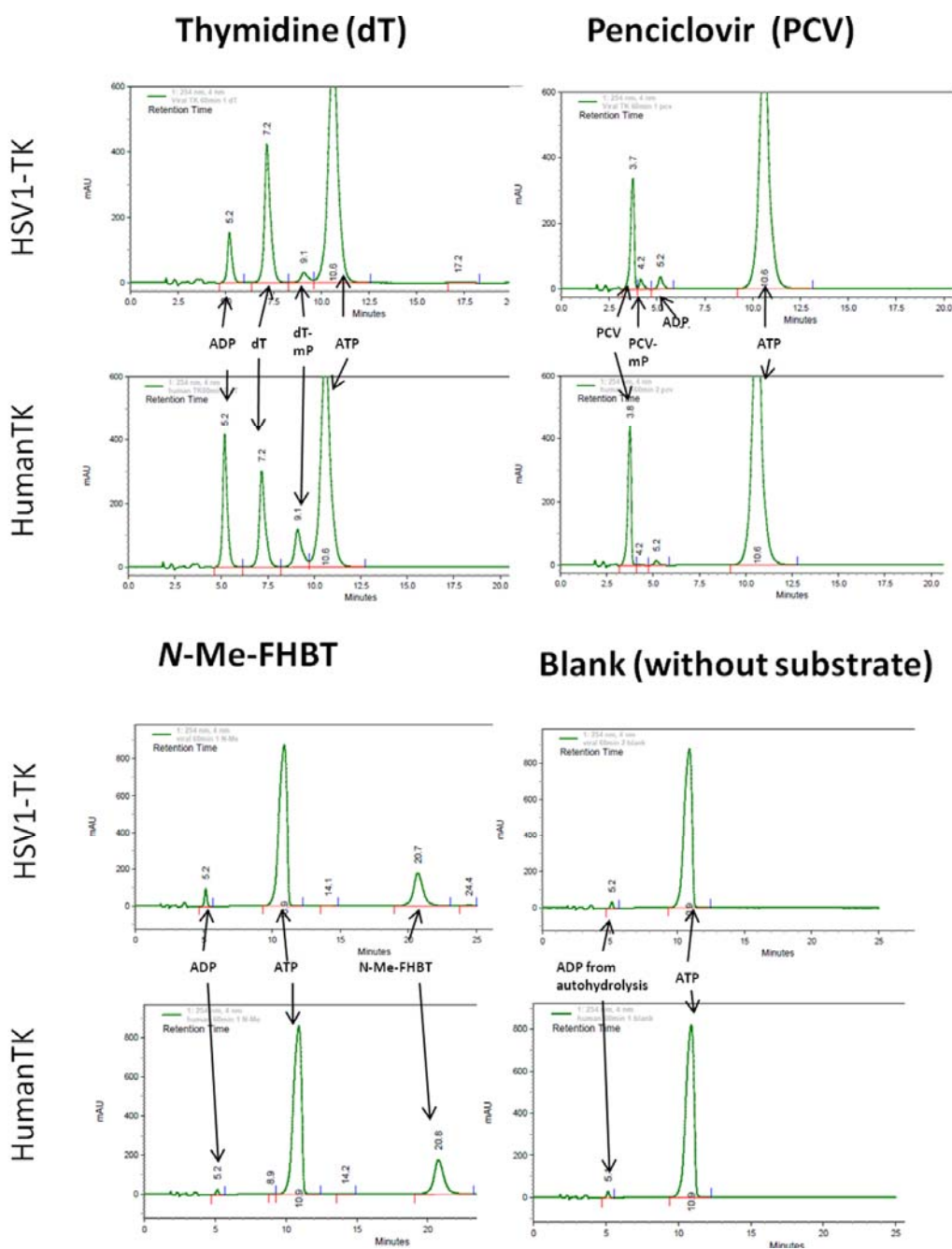


**Figure S1.** Phosphorylation pattern assay at 60 min of incubation: The formation of new peaks (ADP and some monophosphorylated compounds) have been monitored by HPLC coupled with a UV detector at 254 nm. To assess the functionality of the HSV1-TK and the human-TK enzymes, thymidine (dT) was used as a positive control. It showed ADP formation for both enzymes as expected and monophosphorylated thymidine (dT-mP) could be detected. Penciclovir was used to compare with a well known HSV1-TK but not human-TK substrate. Very small substrate-independent ATP hydrolysis was observed for the blank (no substrate) for both enzymes. These chromatograms clearly show the formation of ADP for PCV (and some speculated monophosphorylated penciclovir (PCV-mP)) and *N*-Me-FHBT with HSV1-TK but not the human-TK.

### 2.3.4 *In vitro* cell uptake studies

HEK293 cells transfected with *HSV1-tk* (HEK293TK+) and control HEK293 cells were incubated with *N*-Me-[<sup>18</sup>F]FHBT or [<sup>18</sup>F]FHBG for 30-240 min. The uptake of [<sup>18</sup>F]FHBG was 5.2 to 81.5-fold higher in HSV1-TK containing HEK293TK+ cells than in control cells. The ratios were 14.5 to 70.0-fold for *N*-Me-[<sup>18</sup>F]FHBT (Fig. 3).

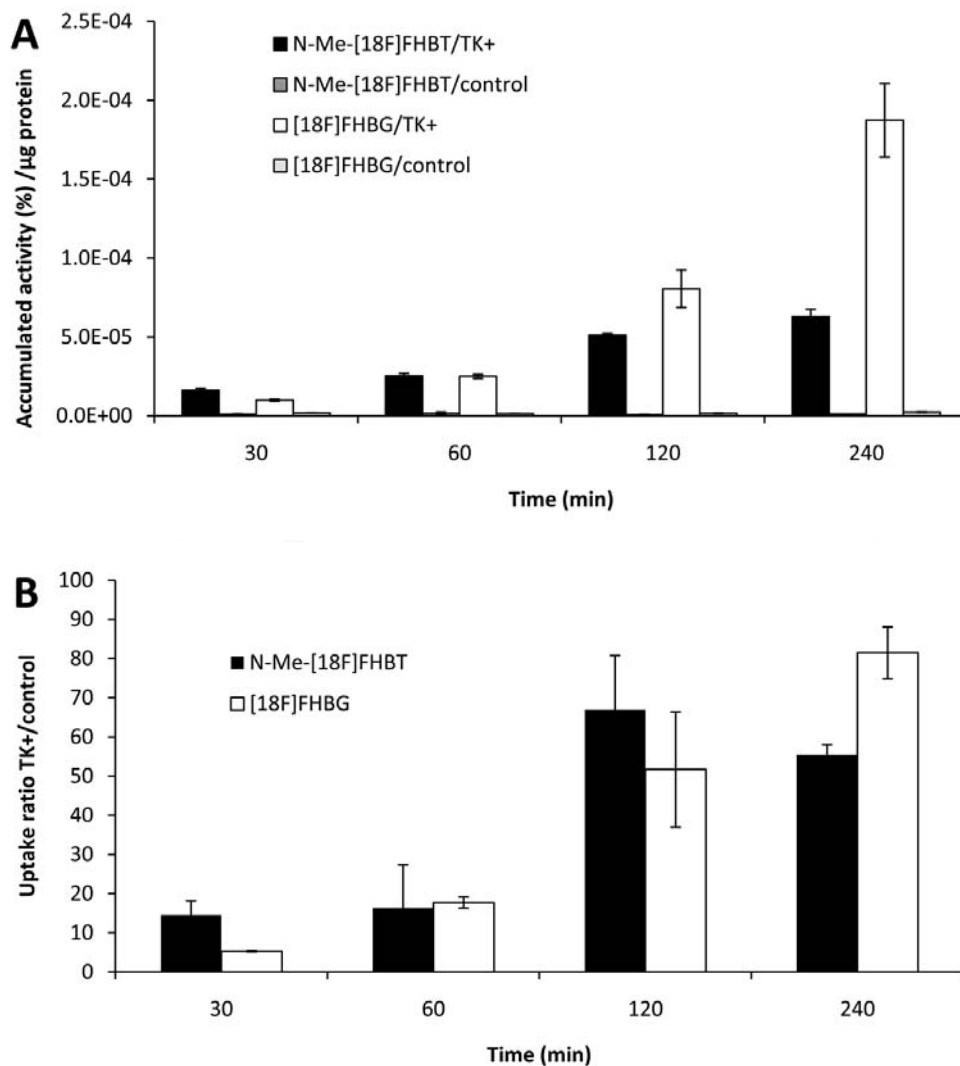


**Figure 3.** Cell uptake studies. Data are expressed as mean±standard deviation of triplicate samples. (A) *N*-Me-[<sup>18</sup>F]FHBT and [<sup>18</sup>F]FHBG net accumulation in HEK293control and HEK293 cells stably expressing the *HSV1-tk* reporter gene as a function of time. (B) Uptake ratio of *N*-Me-[<sup>18</sup>F]FHBT and [<sup>18</sup>F]FHBG in HEK293TK+ cells over HEK293control cells;  $P = 0.04$  at 30 min,  $P > 0.05$  for the other time points (Student *t* test).



### 2.3.5 *In vitro* stability

The stability of *N*-Me-[<sup>18</sup>F]FHBT was tested *in vitro* in PBS at room temperature and in human and mouse plasma at 37 °C. A single radio-peak corresponding to parent *N*-Me-[<sup>18</sup>F]FHBT (retention time 1.2 min) was detected by UPLC. The RCP of *N*-Me-[<sup>18</sup>F]FHBT in PBS, mouse and human plasma was more than 99 % up to 120 min incubation, indicating that the radiotracer is stable in plasma and PBS.

### 2.3.6 Determination of partition coefficient

The lipophilicity of *N*-Me-[<sup>18</sup>F]FHBT was determined by the shake-flask method at physiological pH 7.4. A log  $D_{\text{pH}7.4}$  of  $-0.56 \pm 0.02$  was obtained for *N*-Me-[<sup>18</sup>F]FHBT.

### 2.3.7 Small-animal PET studies with *N*-Me-[<sup>18</sup>F]FHBT and [<sup>18</sup>F]FHBG

Dynamic upper body and static whole body (two beds) PET scans were performed as described in Section 2.3.10. The time frames for the static PET scans, i.e., 60-90 min for *N*-Me-[<sup>18</sup>F]FHBT and 90-120 min for [<sup>18</sup>F]FHBG, were chosen according to the dynamic scans (data not shown) to reach maximal SUV ratios between HEK293TK+ and HEK293control xenografts and between HEK293TK+ xenografts and background (region between the xenografts). Representative PET images of xenograft-bearing mice after *N*-Me-[<sup>18</sup>F]FHBT and [<sup>18</sup>F]FHBG injection, respectively, are shown in Figure 4. Both tracers accumulated in the HEK293TK+ (right shoulder) and to a lesser extent in the HEK293control (left shoulder) xenograft. However, activity in HEK293control xenografts and background activity was lower for [<sup>18</sup>F]FHBG than *N*-Me-[<sup>18</sup>F]FHBT. Both tracers showed high gall bladder and abdominal activity. Table 1 shows the respective SUVs for *N*-Me-[<sup>18</sup>F]FHBT and [<sup>18</sup>F]FHBG. Despite the higher absolute SUV value of *N*-Me-[<sup>18</sup>F]FHBT (60-90 min) than [<sup>18</sup>F]FHBG (90-120 min) in the HEK293TK-positive xenografts, SUV ratios between HEK293TK-positive and HEK293 control xenografts and between TK-positive xenograft and background, were higher for [<sup>18</sup>F]FHBG than for *N*-Me-[<sup>18</sup>F]FHBT due to the higher background activity of *N*-Me-[<sup>18</sup>F]FHBT.

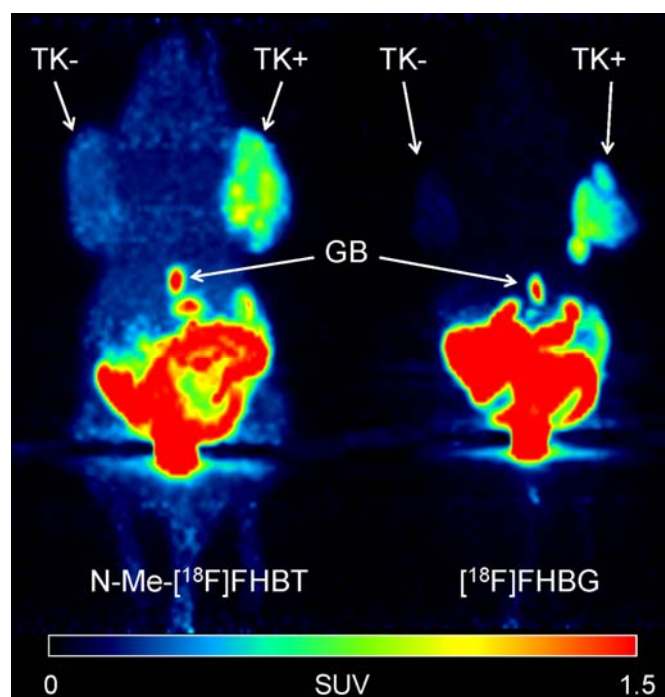


**Figure 4.** *N*-Me- $^{18}\text{F}$ FHBT and  $^{18}\text{F}$ FHBG PET images (maximum-intensity projections) of xenograft-bearing nude mice. Left mouse, *N*-Me- $^{18}\text{F}$ FHBT (10.2 MBq injected), scan time 60-90 min after injection; right mouse:  $^{18}\text{F}$ FHBG (14.8 MBq injected), scan time 90-120 min after injection. Left shoulder, HEK293control xenograft (TK-); right shoulder, HEK293TK+ xenograft (TK+). GB, gall bladder. Anesthesia: 2-3 % isoflurane in air/oxygen.

**Table 1.** Paired comparison of probe accumulation ( $\text{SUV}_{\text{PET}}$ ) in *HSV1-tk* transgenic and control HEK293 xenografts

Measurement <sup>a</sup>	60-90 min	90-120 min
	<i>N</i> -Me- $^{18}\text{F}$ FHBT	$^{18}\text{F}$ FHBG
SUV TK+ xenograft <sup>b</sup>	0.36 ± 0.05	0.26 ± 0.04
SUV control xenograft	0.17 ± 0.01	0.027 ± 0.011
SUV abdomen	0.060 ± 0.023	0.096 ± 0.055
SUV background <sup>b</sup>	0.15 ± 0.01	0.019 ± 0.005
SUV ratio		
TK+/control	2.1 ± 0.2	11.9 ± 7.8
TK+/background	2.4 ± 0.3	14.5 ± 5.0

<sup>a</sup> Data are from 3 animals each. <sup>b</sup>  $P \leq 0.05$  for the ratio of (SUV TK+ xenograft / SUV control xenograft) and for the ratio of (SUV TK+ xenograft / SUV background) for *N*-Me- $^{18}\text{F}$ FHBT and  $^{18}\text{F}$ FHBG (Student *t* test).

### 2.3.8 *Ex vivo* biodistribution of *N*-Me-[<sup>18</sup>F]FHBT and [<sup>18</sup>F]FHBG in xenograft-bearing mice

Biodistribution data for *N*-Me-[<sup>18</sup>F]FHBT and for [<sup>18</sup>F]FHBG in xenograft-bearing mice are shown in Table 2. Both tracers showed significantly higher uptake into the HEK293TK+ than the HEK293control xenografts. The uptake into the HEK293TK+ xenografts was not significantly different for both tracers, however, the ratio between TK+ and control xenograft uptake was lower for *N*-Me-[<sup>18</sup>F]FHBT (1.9±0.3, n=4) than [<sup>18</sup>F]FHBG (16.6±8.8, n=3). In general, background tissue activities were higher for *N*-Me-[<sup>18</sup>F]FHBT than for [<sup>18</sup>F]FHBG. The distribution and elimination patterns were similar for both compounds with high activity in urine, bile and intestine. Radioactivity in bone was low.

**Table 2.** Biodistribution data (SUV<sub>biodis</sub>) of *N*-Me-[<sup>18</sup>F]FHBT and [<sup>18</sup>F]FHBG in xenograft-bearing mice

Tissue	<i>N</i> -Me-[ <sup>18</sup> F]FHBT		[ <sup>18</sup> F]FHBG		
	at 90 min		at 120 min		
Blood	0.14	± 0.04	0.010	±	0.003
Xenograft TK+	0.32	± 0.02	0.35	±	0.07
Xenograft control	0.18	± 0.05	0.024	±	0.006
Spleen	0.13	± 0.04	0.038	±	0.017
Liver	0.16	± 0.05	0.025	±	0.006
Kidney	0.52	± 0.42	0.058	±	0.014
Lung	0.23	± 0.21	0.014	±	0.004
Bone	0.15	± 0.03	0.032	±	0.006
Heart	0.14	± 0.04	0.010	±	0.002
Brain	0.029	± 0.01	0.001	±	0.000
Stomach w. content	0.11	± 0.03	0.026	±	0.025
Intestine w. content	0.94	± 0.19	1.87	±	0.27
Pancreas	0.12	± 0.01	0.019	±	0.007
Muscle	0.14	± 0.05	0.009	±	0.002
Thyroid	0.19	± 0.09	0.022	±	0.005
Gallbladder	4.3	± 3.5	2.1	±	1.4
Urine	38 to 252		6 to 29		

Data are the mean±standard deviation of four animals for *N*-Me-[<sup>18</sup>F]FHBT (ID 14-21 MBq per animal) and three animals for [<sup>18</sup>F]FHBG (ID 19-26 MBq per animal).  $P \leq 0.05$  for the ratio of (xenograft TK+ / xenograft control) and for the ratio of (xenograft TK+ / blood) for *N*-Me-[<sup>18</sup>F]FHBT and [<sup>18</sup>F]FHBG (Student *t* test).

### **2.3.9 *Ex vivo* metabolite studies**

Plasma, urine and xenograft tissues were analyzed for radiometabolites using radio-UPLC. Unaltered parent compound and two major radiometabolites, both with a higher hydrophilicity than the parent compound, were found in urine. The analysis indicated that 86 % of the radioactivity in urine at 30 min and 48 % at 120 min after tracer injection was parent compound. No radioactive peak was detectable in plasma 120 min after injection. In HEK293TK+ xenograft tissue extracts, 76 % of the radioactivity was associated with the parent compound at 30 min postinjection and one new peak, more polar than the parent compound, appeared with the same retention time as the most hydrophilic radiometabolite in urine. At 120 min post-injection, only this polar radiometabolite was detected. For the HEK293control xenograft tissue extracts, only one radioactive peak corresponding to *N*-Me-[<sup>18</sup>F]FHBT was found 30 min post-injection, at 120 min the activity was below detection limit.

## 2.4 Discussion

We successfully synthesized non-radioactive *N*-Me-FHBT using a five-step reaction sequence as shown in Scheme 1. The chemical yields of the various steps ranged from 22 to 89 %. The tosylate precursor was obtained following a known literature procedure [93]. Although a low yield of 5 % was accomplished during the tosylation step, this yield was sufficient for our purposes. All non-radioactive compounds were characterized by  $^1\text{H}$  and  $^{13}\text{C}$ -NMR as well as with mass spectroscopy.

High specificity towards the HSV1-TK enzyme is essential for HSV1-TK gene expression monitoring substrates. To verify whether *N*-Me-FHBT was a substrate for the HSV1-TK, *in vitro* phosphorylation experiments were carried out. The observed phosphorylation of the non-radioactive compound, *N*-Me-FHBT, by HSV1-TK but not by the hTK indicated substrate specificity. The promising *in vitro* specificity of *N*-Me-FHBT for the viral TK and not the human TK encouraged us to perform a further evaluation of the compound. The radiosynthesis of *N*-Me- $^{18}\text{F}$ FHBT was performed using a two-step reaction sequence as shown in Scheme 2. Nucleophilic substitution of the tosyl group in compound **10** with  $^{18}\text{F}$ -fluoride gave the methoxytrityl protected intermediate **11** in ca. 25 % radiochemical yield. Subsequent hydrolysis of the methoxytrityl group afforded the target compound  $^{18}\text{F}$ -**5** in an overall maximal radiochemical yield of 5 % ( $n > 10$ ). The radiochemical yield of  $^{18}\text{F}$ -**5** was not optimized, however, the overall low radiochemical yield of 5 % is explained by the formation of an unidentified radioactive side-product during the hydrolysis step. Optimization strategies including variations in reaction time and temperature could possibly increase the total RCY. *N*-Me- $^{18}\text{F}$ FHBT could be prepared in 120 min with a high radiochemical purity as analyzed by HPLC.

Since *N*-Me- $^{18}\text{F}$ FHBT is a pyrimidine derivative, ideally, it would be more appropriate to compare the *in vitro* and *in vivo* results with a pyrimidine derivative such as  $^{18}\text{F}$ FEAU or  $^{18}\text{F}$ FMAU. We decided to compare the biological data of *N*-Me- $^{18}\text{F}$ FHBT with the purine analog,  $^{18}\text{F}$ FHBG, because it is the best established PET ligand for HSV1-TK imaging and is also considered the “gold standard” in clinical trial studies for reporter gene imaging with PET [6, 11, 12].

We performed *in vitro* cell uptake studies with *N*-Me-[<sup>18</sup>F]FHBT initially since accumulation of the substrate on target site (HSV1-TK expressing cells) is crucial for PET imaging. In this cell uptake study, *N*-Me-[<sup>18</sup>F]FHBT was shown to accumulate in the HEK293 *HSV1-tk* transfected cell line but not in control cells. The uptake ratios of transfected to non-transfected cells were similar for the gold standard, [<sup>18</sup>F]FHBG, and our new compound. At an early time point of 30 min, a faster accumulation of *N*-Me-[<sup>18</sup>F]FHBT was observed compared to [<sup>18</sup>F]FHBG, whereas for later time points no statistically significant differences were observed between both compounds. Cell uptake depends on the cell line and the transfection efficiency. In our study, the uptake ratios of [<sup>18</sup>F]FHBG were in the same range as reported for HT-29 human colon cancer cells (transduced with the retroviral vector G1Tk1SvNa) [94].

*In vitro* stability studies revealed that *N*-Me-[<sup>18</sup>F]FHBT is stable over 120 min in human and mouse plasma, as well as in PBS. These *in vitro* findings suggest that this C-6 substituted pyrimidine is a candidate for imaging HSV1-TK expression. *In vivo* studies, including biodistribution and PET imaging were thus performed to evaluate the disposition of this new pyrimidine compound substituted in C-6 position and methylated in N-1 position in HSV-1 TK xenograft bearing mice. In general, the PET images of *N*-Me-[<sup>18</sup>F]FHBT are consistent with the biodistribution data reflecting the significant uptake of *N*-Me-[<sup>18</sup>F]FHBT into HEK293TK+ xenografts over HEK293 control xenografts. The fact that the biodistribution data did not confirm the higher HEK293TK+ SUV for *N*-Me-[<sup>18</sup>F]FHBT can be assigned to the differences in kinetics of the two tracers. While the SUV of [<sup>18</sup>F]FHBG was relatively constant during the PET scans, the SUV of *N*-Me-[<sup>18</sup>F]FHBT decreased by ca 25 % from the start to the end of PET acquisition. SUVs from the PET scans are averaged over the scan duration while the biodistribution data are from 90 and 120 min after injection, respectively, i.e., time points corresponding to the end time points of the PET acquisitions.

Radioactivity in the background region of interest in PET was not higher than that in the HEK293control xenograft and most tissues showed similar or lower radioactivity levels than the control xenograft in the biodistribution study. This indicates that both tracers are not substrates for endogenous murine TK and thus suitable for preclinical gene therapy studies with *HSV1-tk* as reporter gene.

The appearance of a more polar radiometabolite in the HEK293TK+ xenografts is in line with the hypothesized phosphorylation of *N*-Me-[<sup>18</sup>F]FHBT by HSV1-TK. PET images and *ex vivo*

biodistribution data suggest that *N*-Me-[<sup>18</sup>F]FHBT radioactivity is excreted via urine and bile. Similar elimination pathways were observed in a human dosimetry study of [<sup>18</sup>F]FHBG, where the organs receiving the highest absorbed doses were the urinary bladder, kidneys and gut [82]. The radioactivity accumulation of *N*-Me-[<sup>18</sup>F]FHBT in intestines was lower than that of [<sup>18</sup>F]FHBG and this has the positive effect of reducing the abdominal background for *N*-Me-[<sup>18</sup>F]FHBT, which is one of the main goals for many of the compounds used to image HSV1-TK expression. The advantage of reduced abdominal background due to high renal clearance has also been observed for other pyrimidines such as [<sup>18</sup>F]FFAU [95]. However, the difference may also be related to the different time windows of analysis, i.e. 60 to 90 min for *N*-Me-[<sup>18</sup>F]FHBT and 90 to 120 min for [<sup>18</sup>F]FHBG.

We expect similar pharmacokinetic and elimination behavior of our compound in humans with bladder as the dose limiting organ. *N*-Me-[<sup>18</sup>F]FHBT is quite hydrophilic ( $\log D_{\text{pH}7.4} = -0.56$ ) and specialized transport systems may be required for its transport into cells. The presence or absence of nucleoside transporters in cells depending on the cell type and the recognition of the PET tracer by these transporters may, therefore, have an important impact on the pharmacokinetics. There are multiple carriers for the transport of nucleosides that are either of the facilitated diffusion type or of the concentrative Na<sup>+</sup>/cotransport type which exhibit both broad substrate specificities for pyrimidine and purine nucleosides [96-98]. We speculate *N*-Me-[<sup>18</sup>F]FHBT may be transported via a different transporter system which would result in different levels of radioactivity accumulation in normal tissues and HSV1-TK gene expressing tissues of both PET ligands. This would explain why *N*-Me-[<sup>18</sup>F]FHBT shows a higher background activity in most tissues including blood and HEK293control xenografts than [<sup>18</sup>F]FHBG. An advantage of *N*-Me-[<sup>18</sup>F]FHBT, however, is the negligible low bone uptake as no defluorination was observed unlike [<sup>18</sup>F]FHBG which sometimes shows *in vivo* defluorination [94].

## 2.5 Conclusion

We have successfully prepared *N*-Me-[<sup>18</sup>F]FHBT and showed that this *N*-1 methylated C-6 pyrimidine derivative is a substrate for HSV1-TK, but not for the human TK. *N*-Me-[<sup>18</sup>F]FHBT accumulated to a high extent in HEK293TK+ cells but not significantly in non-transfected cells. *In vitro* data showed high plasma stability. Significant accumulation in HSV1-TK transfected cells was observed *in vivo*. Within the first 60 min after tracer application, SUVs in HEK293TK+ xenografts were higher for *N*-Me-[<sup>18</sup>F]FHBT than [<sup>18</sup>F]FHBG. However, a general higher background resulted in lower SUV ratios of HEK293TK+/HEK293 control compared to [<sup>18</sup>F]FHBG. Lower activity in intestines compared to [<sup>18</sup>F]FHBG may be an advantage of this new compound reducing the impact of the observed activity in the abdominal region. Although *N*-Me-[<sup>18</sup>F]FHBT is not superior to [<sup>18</sup>F]FHBG, we clearly have demonstrated the feasibility of using *N*-Me-[<sup>18</sup>F]FHBT, a C-6 substituted pyrimidine derivative, as a PET probe to monitor HSV1-TK gene expression *in vivo*.

**Acknowledgment.** We thank Dr. Linjing Mu and Cindy Fischer for their support and help during stability studies and Claudia Keller and Petra Wirth for their assistance in the *in vivo* and *ex vivo* experiments. We thank Dr. Svetlana Selivanova for fruitful discussions and sharing radiochemistry knowledge. We thank Dr Jason Holland for reading through the manuscript and his comments. Financial support for this study was provided by the Swiss Science National Foundation (Project Nr. 31003A\_126963) and Ministry of Science of the Republic of Croatia (Project Nr. 125-0982464-2925).







# **Synthesis and preclinical evaluation of a new C-6 alkylated pyrimidine derivative as a PET imaging agent for HSV1-*tk* gene expression**

Ursina Müller, Tobias L. Ross, Charlene Ranadheera, Adrienne Müller, Mariana Born, Evelyn Trauffer, Stefanie D. Krämer, Simon M. Ametamey

*Nuclear Medicine and Biology*

Author contributions:

Ursina Müller carried out the syntheses including development of radiolabeling, organized and performed *in vitro* and *in vivo* experiments and wrote the paper.

Tobias L. Ross established the synthetic strategies and contributed to the radiolabeling.

Charlene Ranadheera developed the cell line together with Mariana Born and contributed to the enzyme production.

Adrienne Müller carried out the western blots and the *in vivo* studies and evaluated the PET data.

Stefanie Krämer carried out *in vivo* studies and evaluated the PET data.

Evelyn Trauffer performed the upscale of the precursor for radiolabeling.



### 3.1 Introduction

Reporter gene imaging with positron emission tomography (PET) is a powerful non-invasive tool to study different biological processes in preclinical settings and currently offers a great potential for translation to clinical use. It allows for monitoring different molecular cellular processes such as transcriptional regulation, protein-protein interactions, cell targeting and cell trafficking of e.g. immune cell, cancer cells or stem cells and targeted drug action [10]. The gene encoding herpes simplex virus type 1 thymidine kinase (HSV1-*tk*) is commonly used as a reporter gene in preclinical studies in combination with small animal PET. Uptake into cells of a PET reporter probe followed by selective phosphorylation by HSV1-TK leads to metabolic trapping of the radiotracer in HSV1-TK expressing cells, thus providing indirect information about the location, extent and duration of expression of the gene of interest. Several nucleoside analogs that are selectively phosphorylated by HSV1-TK have been synthesized [21, 78].

Nucleosides are transported into the cells mainly via two types of transporters, the concentrative (CNT, SLC28) and equilibrative (ENT, SLC29) nucleoside transporters. Besides providing uptake into the cells of interest, these transporters can have an impact on the general biodistribution of nucleoside PET probes as recently shown for the mammalian thymidine kinase-1 (TK1) substrate 3'-deoxy-3'-[<sup>18</sup>F]fluorothymidine [<sup>18</sup>F]FLT and ENT1 [99].

HSV1-TK phosphorylates a broad range of nucleoside analogs, and its expression can be imaged with several substrates including pyrimidine derivatives 5-[<sup>124/131</sup>I]-2'-deoxy-2'-fluoro-1-β-D-arabino-uracil ([<sup>124/131</sup>I]FIAU), 2'-deoxy-2'-[<sup>18</sup>F]-fluoro-5-ethyl-1-β-D-arabinofuranosyl-uracil ([<sup>18</sup>F]FEAU), or acycloguanosine derivatives, such as 9-(4-[<sup>18</sup>F]-fluoro-3-[hydroxymethyl]butyl)guanine ([<sup>18</sup>F]FHBG) (Fig. 1) [30, 32, 40, 79, 83]. The high selectivity for viral over mammalian TK is a prerequisite for a good probe for HSV1-TK. FIAU is an example with suboptimal selectivity for HSV1-TK as it showed some accumulation in xenografts devoid of viral TK due to the phosphorylation by cellular TK1 [80]. FHBG on the other hand, exhibits high abdominal radioactivity concentrations due to hepatobiliary elimination. This makes tracking of the reporter gene close to the abdomen impossible. In addition, when compared to pyrimidines, FHBG is less sensitive towards the native HSV1-TK [80-82]. The development of a

radiotracer with optimal distribution between HSV1-TK expressing cells and normal tissues remains an ambitious goal for reporter gene imaging.

In the search for improved PET radiotracers for HSV1-*tk* gene expression monitoring we reported previously on a number of C-6 alkylated pyrimidine derivatives and showed that these new pyrimidine derivatives have high binding affinities for HSV1-TK and exhibit no cytotoxic effects [45, 84]. In this work, we report on the development and evaluation of 6-((1-fluoro-3-hydroxypropan-2-yloxy)methyl)-5-methylpyrimidine-2,4(1*H*,3*H*)-dione (FHOMP), a pyrimidine nucleoside substituted on the C-6 position with a side chain in analogy to the antiviral drug ganciclovir and the HSV1-TK PET tracer 9-((3-[<sup>18</sup>F]fluoro-1-hydroxy-2-propoxy)-methyl)guanine [<sup>18</sup>F]FHPG (Fig. 1). We describe the synthesis of the reference standard and precursor, as well as the radiosynthesis of [<sup>18</sup>F]FHOMP in a two-step reaction sequence. The latter was achieved by N-1 protection of the precursor preventing intramolecular cyclization between N-1 and the acyclic moiety at C-6 during the radiosynthesis. We further report on the *in vitro* and *in vivo* evaluation of [<sup>18</sup>F]FHOMP with HSV1-TK positive and control HEK293 (human embryonic kidney) cells and xenografts. The well-established radiotracer [<sup>18</sup>F]FHBG was used as reference for the biological evaluation. Furthermore, we investigated the effect of ENT1 inhibition on the biodistribution of [<sup>18</sup>F]FHOMP. The transporter is expressed in many human, rat and mouse tissues [54, 56, 100, 101] and may, therefore, influence the distribution of [<sup>18</sup>F]FHOMP.

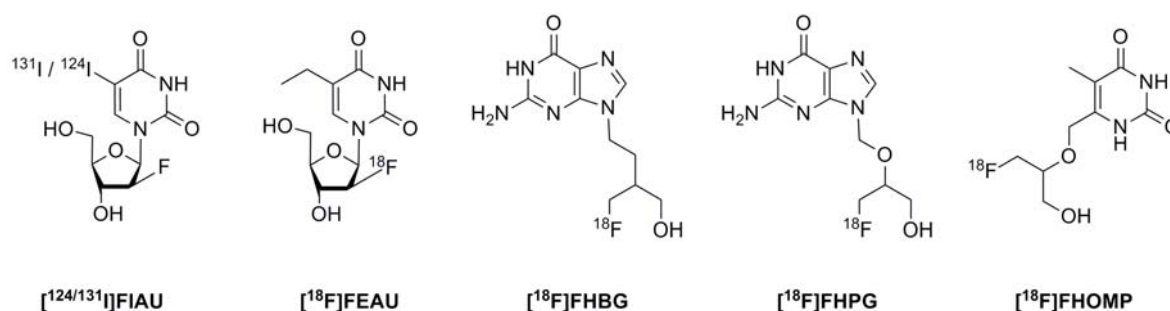


**Figure 1.** Chemical structures of 5-[<sup>124/131</sup>I]-2'-deoxy-2'-fluoro-1-β-D-arabino-uracil ([<sup>124/131</sup>I]FIAU), 2'-deoxy-2'-[<sup>18</sup>F]-fluoro-5-ethyl-1-β-D-arabinofuranosyl-uracil ([<sup>18</sup>F]FEAU), 9-(4-[<sup>18</sup>F]-fluoro-3-(hydroxymethyl)butyl)guanine ([<sup>18</sup>F]FHBG), 9-((3-[<sup>18</sup>F]fluoro-1-hydroxy-2-propoxy)-methyl)guanine ([<sup>18</sup>F]FHPG) and 6-((1-[<sup>18</sup>F]-fluoro-3-hydroxypropan-2-yloxy)methyl)-5-methylpyrimidine-2,4(1*H*,3*H*)-dione ([<sup>18</sup>F]FHOMP).

## 3.2 Materials and Methods

### 3.2.1 General

All reagents and solvents were purchased from Sigma-Aldrich Chemie GmbH or VWR International AG. All chemicals were used as supplied unless stated otherwise. Dulbecco's modified Eagle's medium (DMEM+GlutaMAX-I) with a high glucose concentration (4.5 g/L) and pyruvate, trypsin 0.25% with EDTA, geneticine (G418) and fetal bovine serum (FBS) were purchased from Gibco. The precursor *N*<sup>2</sup>-(*p*-Anisyldiphenylmethyl)-9-[(4-(*p*-toluolsulfonyloxy))-3-(*p*-anisyldiphenylmethoxymethyl)butyl]guanine (tosyl-FHBG) and the reference compound (9-(4-fluoro-3-[hydroxymethyl]butyl)guanine) were purchased from ABX GmbH, Germany. No-carrier-added aqueous [<sup>18</sup>F]fluoride ion was produced on an IBA Cyclone 18/9 cyclotron by irradiation of 2.0 mL water target (for a large volume target) or 0.585 mL (for a small volume target), using a 18 MeV proton beam on 98% enriched [<sup>18</sup>O]water using the <sup>18</sup>O(p,n)<sup>18</sup>F nuclear reaction. No-carrier added <sup>18</sup>F-fluoride (~28-86 GBq) was trapped on an anion exchange cartridge (Sep-Pak Light Accell Plus QMA; Waters AG), preconditioned with 5 mL of aqueous 0.5 M potassium carbonate solution and 5 mL of water. [<sup>18</sup>F]FHBG was prepared as previously reported [85].

### 3.2.2 Cell line and transfection

HEK293 human embryonic kidney cells were obtained from DMSZ (Braunschweig, Germany). Cells were stably transfected with a plasmid encoding the wild-type HSV1-*tk* gene (HEK293TK+ cells). In addition to the HSV1-*tk* gene, the plasmid contained a red fluorescent protein (*RFP*) gene, and G418 resistance gene. The plasmid was kindly provided by Prof. Sanjiv Sam Gambhir, Department of Radiology – Nuclear Medicine, Stanford University, Palo Alto CA, USA. Plasmid DNA was linearized by digestion using the restriction enzyme BgIII (10 u/μL, Promega) at 37 °C overnight and was subsequently purified using the QIAquick Purification Kit (Qiagen) as recommended by the manufacturer. The linearized DNA was transfected into 60-80% confluent HEK293 cells using Lipofectamine 2000 (Invitrogen) as recommended by the manufacturer. The transfection medium was removed after 24 hours and replaced with DMEM+GlutaMAX-I medium supplemented with 10% FBS and G418 (300 μg/mL) to select for the HSV-*tk* transgenic

cells. Cells were detached with trypsin/EDTA (Invitrogen) and stocks were frozen in liquid nitrogen. Resuscitated cells were used for a maximum of 10 passages. HSV1-TK expression was verified indirectly by visualizing the RFP by flow cytometry on a FACSCalibur (BD Biosciences) immediately after transfection and by fluorescent microscopy after freezing and resuscitation of the cells. In flow cytometry, 71% of transfected cultures were positive for the transgene. In fluorescence microscopy, resuscitated HEK293TK+ cells showed a strong signal at the respective wavelength which was absent in the parent cells (data not shown).

### **3.2.3 Immunoblot analysis**

The HSV1-TK expression in resuscitated HEK293TK+ and HEK293 cells and xenograft tissues was tested by immunoblot analysis. Proteins from cell cultures or xenograft lysates were separated by 10% SDS-polyacrylamide gel electrophoresis according to standard protocols (Bio-Rad) at 100 V for 90 min and transferred onto a PVDF blotting membrane at 60 mA for 90 min. The blots were blocked in 5% dried milk in Tris-buffered saline-Tween-20 (TBS-T) and processed for immunostaining with an anti-HSV1-TK polyclonal antibody (1:500, Santa Cruz Biotechnology) over night at 4 °C. After washing with TBS-T, the membranes were incubated with rabbit anti-goat IgG Peroxidase Conjugate (Sigma-Aldrich) for 1 h at room temperature. The antigen-antibody complexes were detected by enhanced chemoluminescence (ECL, Amersham, Buckinghamshire, UK).

### **3.2.4 Animals**

Animal studies were approved by the Veterinary Office of Canton Zurich and complied with Swiss laws and guidelines on animal protection and husbandry. Subcutaneous xenografts were produced in 7 weeks old female NMRI nude mice (Charles River, Sulzfeld, Germany) by subcutaneous injection in the shoulder region of  $5 \times 10^6$  cells in 100  $\mu$ L PBS, pH 7.4, under 2-3% isoflurane (Abbott) anesthesia. Transgenic HEK293TK+ cells were injected on the left side, control HEK293 (HEK293 control) cells on the right side. Xenograft growth and body weight were monitored regularly. Experiments were conducted when the xenografts reached a volume between 1 and 2  $\text{cm}^3$ , 3-4 weeks after subcutaneous inoculation.



### 3.2.5 Analytic and chromatographic methods

Pre-coated Merck silica gel 60F-254 plates were used for thin layer chromatography and the spots were detected under UV light (254 nm). Column chromatography was performed using silica gel (0.040-0.063 mm) Fluka; glass column was slurry-packed under gravity. The  $^1\text{H}$ ,  $^{13}\text{C}$  and  $^{19}\text{F}$  NMR spectra were recorded at 23 °C on a Bruker Avance 400 ( $^1\text{H}$ , 400 MHz;  $^{13}\text{C}$ , 100 MHz;  $^{19}\text{F}$ , 376 MHz) spectrometer using  $\text{CDCl}_3$  or  $\text{DMSO-d}_6$  as the solvent. Chemical shifts (ppm) were determined relative to internal  $\text{CHCl}_3$  ( $^1\text{H}$ ,  $\delta$  7.24;  $\text{CDCl}_3$ ), internal  $\text{CDCl}_3$  ( $^{13}\text{C}$ ,  $\delta$  77.0,  $\text{CDCl}_3$ ), internal  $\text{DMSO-d}_5$  ( $^1\text{H}$ ,  $\delta$  2.49;  $\text{DMSO-d}_6$ ), or internal  $\text{DMSO-d}_6$  ( $^{13}\text{C}$ ,  $\delta$  39.5,  $\text{DMSO-d}_6$ ). For  $^{19}\text{F}$  NMR measurements,  $\text{CFCl}_3$  was used as the internal standard. Values of the coupling constant,  $J$ , are given in hertz (Hz). Low-resolution mass spectra (LRMS) were recorded with a Micromass Quattro micro API LC-ESI. High resolution mass spectra (HRMS) were recorded with a Bruker FTMS 4.7T BioAPEXII (ESI).

Analytic radio-high performance liquid chromatography (HPLC) of [ $^{18}\text{F}$ ]FHOMP was performed on an Agilent 1100 series HPLC system equipped with a UV multi-wavelength detector and a Raytest Gabi Star detector using a Gina software. [ $^{18}\text{F}$ ]FHOMP was analyzed on a reversed-phase column, (Gemini C18, 250 x 4.6 mm, particle size: 5  $\mu\text{m}$ , Phenomenex) using a flow rate of 1 mL/min (UV detection at 267 nm) and a gradient as follows: Eluent A was water, eluent B was acetonitrile. The gradient was from 100% A to 90% A and 10% B at 0-15 min, then isocratic at 90% A from 15-20 min, then to 100% A from 20-21 min followed by 100% A isocratic from 21-25 min.

Semi-preparative radio-HPLC was performed on an HPLC system equipped with a Merck-Hitachi L-6200A intelligent pump, a Knauer variable-wavelength ultraviolet detector and an Eberline radiation monitor. [ $^{18}\text{F}$ ]FHOMP was purified on a reversed phase column, (Gemini C18, 250 x 10 mm, particle size: 5  $\mu\text{m}$ , Phenomenex) using a flow rate of 4 mL/min and a gradient as follows: Eluent A was water, eluent B was ethanol. After 10 min isocratic 100% A the gradient was from 100% A to 90% A and 10% B at 10-30 min.

For the determination of the microsomal stability of [ $^{18}\text{F}$ ]FHOMP Ultra Performance Liquid Chromatography (UPLC) was performed using a Waters ACQUITY UPLC<sup>®</sup> system equipped with a Berthold FlowStar LB513 radioactivity flow through detector (coincidence detection) and a Waters ACQUITY UPLC<sup>®</sup> BEH 2.1 x 50 mm, 1.7  $\mu\text{m}$  C<sub>18</sub> reversed-phase analytic column. Elution was performed at a flow of 0.6 mL/min and a wavelength of 267 nm with a gradient from

100% A (sodium phosphate buffer, pH 7.0) and 0 % B (acetonitrile) to 90% A and 10% B over a 1.5-min period, then a gradient to 30% A and 70% B until 2 min followed by a constant flow of 30% A and 70% B until 3.0 min, then a gradient to 100% A and 0% B to 3.1 min followed by a constant flow of 100% A until 3.2 min.

### 3.2.6 Synthesis of reference FHOMP (6)

**6-(Chloromethyl)-5-methylpyrimidine-2,4(1*H*,3*H*)-dione (1).** Compound **1** was synthesized according to published protocols starting from 5,6-dimethylpyrimidine-2,4(1*H*,3*H*)-dione [102]. <sup>1</sup>H NMR (400 MHz, DMSO-*d*<sub>6</sub>): δ 1.82 (s, 3H, CH<sub>3</sub>), 4.43 (s, 2H, CH<sub>2</sub>), 10.87 (s, 1H, N1*H*), 11.16 (s, 1H, N3*H*) ppm. <sup>13</sup>C NMR (100 MHz, DMSO-*d*<sub>6</sub>): δ 9.1, 39.4, 107.4, 145.3, 150.6, 164.8 ppm. LRMS (ESI+) *m/z* 174.71 (*M*+H)<sup>+</sup>.

**2-(Benzyloxymethyl)oxirane (3).** Compound **3** was prepared by benzylation of (±)-glycidol (**2**) by following published methods [103]. <sup>1</sup>H NMR (400 MHz, CDCl<sub>3</sub>): δ 2.62 (dd, 1H, *J* = 5.0, 2.7 Hz, CH-CH<sub>2</sub>-O), 2.80 (dd, 1H, *J* = 4.9, 4.1 Hz, CH-CH<sub>2</sub>-O), 3.19 (m, 1H, CH), 3.45 (dd, 1H, *J* = 11.5, 5.7 Hz, O-CH<sub>2</sub>), 3.72 (dd, 1H, *J* = 14.1, 7.1 Hz, O-CH<sub>2</sub>), 4.60 (dd, 2H, *J* = 23.2, 11.9 Hz, Ph-CH<sub>2</sub>-O), 7.26-7.38 (m, 5H, Ph) ppm. HRMS (ESI+) *m/z* found 164.0830, calcd 164.0837 for C<sub>10</sub>H<sub>12</sub>O<sub>2</sub>.

**1-(Benzyloxy)-3-fluoropropan-2-ol (4).** Epoxide **3** was selectively opened via fluorination using TBABF-KHF<sub>2</sub> according to published methods [104]. <sup>1</sup>H NMR (400 MHz, CDCl<sub>3</sub>): δ 2.54 (bs, 1H, OH), 3.58 (m, 2H, O-CH<sub>2</sub>-CH), 4.05 (m, 1H, O-CH<sub>2</sub>-CH), 4.46 (ddd, 1H, *J*<sub>H,F</sub> = 47.5 Hz, *J*<sub>H,H</sub> = 18.3, 9.7 Hz, F-CH<sub>2</sub>), 4.48 (ddd, 1H, *J*<sub>H,F</sub> = 47.5 Hz, *J*<sub>H,H</sub> = 18.3, 9.7 Hz, F-CH<sub>2</sub>), 4.57 (s, 2H, Ph-CH<sub>2</sub>-O), 7.29-7.39 (m, 5H, Ph) ppm. <sup>13</sup>C NMR (100 MHz, CDCl<sub>3</sub>): δ 69.3 (d, *J*<sub>C,F</sub> = 20.5 Hz), 70.0 (d, *J*<sub>C,F</sub> = 6.8), 73.5, 83.9 (d, *J*<sub>C,F</sub> = 169.9 Hz), 127.8, 127.9, 128.5, 137.6 ppm. <sup>19</sup>F NMR (376 MHz, CDCl<sub>3</sub>): δ -232.1 (dt, 1F) ppm. HRMS (ESI+) *m/z* found 184.0893, calcd 184.0899 for C<sub>10</sub>H<sub>13</sub>FO<sub>2</sub>.

**6-((1-(Benzyloxy)-3-fluoropropan-2-yloxy)methyl)-5-methylpyrimidine-2,4(1*H*,3*H*)-dione (5).** NaH (60% in mineral oil, 39 mg, 1.629 mmol) was added to a solution of **4** (100 mg, 0.586 mmol) in THF (17 mL) at 0 °C. The mixture was stirred for 30 min at room temperature.

Compound **1** (55.4 mg, 0.317 mmol) was added at 0 °C and the reaction was stirred for 5 min at 0 °C. After allowing to reach room temperature, the mixture was heated to reflux for 16 h. The reaction was cooled to room temperature, quenched with ice and water, diluted with ethylacetate and washed with water and brine. The organic phase was dried over MgSO<sub>4</sub> and concentrated. The residue was purified by column chromatography on silica gel (CH<sub>2</sub>Cl<sub>2</sub> : CH<sub>3</sub>OH = 30 : 1) to afford **5** (46.6 mg, 46%). <sup>1</sup>H NMR (400 MHz, DMSO-d<sub>6</sub>): δ 1.75 (s, 3H, CH<sub>3</sub>), 3.57 (dd, 2H, *J* = 5.5, 1.0 Hz, BnO-CH<sub>2</sub>), 3.83 (m, 1H, CH), 4.41 (s, 2H, C6-CH<sub>2</sub>), 4.52 (s, 2H, Ph-CH<sub>2</sub>), 4.55 (m, 2H, CH<sub>2</sub>-F), 7.32 (m, 5H, Ph), 10.46 (s, 1H, N1H), 11.07 (s, 1H, N3H) ppm. <sup>13</sup>C NMR (100 MHz, DMSO-d<sub>6</sub>): δ 9.0, 65.2, 68.1 (d, *J*<sub>C,F</sub> = 8.5 Hz), 72.4, 77.2 (d, *J*<sub>C,F</sub> = 18.5 Hz), 82.7 (d, *J*<sub>C,F</sub> = 167.4 Hz), 106.0, 127.5, 128.3, 138.0, 145.9, 150.7, 164.9 ppm. <sup>19</sup>F NMR (376 MHz, DMSO-d<sub>6</sub>): δ -230.1 (dt, 1F) ppm. LRMS (ESI+) *m/z* 322.68 (*M*+H)<sup>+</sup>.

**6-((1-Fluoro-3-hydroxypropan-2-yloxy)methyl)-5-methylpyrimidine-2,4(1H,3H)-dione (6).**

Palladium on activated carbon 10% (15 mg, 0.014 mmol Pd) was added to a 10 mL-reacti-vial containing **5** (46.6 mg, 0.145 mmol). Methanol (1 mL) was added and the system was flushed with argon. H<sub>2</sub> gas was bubbled into the system using a balloon. Having the system saturated with H<sub>2</sub>, the balloon was removed and the closed system was heated to 80 °C for 20 h. After cooling to room temperature and filtration through celite (CH<sub>3</sub>OH) the crude was purified by column chromatography on silica gel (CH<sub>2</sub>Cl<sub>2</sub> : CH<sub>3</sub>OH = 20 : 1) to obtain **6** (17 mg, 50%). <sup>1</sup>H NMR (400 MHz, DMSO-d<sub>6</sub>): δ 1.74 (s, 3H, CH<sub>3</sub>), 3.51 (t, 2H, *J* = 10.4 Hz, CH<sub>2</sub>-OH), 3.63 (m, 1H, CH), 4.41 (s, 2H, C6-CH<sub>2</sub>), 4.47 (m, 2H, CH<sub>2</sub>-F), 5.02 (t, 1H, *J* = 11.3 Hz, OH), 10.40 (s, 1H, N1H), 11.04 (s, 1H, N3H) ppm. <sup>13</sup>C NMR (100 MHz, DMSO-d<sub>6</sub>): δ 8.8, 59.4 (d, *J*<sub>C,F</sub> = 6.7 Hz), 64.9, 79.2 (d, *J*<sub>C,F</sub> = 14.2 Hz), 82.1 (d, *J*<sub>C,F</sub> = 133.1 Hz), 105.2, 146.2, 150.6, 164.8 ppm. <sup>19</sup>F NMR (376 MHz, DMSO-d<sub>6</sub>): δ -230.4 (1F) ppm. HRMS (ESI+) *m/z* found 233.0932, calcd 233.0932 for C<sub>9</sub>H<sub>14</sub>FN<sub>2</sub>O<sub>4</sub>.

### 3.2.7 Synthesis of precursor 12

**6-((1,3-Bis(benzyloxy)propan-2-yloxy)methyl)-5-methylpyrimidine-2,4(1H,3H)-dione (8).**

NaH (60% in mineral oil, 124.5 mg, 3.11 mmol) was added to a solution of 1,3-bis(benzyloxy)propan-2-ol (**7**) (213 μL, 0.86 mmol) in THF (10 mL) at 0 °C. The mixture was stirred for 60 min at room temperature. A solution of **1** (147.1 mg, 0.84 mmol) in THF (5 mL)

was added at 0 °C over 40 min. The reaction was stirred at room temperature for 30 min and heated to reflux for 19 h. After this time, the mixture was concentrated, treated with ice water and neutralized. The solution was extracted with ethylacetate. The combined organic phases were dried over MgSO<sub>4</sub> and concentrated. The residue was purified by column chromatography on silica gel (CH<sub>2</sub>Cl<sub>2</sub> : CH<sub>3</sub>OH = 40 : 1) to afford **8** (168.5 mg, 49%) as yellow solid. <sup>1</sup>H NMR (400 MHz, DMSO-d<sub>6</sub>): δ 1.72 (s, 3H, CH<sub>3</sub>), 3.55 (m, 4H, BnO-CH<sub>2</sub>), 3.78 (m, 1H, CH), 4.43 (s, 2H, C6-CH<sub>2</sub>), 4.50 (s, 4H, Ph-CH<sub>2</sub>), 7.32 (m, 10H, Ph), 10.36 (s, 1H, N1H), 11.04 (s, 1H, N3H) ppm. <sup>13</sup>C NMR (100 MHz, DMSO-d<sub>6</sub>): δ 8.8, 65.2, 69.5, 72.2, 77.9, 105.1, 127.4, 127.4, 128.1, 138.1, 146.4, 150.5, 162.7 ppm. LRMS (ESI+) m/z 410.76 (M+H)<sup>+</sup>.

**6-((1,3-Bis(benzyloxy)propan-2-yloxy)methyl)-1,3-bis(methoxymethyl)-5-methylpyrimidine-2,4(1H,3H)-dione (9)**. Compound **8** (65 mg, 0.158 mmol) was dissolved in DIPEA (300 μL) and dichloromethane (450 μL) and the mixture was stirred for 30 min. Chlorotrimethylsilane (60 μL, 0.473 mmol) was added and the reaction was stirred for 30 min. After this time, methoxymethyl chloride (MOMCl) (70 μL, 0.92 mmol) was added. After 1 h, additional MOMCl (250 μL, 3.29 mmol) was added. After 22 h, the reaction was diluted with ethylacetate, washed with saturated aqueous NaHCO<sub>3</sub> solution and extracted with ethylacetate. The combined organic phases were combined, washed with brine, dried over Na<sub>2</sub>SO<sub>4</sub> and concentrated in vacuo. The crude product was purified by column chromatography on silica gel (ethylacetate : hexane = 1:1) to yield **9** (77 mg, 97%). <sup>1</sup>H NMR (400 MHz, CDCl<sub>3</sub>): δ 2.01 (s, 3H, CH<sub>3</sub>), 3.34 (s, 3H, N3-MOMCH<sub>3</sub>), 3.43 (s, 3H, N1-MOMCH<sub>3</sub>), 3.57 (m, 4H, BnO-CH<sub>2</sub>), 3.81 (m, 1H, CH), 4.52 (s, 4H, Ph-CH<sub>2</sub>), 4.68 (s, 2H, C6-CH<sub>2</sub>), 5.39 (s, 2H, N3-MOMCH<sub>2</sub>), 5.42 (s, 2H, N1-MOMCH<sub>2</sub>), 7.27-7.37 (m, 10H, Ph) ppm. <sup>13</sup>C NMR (100 MHz, CDCl<sub>3</sub>): δ 11.1, 57.0, 57.9, 64.4, 70.5, 72.7, 73.7, 75.1, 78.6, 111.9, 127.8, 127.9, 128.5, 137.8, 145.0, 152.5, 163.6 ppm. LRMS (ESI+) m/z 498.80 (M+H)<sup>+</sup>.

**6-(((1,3-Dihydroxypropan-2-yl)oxy)methyl)-1,3-bis(methoxymethyl)-5-methylpyrimidine-2,4(1H,3H)-dione (10)**. To a solution of **9** (300 mg, 0.60 mmol) in ethanol (23 mL), Pd(OH)<sub>2</sub> on activated carbon 20% (382.5 mg, 0.54 mmol) and cyclohexene (4.5 mL) were added and the reaction was heated to reflux for 70 min. After cooling, the mixture was filtered through celite (ethylacetate) and the solvent was evaporated to yield **10** (179 mg, 93%) as light-yellow oil. <sup>1</sup>H

NMR (400 MHz, CDCl<sub>3</sub>):  $\delta$  2.09 (s, 3H, CH<sub>3</sub>), 2.32 (bs, 2H, OH), 3.45 (s, 3H, N3-MOMCH<sub>3</sub>), 3.48 (s, 3H, N1-MOMCH<sub>3</sub>), 3.62 (m, 1H, CH), 3.78 (ddd, 4H,  $J = 30.2, 11.8, 3.7$  Hz, OH-CH<sub>2</sub>), 4.70 (s, 2H, C6-CH<sub>2</sub>), 5.41 (s, 2H, N3-MOMCH<sub>2</sub>), 5.49 (s, 2H, N1-MOMCH<sub>2</sub>) ppm. <sup>13</sup>C NMR (100 MHz, CDCl<sub>3</sub>):  $\delta$  11.3, 57.5, 58.0, 62.7, 64.0, 72.8, 75.4, 80.8, 112.0, 144.6, 152.4, 163.3 ppm. LRMS (ESI+)  $m/z$  318.70 ( $M+H$ )<sup>+</sup>.

**6-(((1-Hydroxy-3-((4-methoxyphenyl)diphenylmethoxy)propan-2-yl)oxy)methyl)-1,3-bis(methoxymethyl)-5-methylpyrimidine-2,4(1H,3H)-dione (11).** To a solution of **10** (20 mg, 0.063 mmol) in DMF (0.4 mL) triethylamine (9.5 mg, 0.094 mmol) was added and the mixture was stirred at room temperature for 10 min. 4-methoxytritylchloride (20 mg, 0.064 mmol) and catalytic amount of DMAP were added and the reaction was stirred for 2 h at room temperature. The mixture was diluted with ethylacetate, washed with water and brine, dried over MgSO<sub>4</sub> and concentrated. The residue was purified by column chromatography on silica gel (ethylacetate : hexane 1:4 to ethylacetate : hexane 1:1) to afford **11** (11.2 mg, 30%). <sup>1</sup>H NMR (400 MHz, CDCl<sub>3</sub>):  $\delta$  1.95 (s, 3H, CH<sub>3</sub>), 2.31 (bs, 1H, OH), 3.21 (m, 2H, MMTrO-CH<sub>2</sub>), 3.35 (s, 3H, N3-MOMCH<sub>3</sub>), 3.36 (s, 3H, N1-MOMCH<sub>3</sub>), 3.57 (m, 2H, OH-CH<sub>2</sub>), 3.63 (m, 1H, CH), 3.73 (s, 3H, MMTrCH<sub>3</sub>), 4.57 (dd, 2H,  $J = 52.6, 11.7$  Hz, C6-CH<sub>2</sub>), 5.34 (m, 4H, MOMCH<sub>2</sub>), 6.77 (m, 2H, CH-C-O-CH<sub>3</sub>), 7.14-7.36 (m, 12H, MMTrCH) ppm. <sup>13</sup>C NMR (100 MHz, CDCl<sub>3</sub>):  $\delta$  11.3, 55.2, 57.5, 57.9, 63.0, 63.5, 64.2, 72.7, 75.3, 80.5, 87.0, 111.8, 113.2, 127.1, 127.9, 128.3, 130.3, 135.1, 144.0, 144.7, 152.4, 158.7, 163.4 ppm. LRMS (ESI+)  $m/z$  612.87 ( $M+H$ )<sup>+</sup>.

**2-((1,3-Bis(methoxymethyl)-5-methyl-2,6-dioxo-1,2,3,6-tetrahydropyrimidin-4-yl)methoxy)-3-((4-methoxyphenyl)diphenylmethoxy)propyl 4-methylbenzenesulfonate (12).** Compound **11** (11.2 mg, 0.019 mmol) was suspended in pyridine (0.3 mL) and stirred at room temperature for 30 min. Tosylchloride (16.4 mg, 0.086 mmol) dissolved in dichloromethane (0.1 mL) was added and the mixture was stirred for 2 h at 30 °C. A catalytic amount of DMAP was added and the reaction was heated at 30 °C for 17 h. The mixture was quenched with water and diluted with ethylacetate. The mixture was washed with 1M CuSO<sub>4</sub> solution and extracted with ethylacetate. The combined organic phases were dried over MgSO<sub>4</sub> and concentrated. The residue was purified by column chromatography on silica gel (ethylacetate : hexane = 1:1) to obtain **12** (6.4 mg, 45%). <sup>1</sup>H NMR (400 MHz, CDCl<sub>3</sub>):  $\delta$  1.92 (s, 3H, CH<sub>3</sub>), 2.44 (s, 3H, TsCH<sub>3</sub>), 3.21 (d, 2H,  $J = 19.1$  Hz

MMTrO-CH<sub>2</sub>), 3.36 (s, 3H, N3-MOMCH<sub>3</sub>), 3.43 (s, 3H, N1-MOMCH<sub>3</sub>), 3.61-3.67 (m, 1H, CH), 3.80 (s, 3H, MMTrCH<sub>3</sub>), 4.03 (dd, 1H, <sup>2</sup>J = 10.6, <sup>3</sup>J = 3.2 Hz, TsO-CH<sub>2</sub>), 4.10 (dd, 1H, <sup>2</sup>J = 10.6, <sup>3</sup>J = 3.2 Hz, TsO-CH<sub>2</sub>), 4.53 (dd, 2H, J = 13.3, 11.7 Hz, C6-CH<sub>2</sub>), 5.32 (m, 2H, N3-MOMCH<sub>2</sub>), 5.39 (s, 2H, N1-MOMCH<sub>2</sub>), 6.81 (m, 2H, S-C-CH-CH), 7.21-7.36 (m, 14H, tritylCH), 7.74 (m, 2H, S-C-CH) ppm. <sup>13</sup>C NMR (100 MHz, CDCl<sub>3</sub>): δ 11.2, 21.7, 55.2, 57.1, 57.9, 62.5, 64.3, 69.6, 72.7, 75.0, 77.5, 87.0, 112.0, 113.3, 127.2, 127.9, 128.2, 129.9, 130.3, 132.7, 134.8, 143.8, 143.8, 144.3, 145.1, 152.3, 158.8, 163.4 ppm. HRMS (ESI+) m/z found 767.2618 for [C<sub>40</sub>H<sub>44</sub>N<sub>2</sub>NaO<sub>10</sub>S]<sup>+</sup>, calcd 767.2609 for [C<sub>40</sub>H<sub>44</sub>N<sub>2</sub>NaO<sub>10</sub>S]<sup>+</sup>.

### 3.2.8 Radiosynthesis of [<sup>18</sup>F]FHOMP (<sup>18</sup>F-6)

The no-carrier-added <sup>18</sup>F-fluoride was trapped on the anion exchange cartridge and directly eluted into a 5-mL sealed reaction vessel using a solution of tetrabutylammonium hydroxide (27.8 mg) in 0.6 mL of methanol. The solvent was removed at 90 °C under reduced pressure and a stream of nitrogen. Subsequently, water was removed by azeotropic distillation with acetonitrile (3 x 1 mL) under reduced pressure and a stream of nitrogen at 90 °C. The vial was kept at room temperature for additional 5 min under vacuum. To this dried [<sup>18</sup>F]TBAF salt was added a solution of the tosylate precursor **12** (4 mg) in 0.3 mL *tert*-butanol and anhydrous acetonitrile (4:1). The reaction mixture was heated for 30 min at 110 °C. After cooling, the crude product was passed through an SPE cartridge (Sep-Pak silica, Waters AG) to remove TBA and unreacted fluoride. The cartridge was washed with acetonitrile (3 x 0.5 mL). The solvent was evaporated at 90 °C under a stream of nitrogen to dryness. For hydrolysis, 0.6 mL of conc. HCl was added and the mixture was heated for 10 min at 110 °C. The vial was cooled, neutralized with 4 M NaOH (1.5 mL) and diluted with 0.6 M phosphate buffer to a total volume of 5 mL. The crude product was injected onto the semi-preparative radio-HPLC column for HPLC purification. The desired product fraction was collected at approximately 19 min (max. 5% ethanol in water) and directly passed through a sterile filter into a sterile and pyrogen-free vial. Radiochemical yield was determined after purification, and on the basis of starting activity.

### 3.2.9 *In vitro* phosphorylation of FHOMP

Phosphorylation of FHOMP, penciclovir (PCV) as a well known substrate for HSV1-TK but not the human TK (hTK) and deoxythymidine (dT; positive control to assess the functionality of both HSV1-TK and human TK, hTK) by HSV1-TK and hTK were monitored by HPLC as described previously [105]. In brief, 1-5 mM substrate were incubated with 3  $\mu$ g of HSV1-TK or hTK and 5 mM ATP in a buffer solution (pH 7.4) at 37 °C and quenched after 20 and 60 min. The recombinant enzymes, HSV1-TK and hTK, were expressed and purified according to a previously published protocol [87]. The formation of adenosine-diphosphate (ADP) was monitored. A blank reaction (without substrate) was run concurrently to account for substrate-independent ATP hydrolysis.

### 3.2.10 Accumulation of [ $^{18}$ F]FHOMP in HEK293TK+ and HEK293 control cells

Uptake of [ $^{18}$ F]FHOMP and [ $^{18}$ F]FHBG into HEK293TK+ and HEK293 control cells was determined according to a previously published protocol [105]. In brief, cells were incubated in a 12-well culture plate with 1 mL medium containing 130 kBq [ $^{18}$ F]FHOMP or [ $^{18}$ F]FHBG per well. The radioactivity of the cell lysate and the combined incubation medium and washing solutions, respectively, were measured in a gamma counter (Wizard, Perkin Elmer) at the indicated time points. Radioactivity of the cell lysates was normalized to total protein determined in 50  $\mu$ L cell lysate with the *DC*<sup>TM</sup> Protein Assay Kit I (Bio Rad, Hercules CA). Cell uptake was calculated as the percent accumulated radioactivity per mg protein ((dpm cells x 100 / (dpm cells + dpm medium))/mg protein) and corresponding uptake ratios between HEK293TK+ and HEK293 control cells were calculated [90].

### 3.2.11 Determination of partition coefficient

The log  $D_{\text{pH}7.4}$  of [ $^{18}$ F]FHOMP and [ $^{18}$ F]FHBG in 1-octanol/PBS was determined by the shake-flask method as previously described [105]. [ $^{18}$ F]FHOMP or [ $^{18}$ F]FHBG (~1.5 MBq) was added in 5  $\mu$ L water containing 5% ethanol to vials containing 0.5 mL each of 1-octanol and PBS. The vials were shaken for 20 min at room temperature and the phases were separated by

centrifugation. The radioactivity was measured in 50  $\mu\text{L}$  of each phase with a gamma counter (Wizard, Perkin Elmer). Measurements were performed in triplicates and  $\log D_{\text{pH}7.4}$  values were calculated as the logarithmic ratio of the counts in the octanol and PBS samples.

### 3.2.12 *In vitro* metabolism with liver microsomes

[ $^{18}\text{F}$ ]FHOMP metabolism by microsomal enzymes was investigated *in vitro* employing pooled mouse or human liver microsomes (BD Biosciences). The test compound (17 MBq) or 34  $\mu\text{M}$  testosterone (positive control), was preincubated for 5 min with NADPH regenerating system (NADPH-RS; BD Biosciences) according to the manufacturers protocol in 0.1 M phosphate buffer (pH 7.4) at 37  $^{\circ}\text{C}$  before addition of the microsome suspension (0.5 mg protein per mL). A suspension of microsomes without NADPH-RS and a suspension of NADPH-RS without microsomes were used as negative controls. At different time points (0, 10, 20, 60, 90, and 120 min) 100  $\mu\text{L}$  samples were withdrawn and the enzymatic reactions were stopped and proteins precipitated with an equal volume of ice-cold acetonitrile. Samples were centrifuged at 13200 rpm for 3 min to obtain the supernatant which was filtered (0.45  $\mu\text{m}$ ), and diluted 1:1 with 0.05 M sodium phosphate buffer (pH 7.0) to be analyzed by Waters ACQUITY UPLC<sup>®</sup> system as described. Samples of the formulated solution in water containing 5% ethanol and stored at room temperature were used to check for chemical decomposition.

### 3.2.13 Blood radioactivity-time curve and biological half-life of [ $^{18}\text{F}$ ]FHOMP

To estimate the biological blood half-life of [ $^{18}\text{F}$ ]FHOMP, three mice (female NMRI nude mice, 21-25 g; Charles River) were injected into a lateral tail vein with 9-12 MBq [ $^{18}\text{F}$ ]FHOMP in 100  $\mu\text{L}$  saline containing maximal 5% ethanol. Blood samples were drawn through the contra-lateral tail vein at several time points from 2 to 120 min after injection. The radioactivity in each blood sample was measured with a gamma counter (Wizard, Perkin Elmer), corrected for radioactivity decay and the percentage of injected dose per g blood (%ID/g) was calculated and plotted against the time point of blood withdrawal. Radioactivity-time curves were fitted with a mono-exponential function  $\%ID/g(t) = \%ID/g(0) \times e^{-kt}$ , where %ID/g(0) is the fitted starting blood radioactivity at time 0,  $k$  is the rate constant in  $\text{min}^{-1}$  and  $t$  the time in min. Biological half-life values were calculated as  $t_{1/2} = \ln 2/k$ .



### 3.2.14 Small-animal PET

Xenograft bearing mice (21-30 g) were administered 17-24 MBq [ $^{18}\text{F}$ ]FHOMP (n = 5) or 7-25 MBq [ $^{18}\text{F}$ ]FHBG (n = 5) in 100  $\mu\text{L}$  saline containing  $\leq 5\%$  ethanol via tail vein injection. Anesthesia was induced with 2-3% isoflurane (Abbott) in air-oxygen 5 min prior to PET/CT acquisition. Depth of anesthesia and temperature were controlled as described previously [91]. PET/CT scans were performed with a GE VISTA eXplore PET/CT tomograph with an axial field of view of 4.8 cm [92]. Dynamic (one bed position, list mode) and static (two bed positions, 15 min upper body followed by 15 min lower body) scans were acquired over 90 and 30 min, respectively. Data were reconstructed by 2D ordered-subset expectation maximization (2D OSEM), dynamic scans were reconstructed into 5 min time frames. Region of interest analysis was conducted with the software PMOD 3.2 (PMOD, Switzerland). Volumes of interest (VOIs) were drawn according to the CT images and the average background activity was estimated from a sphere with a volume of ca 0.5  $\text{cm}^3$  between the two xenografts. VOIs for abdominal average activity were drawn according to the PET images, outlining regions with higher than background activity excluding gall and urinary bladders. Standardized uptake values (SUVs) were calculated from the VOI average activities per  $\text{cm}^3$  multiplied with the body weight (with 1 g corresponding to 1  $\text{cm}^3$ ) and divided by the injected activity dose (all decay corrected).

### 3.2.15 *Ex vivo* biodistribution studies of [ $^{18}\text{F}$ ]FHOMP and [ $^{18}\text{F}$ ]FHBG

To perform *ex vivo* biodistribution studies of [ $^{18}\text{F}$ ]FHOMP and [ $^{18}\text{F}$ ]FHBG, HEK293 control and HEK293TK+ xenograft bearing nude mice (25-30 g) were administered 4.7-5.1 MBq [ $^{18}\text{F}$ ]FHOMP (n = 4) or 4.5-5.0 MBq [ $^{18}\text{F}$ ]FHBG (n = 3) in 100  $\mu\text{L}$  saline containing  $\leq 5\%$  ethanol via tail-vein injection. Animals were sacrificed and dissected 60 min after injection, organs and tissue samples were weighed and the radioactivity determined in a gamma counter. The time point of dissection was chosen according to dynamic PET scans and at a time-point when [ $^{18}\text{F}$ ]FHOMP activity ratios between HEK293TK+ and control xenografts were highest. Decay corrected radioactivity was expressed in analogy to the SUV as the ratio between the detected activity per gram tissue and the injected dose per gram body weight ( $\text{SUV}_{\text{biodis}}$ ).

### **3.2.16 Effect of ENT1 inhibition on [<sup>18</sup>F]FHOMP PET and *ex vivo* biodistribution**

Four mice (19-23 g) received each 15 mg/kg ENT1 inhibitor nitrobenzylmercaptapurine ribonucleoside phosphate (NBMPR-P; generously provided by Dr. Wendy Gati, Department of Pharmacology, University of Alberta, Edmonton Canada) dissolved in aqua ad injectabilia via intraperitoneal injection. At this dosage, NBMPR-P inhibits ENT1 with no observed animal toxicity [106]. One hour after NBMPR-P administration, [<sup>18</sup>F]FHOMP (4.0-6.4 MBq) was injected in 100 µL water containing maximal 5% ethanol via a lateral tail vein. At 60 min after radiotracer injection, three animals were sacrificed by decapitation under isoflurane anesthesia. Organs and tissues were removed, and the accumulated radioactivity was measured in the gamma-counter and expressed as described in Section 3.3.15. A static whole body PET scan from 60-90 min was acquired with one mouse according to Section 3.3.14.

### 3.3 Results

#### 3.3.1 Cell line and xenograft characterization

The HEK293TK+ cell line and HEK293TK+ xenograft tissue showed an intense immunoreactive band for HSV1-TK protein located at 45 kDa by Western Blot analysis (Fig. 2). Purified HSV1-TK protein (see Section 3.3.9.) served as positive control. The HEK293 control cells and HEK293 control xenograft tissue did not show this band.

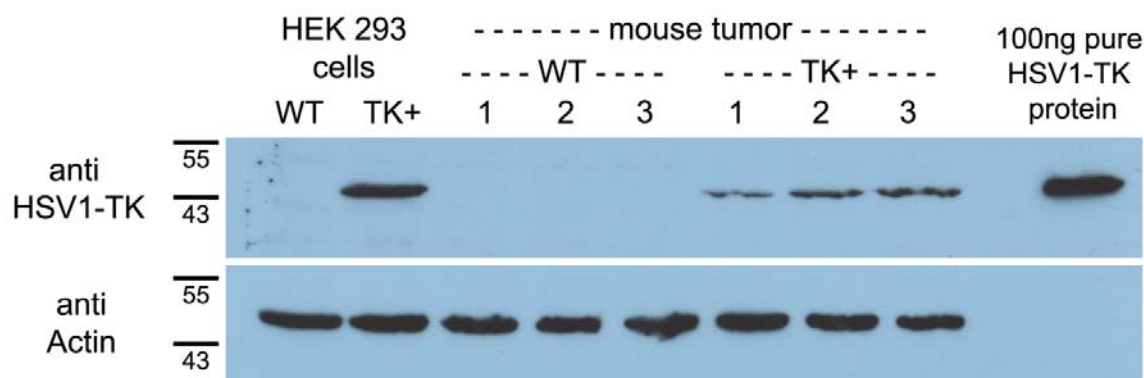
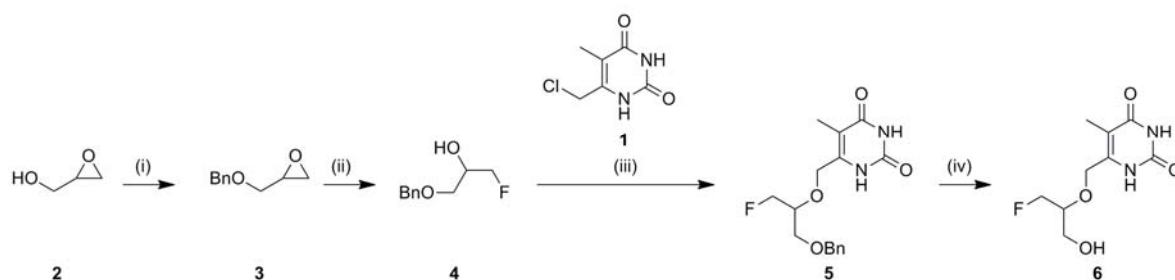


**Figure 2.** Western blot analysis of HSV1-TK expression in transfected (TK+) and nontransfected control (WT) cells (HEK293) and xenograft tissues (tumor) using anti-HSV1-TK polyclonal antibody. Purified HSV1-TK protein served as positive control. Actin expression verified that the same amount of protein was loaded per lane.

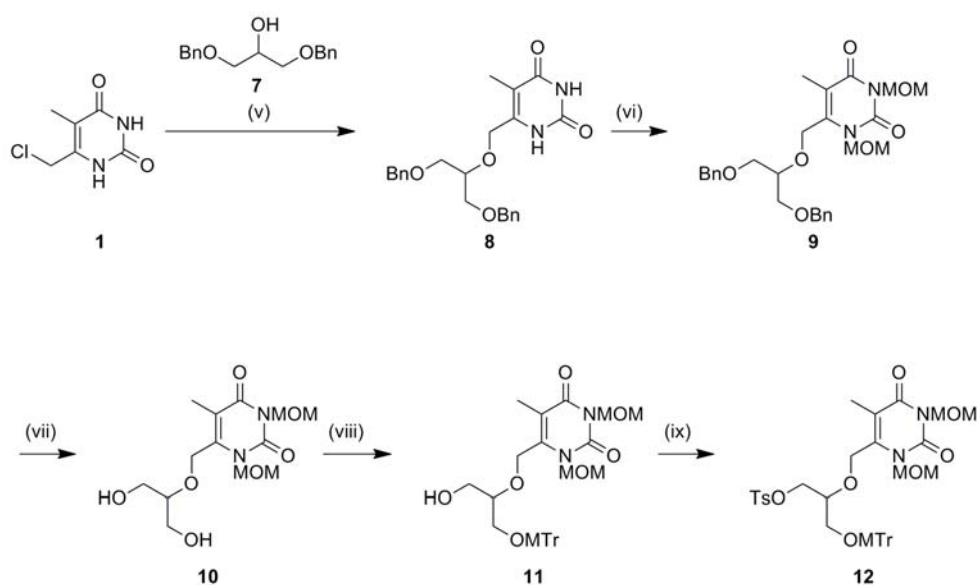
#### 3.3.2 Syntheses of reference FHOMP (6) and precursor 12

The synthesis of reference compound **6** started from glycidol **2** (Scheme 1) which was transformed to benzyloxy fluoropropanol **4** in 44% yield as reported previously [103, 104]. Alcohol **4** was reacted with pyrimidine **1** which was synthesized according to a published method [102] to yield benzylated compound **5** in 46%. Deprotection of the benzyl group in **5** was achieved by treatment with Pd/C and hydrogen to afford target compound **6** in 50% yield.



**Scheme 1.** Synthesis of reference FHOMP (**6**): (i) NaH, BnBr, THF; (ii) TBABF-KHF<sub>2</sub>, heptane, 128 °C; (iii) NaH, 6-(chloromethyl)-5-methylpyrimidine-2,4(1*H*,3*H*)-dione, THF, reflux; (iv) 10% Pd/C, H<sub>2</sub>, MeOH, reflux

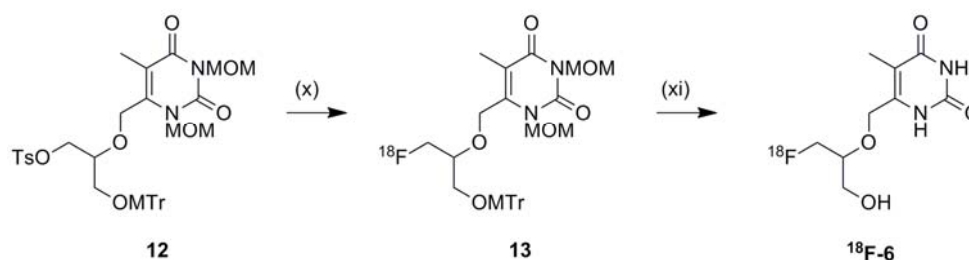
For the synthesis of the precursor (Scheme 2), pyrimidine **1** was reacted with dibenzylated alcohol **7** in THF using NaH as a base to afford compound **8** in 49% yield. Treatment of **8** with Me<sub>3</sub>SiCl and DIPEA and subsequent reaction with MOMCl in analogy to a published procedure [107] gave N-1 and N-3 protected pyrimidine **9** in 97% yield. Pyrimidine **9** was debenzylated by *in situ* transfer-hydrogenation with Pd(OH)<sub>2</sub> on carbon and cyclohexene to yield diol **10** in 93%. Diol **10** was treated with methoxytritylchloride (MTrCl) to afford MTr-protected alcohol **11** in 30% yield. The tosylate precursor **12** was obtained in 45% yield after reacting MTr-protected alcohol **11** with tosylchloride.



**Scheme 2.** Synthesis of tosylate precursor **12**: (v) **7**, NaH, THF, reflux; (vi) 1. TMSCl, DIPEA, DCM; 2. MOMCl; (vii) Pd(OH)<sub>2</sub>, cyclohexene, EtOH, reflux; (viii) MTrCl, TEA, DMAP, DMF; (ix) TsCl, DMAP, pyridine, 30 °C

### 3.3.3 Radiosynthesis of [ $^{18}\text{F}$ ]FHOMP ( $^{18}\text{F}$ -6)

Tosyl precursor **12** was directly labeled with  $^{18}\text{F}$  via nucleophilic substitution using [ $^{18}\text{F}$ ]TBAF followed by acidic cleavage of all protecting groups (Scheme 3). The nucleophilic  $^{18}\text{F}$ -fluorination was performed in *tert*-butanol and acetonitrile (4:1) at 110 °C for 30 min to afford  $^{18}\text{F}$ -labeled intermediate **13**. The incorporation yield was 88% by radio-UPLC analysis. The second step involving the acidic hydrolysis of intermediate **13** gave the final compound,  $^{18}\text{F}$ -6, in 51% radiochemical yield after semi-preparative HPLC purification using injectable mobile phase. Typically starting from 28-86 GBq,  $^{18}\text{F}$ -6 was obtained in a concentration of 1.5-3.6 GBq/mL. The overall decay corrected radiochemical yield was 25%. Quality control by analytical radio-HPLC showed that the radiochemical purity was always greater than 95%. The total synthesis time EOB was about 110 min and the identity of [ $^{18}\text{F}$ ]FHOMP was confirmed by co-injection of the non-radioactive reference compound FHOMP (Fig. 3).



**Scheme 3.** Radiosynthesis of [ $^{18}\text{F}$ ]FHOMP ( $^{18}\text{F}$ -6): (x) [ $^{18}\text{F}$ ]TBAF, *tert*-butanol/ACN 4:1, 110 °C; (xi) conc. HCl, 110 °C

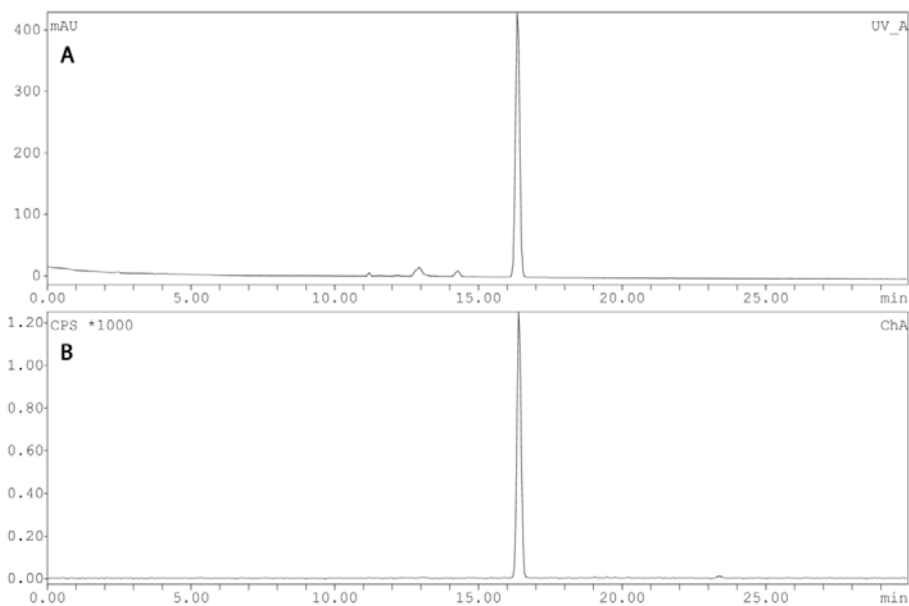


**Figure 3.** HPLC profile of [ $^{18}\text{F}$ ]FHOMP ( $^{18}\text{F}$ -6) after semi-preparative HPLC purification. **A** UV absorption at 254 nm: co-injected non-radioactive FHOMP (6). **B** radio chromatogram: radioactive trace of [ $^{18}\text{F}$ ]FHOMP ( $^{18}\text{F}$ -6).

### 3.3.4 *In vitro* phosphorylation of FHOMP

The selectivity of FHOMP for HSV1-TK over hTK was investigated *in vitro* in a phosphorylation assay with the purified recombinant enzymes. Both recombinant enzymes were functional as concluded from the formation of phosphorylated dT (dT-mP) and ADP after incubation with dT. Increasing ADP concentrations were observed during FHOMP and PCV-control incubation with HSV1-TK and ATP but only autohydrolysis formation of ADP was detected with hTK. These data indicate that FHOMP is indeed a substrate for HSV1-TK but not for hTK (Figure S1).

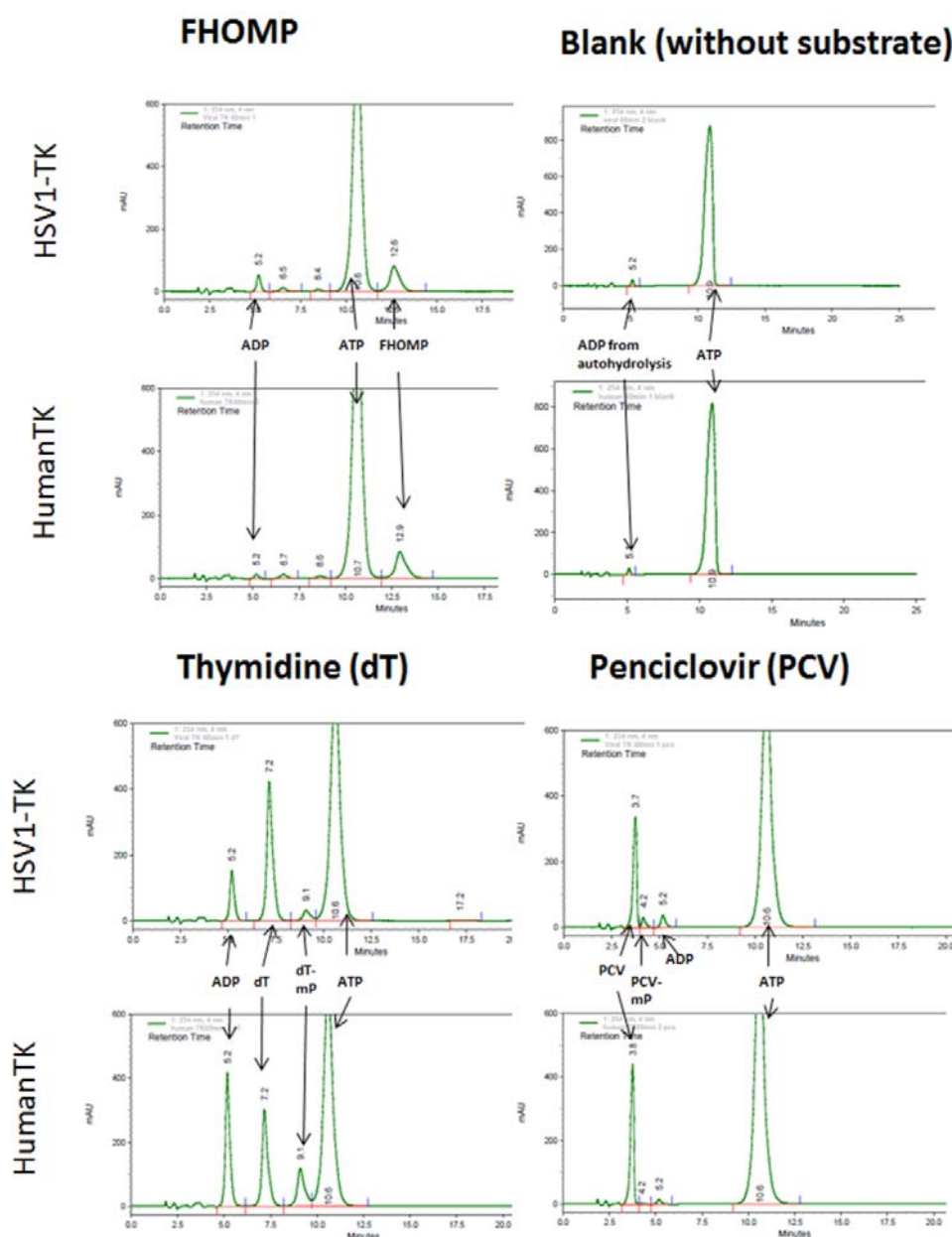


**Figure S1.** Phosphorylation pattern assay at 60 min of incubation: The formation of new peaks (ADP and some monophosphorylated compounds) have been monitored by HPLC coupled with a UV detector at 254 nm. To assess the functionality of the HSV1-TK and the human-TK enzymes, thymidine (dT) was used as a positive control. It showed ADP formation for both enzymes as expected and monophosphorylated thymidine (dT-mP) could be detected. Penciclovir was used to compare with a well known HSV1-TK but not human-TK substrate. Very small substrate-independent ATP hydrolysis was observed for the blank (no substrate) for both enzymes. These chromatograms clearly show the formation of ADP for PCV (and some speculated monophosphorylated penciclovir (PCV-mP)) and FHOMP with HSV1-TK but not the human-TK. The data for dT, PCV and blank have been shown before in [23].

### 3.3.5 *In vitro* cell uptake studies

Figure 4 summarizes the uptake of [ $^{18}\text{F}$ ]FHOMP and [ $^{18}\text{F}$ ]FHBG *in vitro* in HSV1-*tk* transfected (HEK293TK+) and control cells. Cells were incubated for the indicated durations with [ $^{18}\text{F}$ ]FHOMP or [ $^{18}\text{F}$ ]FHBG. The uptake of [ $^{18}\text{F}$ ]FHOMP was 52-fold (30 min incubation) to 244-fold (180 min) higher in HSV1-TK containing HEK293TK+ cells than in control cells. The respective ratios increased from 5 at 30 min to 81 at 240 min for [ $^{18}\text{F}$ ]FHBG. Uptake into control cells was low for [ $^{18}\text{F}$ ]FHOMP with  $3.6\text{E-}04 \pm 7.7\text{E-}05$  %/mg protein and for [ $^{18}\text{F}$ ]FHBG with  $1.8\text{E-}03 \pm 1.3\text{E-}04$  %/mg protein. [ $^{18}\text{F}$ ]FHOMP uptake ratios were significantly ( $P < 0.02$ ; Student *t* test) higher than [ $^{18}\text{F}$ ]FHBG uptake ratios, i.e., 9.9-fold higher at 30 min, 7.1-fold higher at 60 min, and 3.6-fold higher at 120 min.

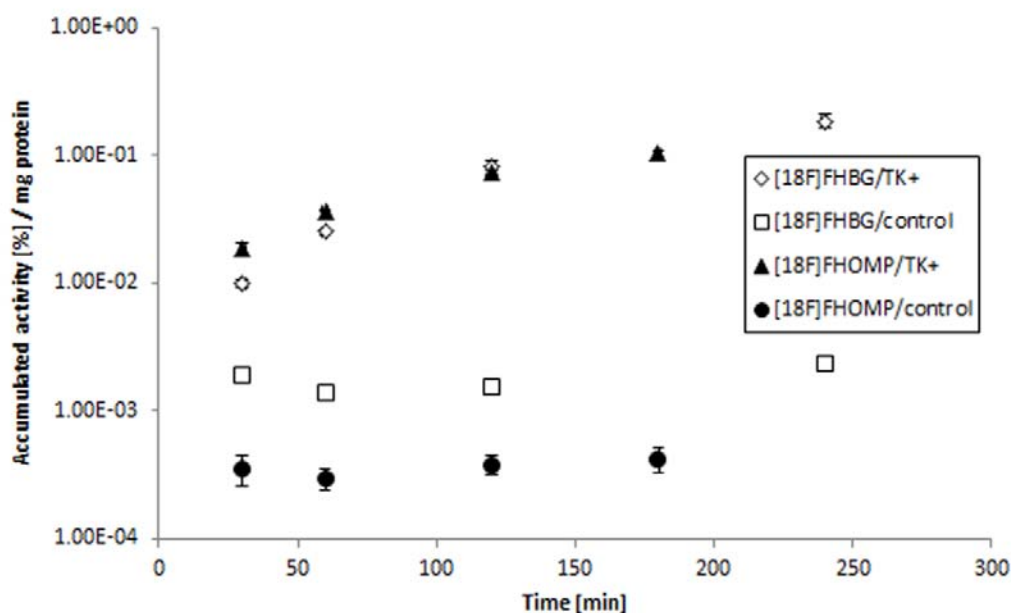


**Figure 4.** *In vitro* uptake (%/mg protein) of [ $^{18}\text{F}$ ]FHOMP and [ $^{18}\text{F}$ ]FHBG in HEK293TK+ cells (TK+) over HEK293 control cells (control). Data are expressed as mean $\pm$ standard deviation of triplicate sample. [ $^{18}\text{F}$ ]FHBG data has been shown before in [105].



### 3.3.6 Octanol/buffer $\log D$ of [ $^{18}\text{F}$ ]FHOMP and [ $^{18}\text{F}$ ]FHBG at pH 7.4

The lipophilicity of [ $^{18}\text{F}$ ]FHOMP and [ $^{18}\text{F}$ ]FHBG was determined by the shake-flask method at physiological pH 7.4. A  $\log D_{\text{pH}7.4}$  of  $-0.87 \pm 0.03$  was obtained for [ $^{18}\text{F}$ ]FHOMP and  $-0.87 \pm 0.01$  for [ $^{18}\text{F}$ ]FHBG, respectively.

### 3.3.7 *In vitro* metabolism by liver microsomes

In mouse or human liver microsomes, over 99% of [ $^{18}\text{F}$ ]FHOMP was still intact after 120 min of incubation at 37 °C. A stability study of the formulated solution (5% ethanol in water) revealed no radioactive degradation products of the parent compound at room temperature over 240 min.

### 3.3.8 Blood radioactivity-time curve and biological half-life of [ $^{18}\text{F}$ ]FHOMP

The averaged blood radioactivity-time curves after [ $^{18}\text{F}$ ]FHOMP intravenous injection in three nude mice, uncorrected for potential metabolites, are shown in Figure 5. The decay-corrected blood radioactivity (%ID/g) decreased with first order kinetics. The radioactivity-time curves were fitted with a mono-exponential function and biological half-life values ( $t_{1/2}$ ) were calculated as described under Methods. The average  $t_{1/2}$  was  $26.2 \pm 4.2$  min.

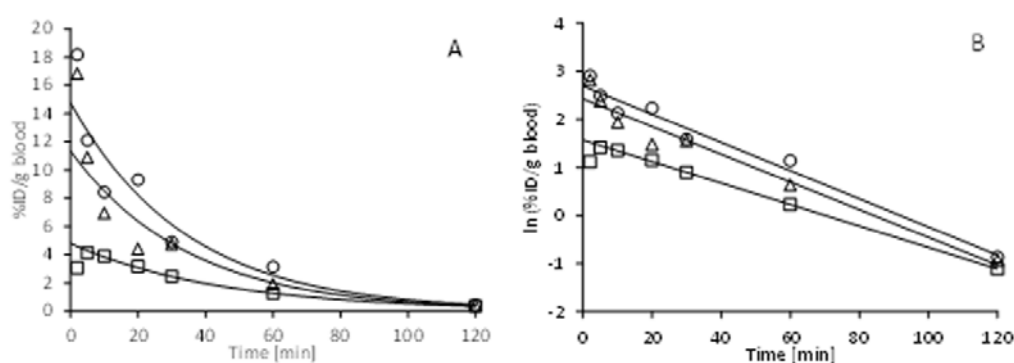


**Figure 5.** Decay-corrected blood radioactivity-time curves after [ $^{18}\text{F}$ ]FHOMP intravenous injection. Linear (A) and semi-logarithmic (B) representations of decay-corrected radioactivity (%ID per g blood) after intravenous injection of [ $^{18}\text{F}$ ]FHOMP. Symbols represent the data of three mice, solid lines are fitted mono-exponential functions (weighted for the squared deviations in the ln plot). The first data point (2 min) of the second animal (squares) was excluded from the fit. Fitted biological half-lives were 23.6 min (circles), 31.1 min (squares), and 24.0 min (triangles).

### 3.3.9 Small-animal PET studies with [ $^{18}\text{F}$ ]FHOMP and [ $^{18}\text{F}$ ]FHBG

Static whole body (two beds, 60-90 min) PET images of xenograft-bearing mice after [ $^{18}\text{F}$ ]FHOMP and [ $^{18}\text{F}$ ]FHBG injection, respectively, are shown in Figure 6. The time frame for the static PET scans was based on the dynamic scans and was chosen when SUV ratios between HEK293TK+ and HEK293 control xenografts and between HEK293TK+ xenografts and background (region between the xenografts) for [ $^{18}\text{F}$ ]FHOMP were highest (data not shown). [ $^{18}\text{F}$ ]FHOMP accumulated in the TK-positive xenograft, consistent with the biodistribution results (see Section 3.4.10.). Uptake in the control xenograft was low and similar to background activity. The hottest spot was the abdomen, followed by the gallbladder and the TK-positive xenograft. [ $^{18}\text{F}$ ]FHBG showed similar imaging characteristics as [ $^{18}\text{F}$ ]FHOMP with a higher abdominal activity, but less intense general background activities.

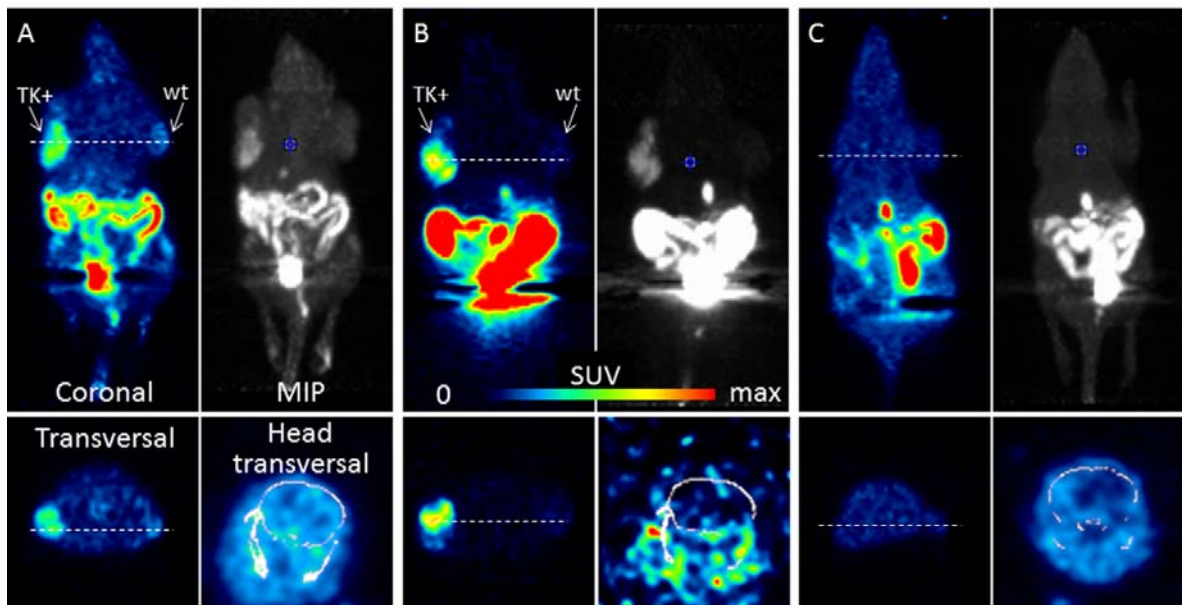


**Figure 6.** PET imaging of [ $^{18}\text{F}$ ]FHOMP and [ $^{18}\text{F}$ ]FHBG. Mice were scanned for 30 min (2 bed positions) 60 min after tracer injection. A, B) HSV1-TK+ (left shoulder) and control (right shoulder) xenograft-bearing mice were injected 12 MBq [ $^{18}\text{F}$ ]FHOMP (A) or 21 MBq [ $^{18}\text{F}$ ]FHBG (B). C) Mouse without xenografts after ENT-1 blockade with NBMPR-P and injection of 18 MBq [ $^{18}\text{F}$ ]FHOMP. Max SUV 1 except for brain sections with max SUV 0.5 (A, B) and 0.1 (C). MIP, maximal intensity projections. Anesthesia: 2-3% isoflurane in air/oxygen.

### 3.3.10 *Ex vivo* biodistribution of [<sup>18</sup>F]FHOMP and [<sup>18</sup>F]FHBG in xenograft-bearing mice

Table 1 summarizes the biodistribution data of [<sup>18</sup>F]FHOMP and [<sup>18</sup>F]FHBG in xenograft-bearing mice at 60 min after radiotracer injection. [<sup>18</sup>F]FHOMP and [<sup>18</sup>F]FHBG radioactivity accumulation was significantly higher in transgenic xenografts than in the control xenografts (P 0.003 and 0.04, respectively). The ratio between TK+ and control xenograft uptake was 2.0±0.8 for [<sup>18</sup>F]FHOMP (n=4) and 3.0±1.2 for [<sup>18</sup>F]FHBG (n=3), the respective TK+ xenograft to blood ratios were 2.1±0.4 and 5.9±2.1. Control xenograft to blood ratios for [<sup>18</sup>F]FHOMP and [<sup>18</sup>F]FHBG were 1.1±0.3 and 2.0±0.2, respectively. The distribution patterns of the two tracers were similar, however, [<sup>18</sup>F]FHOMP exhibited higher activities in most tissues, except intestines and kidneys.

**Table 1.** Biodistribution data (SUV<sub>biodis</sub>) of [<sup>18</sup>F]FHOMP and [<sup>18</sup>F]FHBG in xenograft-bearing mice and of [<sup>18</sup>F]FHOMP in normal mice injected with the ENT1 blocker NBMPR-P (1h before radiotracer) at 60 min after radiotracer injection

Tissue	[ <sup>18</sup> F]FHOMP		[ <sup>18</sup> F]FHBG		[ <sup>18</sup> F]FHOMP + NBMPR-P	
Xenograft TK+	0.34	± 0.02	0.20	± 0.08		
Xenograft control	0.19	± 0.06	0.067	± 0.003		
Blood	0.16	± 0.03	0.034	± 0.002	0.15	± 0.06
Spleen	0.11	± 0.01	0.091	± 0.032	0.08	± 0.03*
Liver	0.16	± 0.01	0.063	± 0.011	0.12	± 0.04
Kidney	0.33	± 0.07	0.39	± 0.12	0.23	± 0.10
Lung	0.13	± 0.002	0.040	± 0.005	0.10	± 0.04
Bone	0.19	± 0.03	0.050	± 0.009	0.12	± 0.04
Heart	0.14	± 0.01	0.034	± 0.005	0.10	± 0.03
Brain	0.099	± 0.006	0.003	± 0.000	0.057	± 0.017*
Stomach w. cont.	0.12	± 0.08	0.026	± 0.011	0.049	± 0.009*
Intestine w. cont.	0.71	± 0.09	1.77	± 0.02	0.55	± 0.13*
Pancreas	0.10	± 0.03	0.065	± 0.028	0.079	± 0.031*
Muscle	0.13	± 0.04	0.041	± 0.010	0.12	± 0.05
Thyroid	0.19	± 0.05	0.041	± 0.010	0.11	± 0.04
Gallbladder	0.5 to 2.4		1.8 to 6.2		1.2 to 2.0	
Urine	14 to 343		120 to 218		14 to 102	

Data are the mean±standard deviation of four animals for [<sup>18</sup>F]FHOMP, three animals each for [<sup>18</sup>F]FHBG and for [<sup>18</sup>F]FHOMP + NBMPR-P. [<sup>18</sup>F]FHOMP and [<sup>18</sup>F]FHBG radioactivity accumulation was significantly higher in transgenic xenografts than in the control xenografts for [<sup>18</sup>F]FHOMP (P 0.003) and for [<sup>18</sup>F]FHBG (0.04).

\*Significantly different from values of [<sup>18</sup>F]FHOMP mice (P ≤ 0.03) (Student *t* test).

### **3.3.11 Effect of ENT1 inhibition on *ex vivo* biodistribution and PET with [<sup>18</sup>F]FHOMP**

To determine whether ENT1 affects [<sup>18</sup>F]FHOMP biodistribution and whether ENT1 inhibition results in lower background radioactivity, mice were analyzed by PET and *post mortem* biodistribution after pre-treatment with the ENT1 inhibitor NBMPR-P and injection of [<sup>18</sup>F]FHOMP. The PET image is shown in Figure 6C. No reduction in background radioactivity was observed compared to the baseline PET image, except a lower uptake into brain. The *ex vivo* biodistribution after ENT1 inhibition (Table 1) showed significantly reduced radioactivity in the brain (P 0.002), spleen (P 0.02), stomach (P 0.002), intestines (P 0.03) and pancreas (P 0.02). However, radioactivity was not reduced in tissues such as muscle and blood which contribute to the general high background in the PET images.

### 3.4 Discussion

Target compound **6** with substrate specificity for HSV1-TK was successfully synthesized in eight steps (Scheme 1) with chemical yields ranging from 46 to 88%. In the synthesis of tosyl precursor **12**, N-1 and N-3 in the pyrimidine ring were protected with MOM groups (Scheme 2) in order to avoid intramolecular cyclization between N-1 and the acyclic moiety at the C-6 position of the pyrimidine ring during radiosynthesis. The protection of the two nitrogens was a critical step and quite challenging probably due to the acidic nature of pyrimidine nitrogen atoms. The treatment of compound **8** with methoxymethylchloride successfully resulted in N-1 and N-3 MOM protection of the dibenzylated compound **9** in an excellent yield of 97%. Standard catalytic hydrogenolysis with H<sub>2</sub> over Pd/C led to a complete reduction of the double bond in pyrimidine **9**. This over reduction has been reported for other pyrimidines [108]. Therefore, an alternative method involving an *in situ* hydrogenation approach using Pd(OH)<sub>2</sub> and cyclohexene system was pursued. In this case, no reduction of the double bond was observed while almost a quantitative conversion of compound **9** to **10** (93%) was achieved within two hours.

For the radiosynthesis of <sup>18</sup>F-**6**, a different synthetic strategy was adapted in order to circumvent a complex multi-step radiosynthesis. This strategy consisted of developing a suitable precursor that would allow the radiosynthesis in a two-step reaction sequence. As such, compound **12** bearing easily cleavable protecting groups and a tosylate leaving group was designed and synthesized in optimal chemical yields. The radiosynthesis of [<sup>18</sup>F]FHOMP (Scheme 3) was accomplished in an overall decay corrected yield of 25%. The optimization of <sup>18</sup>F-fluorination step showed that [<sup>18</sup>F]TBAF was the best fluorinating agent when compared to K[<sup>18</sup>F]F and Cs[<sup>18</sup>F]F. Addition of *tert*-butanol enhanced the incorporation yields up to 88% and a 10-fold higher overall yield was obtained using [<sup>18</sup>F]TBAF combined with *tert*-butanol and acetonitrile. Enhancing the nucleophilicity of fluoride ions and also the rate of the nucleophilic fluorination through the use of protic co-solvents has been reported previously [15]. Deprotection of the intermediate <sup>18</sup>F-**13** was easily achieved with conc HCl. The harsh hydrolysis conditions generated not only the final product but also a more polar unidentified side-product resulting in a 51% radiochemical yield for this step. Formulation of <sup>18</sup>F-**6** without the need to evaporate the mobile phase or trapping on a cartridge is a clear benefit. The radiosynthesis is reliable and robust delivering [<sup>18</sup>F]FHOMP in

high product amounts suitable for preclinical pharmacological *in vitro* as well as *in vivo* evaluations.

Negligible *in vivo* defluorination is a prerequisite for a good  $^{18}\text{F}$ -labeled PET probe as  $^{18}\text{F}$ fluoride accumulates in osseous tissue. Cytochrome P450-mediated defluorination of  $^{18}\text{F}$ FHOMP was excluded *in vitro* with human and mouse liver microsomes. Indeed, no bone uptake of radioactivity was observed *in vivo* in mice after  $^{18}\text{F}$ FHOMP application.

The *in vitro* uptake of  $^{18}\text{F}$ FHOMP into the stably transfected HEK293TK+ cells was significantly higher than in control cells (Fig. 4).  $^{18}\text{F}$ FHOMP showed strikingly higher uptake ratios than  $^{18}\text{F}$ FHBG due to lower uptake into control cells at all investigated time points. For comparison, the highest uptake ratio of *N*-Me- $^{18}\text{F}$ FHBT, also a C-6 substituted pyrimidine derivative, was 70 at 120 min [105]. Based on these results, we expected a high uptake ratio of  $^{18}\text{F}$ FHOMP between HSV1-TK+ and HEK293 control xenografts *in vivo*. The *in vivo* studies showed that the average absolute radioactivity in the transgenic xenografts was higher for  $^{18}\text{F}$ FHOMP than  $^{18}\text{F}$ FHBG. However,  $^{18}\text{F}$ FHBG had a more favorable HSV1-TK+ xenograft/background ratio than  $^{18}\text{F}$ FHOMP owing to its relatively low tissue activity.

Low background activity of  $^{18}\text{F}$ FHBG may be due to more rapid clearance from the blood than  $^{18}\text{F}$ FHOMP resulting in increased TK+/blood or TK+/tissue ratios. Considering the higher intestinal radioactivity of  $^{18}\text{F}$ FHBG and the significantly lower blood concentration at 60 min postinjection, we speculate that a hepatic transporter may be involved that excretes  $^{18}\text{F}$ FHBG more efficiently into the bile than  $^{18}\text{F}$ FHOMP resulting in lower background but higher abdominal activity for  $^{18}\text{F}$ FHBG. In this study, purine derivative  $^{18}\text{F}$ FHBG and pyrimidine derivative  $^{18}\text{F}$ FHOMP were mainly cleared by the hepatobiliary pathway. Generally, in literature, radioactivity of pyrimidines such as  $^{18}\text{F}$ FFAU is favorably excreted via the kidneys [109].

$^{18}\text{F}$ FHOMP,  $^{18}\text{F}$ FHBG and *N*-Me- $^{18}\text{F}$ FHBT exhibited  $\log D_{\text{pH}7.4}$  values between -0.87 and -0.56 [105]. Due to the low lipophilicity of nucleosides and nucleobases in general, cell uptake depends on specific nucleoside transport proteins in the plasma membrane [97, 110]. Nucleoside transport proteins are encoded by two gene families: *SLC28*, encoding for the CNTs, consisting of three isoforms (CNT1-3), which are  $\text{Na}^+$ -dependent symporters, and *SLC29*, encoding for the ENTs consisting of four isoforms (ENT1-4) which are  $\text{Na}^+$ -independent diffusion-limited channels [49, 50]. We investigated whether ENT1, which is expressed in many mammalian

tissues including erythrocytes, brain, vascular endothelium, placenta, heart, liver, lung and colon may contribute to the higher background radioactivity of [ $^{18}\text{F}$ ]FHOMP compared to [ $^{18}\text{F}$ ]FHBG. Inhibition of ENT1 with NBMPR-P significantly reduced brain uptake of [ $^{18}\text{F}$ ]FHOMP, indicating that ENT1 is involved in blood-brain barrier passage of the radiotracer. However, the general background was not reduced by ENT1 inhibition. Thus, other nucleoside transporters or other factors might be responsible for the relatively high background radioactivity as compared to [ $^{18}\text{F}$ ]FHBG.

## 3.5 Conclusion

An efficient and convenient chemical and radiochemical synthesis of a new C-6 substituted pyrimidine derivative 6-((1-fluoro-3-hydroxypropan-2-yloxy)methyl)-5-methylpyrimidine-2,4(1*H*,3*H*)-dione (FHOMP) for HSV1-TK imaging has been developed and accomplished in yields and purity suitable for *in vivo* studies with PET. [<sup>18</sup>F]FHOMP exhibited higher uptake ratios between HEK293TK+ and HEK293 control cells than [<sup>18</sup>F]FHBG *in vitro* but not *in vivo*. The lower ratio *in vivo* is a consequence of the higher general background radioactivity of [<sup>18</sup>F]FHOMP. ENT1 is an important mediator of [<sup>18</sup>F]FHOMP uptake in brain but does not contribute to the relatively high tissue radioactivity in general. Although the *in vivo* properties of [<sup>18</sup>F]FHOMP do not outperform [<sup>18</sup>F]FHBG, the reduced abdominal background radioactivity of [<sup>18</sup>F]FHOMP may be considered an advantage.

**Acknowledgment.** We thank Cindy Fischer, Dr. Linjing Mu and Dominique Leutwiler for their support and help during *in vitro* studies and Claudia Keller and Petra Wirth for their assistance in the *in vivo* and *ex vivo* experiments. We thank Dr. Svetlana Selivanova, Dr. Thomas Betzel, Dr. Aristeidis Chiotellis and Lukas Dialer for fruitful discussions and sharing radiochemistry and chemistry knowledge. We thank Kurt Hauenstein for technical purification support. We thank Dr. Jason Holland for reading through the manuscript and for his fruitful comments. We would like to thank the Flow Cytometry Laboratory of the Institute for Biomedical Engineering UZH and ETH Zurich for technical support. Financial support for this study was provided by the Swiss Science National Foundation (Project Nr. 31003A\_126963).







## **Conclusion and Future Perspectives**



## 4.1 Conclusion and Future Perspectives

Stably expressing HSV1-TK in a HEK293 cell line (HEK293TK+) was successfully established. Both novel tracers, [ $^{18}\text{F}$ ]FHOMP and *N*-Me-[ $^{18}\text{F}$ ]FHBT, allowed the successful PET imaging of HSV1-TK expressing xenografts in mice, and exhibited high *in vivo* stability with negligible defluorination. In combination with *ex vivo* biodistribution studies, [ $^{18}\text{F}$ ]FHOMP and *N*-Me-[ $^{18}\text{F}$ ]FHBT revealed similar uptake properties in HEK293TK+ xenografts, however, compared to [ $^{18}\text{F}$ ]FHBG, both radiotracers showed higher background activities but reduced abdominal background radioactivity. The reduced abdominal background radioactivity is an advantage of the two C-6 substituted pyrimidine derivatives because it may allow HSV1-*tk* gene expression imaging in the abdominal region. Nonetheless, the two novel tracers do not outperform the most commonly used [ $^{18}\text{F}$ ]FHBG *in vivo* due to the aforementioned general higher background tissue radioactivity which needs further investigation. Possible reasons for this higher background radioactivity could be:

- Involvement of hepatic transporter, faster blood clearance of [ $^{18}\text{F}$ ]FHBG
- Phosphorylation by mouse thymidine kinase
- Non-specific uptake via nucleoside transporters (NTs)

To determine whether [ $^{18}\text{F}$ ]FHBG is cleared more rapidly than [ $^{18}\text{F}$ ]FHOMP from the blood into the bile, and therefore, shows higher abdominal activity but a general lower background, it would be of interest to perform an *in vivo* blood clearance assay by taking blood samples of [ $^{18}\text{F}$ ]FHBG and to compare with data observed for [ $^{18}\text{F}$ ]FHOMP. One possible reason for the faster [ $^{18}\text{F}$ ]FHBG blood clearance is that a hepatic transporter may be involved that excretes [ $^{18}\text{F}$ ]FHBG more efficiently into the bile. Solute linked carrier (SLC) transportocytes (e.g. BD Gentest Transporter Models) prepared from transporter-cRNA injected *Xenopus* oocytes could be used to measure transporter-mediated uptake of test tracers. For [ $^{18}\text{F}$ ]FHOMP, the higher levels of radioactivity in the blood could be due to uptake into erythrocytes via nucleoside transporters. For this purpose, uptake studies of the tracers into erythrocytes could be performed.

Even though [ $^{18}\text{F}$ ]FHOMP is not phosphorylated by humanTK or HEK293 control cells, it cannot be excluded that host mouse TK does not phosphorylate [ $^{18}\text{F}$ ]FHOMP in mice. Phosphorylated [ $^{18}\text{F}$ ]FHOMP in blood could contribute to the general higher background radioactivity as well. In addition to existing HSV1-TK and humanTK proteins, mouseTK protein could be produced and incubated with test tracers to study phosphorylation using HPLC analysis. Furthermore, different mouse blood cells could be incubated with test tracers and verified for phosphorylation products.

Another issue is to study whether probe transport across cell and tissue membranes is limiting and affects the images in both target and non-target tissues. Because a wide range of nucleoside transporters are expressed in different cell lines and tissues, a detailed transport study is necessary. For this purpose, yeast producing various recombinant human and rodent nucleoside transporters could be produced and the ability of a PET reporter probe to inhibit uridine uptake could be assessed to provide a measure of the apparent affinities of the NTs. To determine the role of NTs for the C-6 alkylated pyrimidine derivatives and other test tracers, various cell lines or tissue of interest could be analyzed for NT-transcript levels with quantitative real-time polymerase chain reaction (RT-PCR) and uptake into different cell lines with or without NT inhibitors compared.

FEAU as the most promising PET tracer candidate has only been evaluated in rodents but not in humans. FEAU revealed low abdominal background due to renal clearance and no phosphorylation by host kinase. In this regard, clinical results from FEAU are eagerly expected. Nevertheless, clinics still lack the ideal probe. In general, pyrimidines show higher sensitivity towards wild type HSV1-TK than purines and are cleared by kidney, and therefore, profit from low abdominal background in living subjects. In this study, the two C-6 substituted pyrimidines evaluated revealed unexpected hepatobiliary clearance in mice. The aforementioned biological studies, especially the transportocytes assay, could give some answers to the observed hepatobiliary clearance, but it is not clear whether hepatobiliary clearance is due to the C-6 substitution. Therefore, it is crucial to develop and evaluate C-6 substituted pyrimidines that have optimal *in vivo* profile and specificity for HSV1-TK. In this regard, it would be interesting to evaluate [ $^{18}\text{F}$ ]FHBT which revealed high selectivity for HSV1-TK enzyme *in vitro*. Due to the discovered N-1 and N-3 MOM protection, the synthesis of [ $^{18}\text{F}$ ]FHBT may be possible by

reacting already known compound **A** with MOMCl (Fig. 1.). Further chemical transformation would then lead to the expected target compound [ $^{18}\text{F}$ ]FHBT.

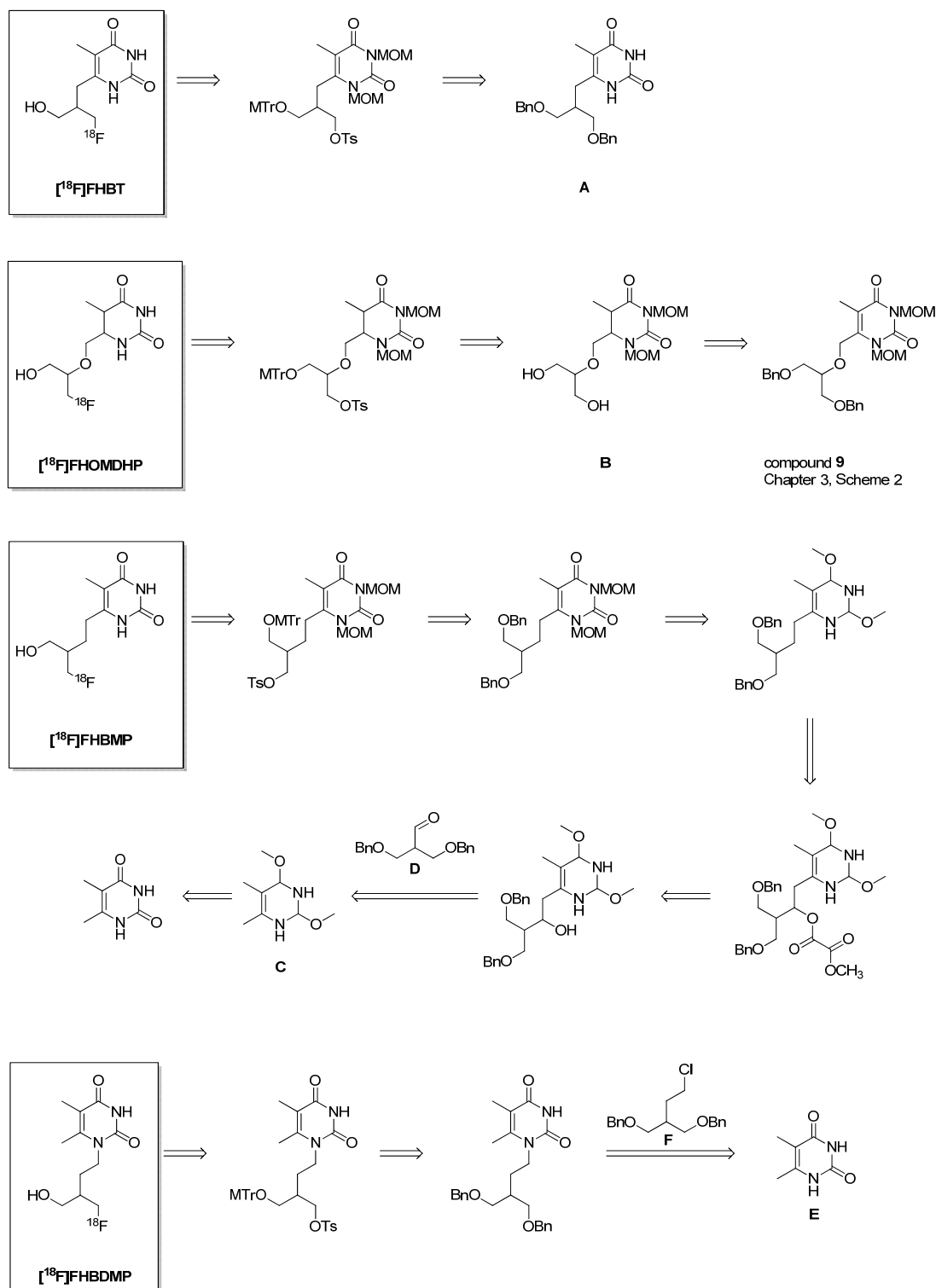


**Figure 1.** Proposed structures of new pyrimidine derivatives as potential HSV1-TK ligands.

Another possible compound could be 6-(((1-[<sup>18</sup>F]-fluoro-3-hydroxypropan-2-yl)oxy)methyl)-5-methyldihydropyrimidine-2,4(1*H*,3*H*)-dione ([<sup>18</sup>F]FHOMDHP) with a reduced pyrimidine ring (Fig. 1.). During the synthesis of [<sup>18</sup>F]FHOMP (described in Chapter 3), intermediate **B** was easily obtained during the reduction of the dibenzylated intermediate **9** (Chapter 3, Scheme 2.) with 10% Pd/C and H<sub>2</sub>. Compound **B** could be further reacted with appropriate reagents to yield [<sup>18</sup>F]FHOMDHP. Furthermore, the introduction of a fluoro-(hydroxymethyl)butyl side chain at the C-6 position in analogy to [<sup>18</sup>F]FHBG (6-(4-[<sup>18</sup>F]-fluoro-3-(hydroxymethyl)butyl)-5-methylpyrimidine-2,4(1*H*,3*H*)-dione, [<sup>18</sup>F]FHBMP) or N-1 position (1-(4-[<sup>18</sup>F]-fluoro-3-(hydroxymethyl)butyl)-5,6-dimethylpyrimidine-2,4(1*H*,3*H*)-dione, [<sup>18</sup>F]FHBDMP) could lead to possible new HSV1-TK substrates. The key step towards [<sup>18</sup>F]FHBMP is the nucleophilic addition of pyrimidine **C** to aldehyde **D**. [<sup>18</sup>F]FHBDMP on the other hand is easily obtained by reacting pyrimidine **E** with chloro compound **F** and further chemical modifications (Fig. 1.). HSV1-TK favors phosphorylation of the hydroxyl group at position 5 of the C-6 substituted side chain, which is given in most of the proposed tracers.







## References

- [1] Blasberg RG and Tjuvajev JG. In vivo molecular-genetic imaging. *J Cell Biochem Suppl* 2002;39:172-83.
- [2] Wolfe D, Mata M, and Fink DJ. A human trial of HSV-mediated gene transfer for the treatment of chronic pain. *Gene Therapy* 2009;16:455-60.
- [3] Griesenbach U and Alton EFWF. Current Status and Future Directions of Gene and Cell Therapy for Cystic Fibrosis. *Bio Drugs* 2011;25:77-88
- [4] Jansen FP and Vanderheyden J-L. The future of SPECT in a time of PET. *Nucl Med Biol* 2007;34:733-5.
- [5] Vassaux G and Groot-Wassink T. In Vivo Noninvasive Imaging for Gene Therapy. *J Biomed Biotechnol* 2003;21:92-101.
- [6] Judenhofer MS, Wehrl HF, Newport DF, Catana C, Siegel SB, Becker M, et al. Simultaneous PET-MRI: a new approach for functional and morphological imaging. *Nat Med* 2008;14:459-65.
- [7] Sangro B, Qian C, Ruiz J, and Prieto J. Tracing Transgene Expression in Cancer Gene Therapy: a Requirement for Rational Progress in the Field. *Mol Imag Biol* 2002;4:27-33.
- [8] Haberkorn U, Altmann A, Mier W, and Eisenhut M. Impact of functional genomics and proteomics on radionuclide imaging. *Seminars in Nuclear Medicine* 2004;34:4-22.
- [9] Peñuelas I, Haberkorn U, Yaghoubi S, and Gambhir S. Gene therapy imaging in patients for oncological applications. *Europ J Nucl Med Mol Imag* 2005;32:S384-S403.
- [10] Kang JH and Chung J-K. Molecular-Genetic Imaging Based on Reporter Gene Expression. *J Nucl Med* 2008;49:164S-79S.
- [11] Ametamey SM, Honer M, and Schubiger PA. Molecular Imaging with PET. *Cheml Rev* 2008;108:1501-16.
- [12] Saha GB. *Fundamentals of Nuclear Pharmacy*. Springer-Verlag New York 2004.
- [13] Wang Y, Seidel J, Tsui BMW, Vaquero JJ, and Pomper MG. Performance Evaluation of the GE Healthcare eXplore VISTA Dual-Ring Small-Animal PET Scanner. *J Nucl Med* 2006;47:1891-900.
- [14] Research R. Image from Riken Research. <http://www.rikenresearch.riken.jp/eng/frontline/6414>.
- [15] Kim DW, Ahn D-S, Oh Y-H, Lee S, Kil HS, Oh SJ, et al. A New Class of SN2 Reactions Catalyzed by Protic Solvents: Facile Fluorination for Isotopic Labeling of Diagnostic Molecules. *J Am Chem Soc* 2006;128:16394-7.
- [16] Chirakal R, Firnau G, Couse J, and Garnett ES. Radiofluorination with  $^{18}\text{F}$ -labelled acetyl hypofluorite: [ $^{18}\text{F}$ ]L-6-fluorodopa. *Int J Appl Rad Isot* 1984;35:651-3.
- [17] Chirakal R, Firnau G, and Garnett EX. High Yield Synthesis of 6- $^{18}\text{F}$ Fluoro-L-Dopa. *J Nucl Med* 1986;27:417-21.
- [18] Chirakal R, Coates G, Firnau G, Schrobilgen GJ, and Nahmias C. Direct radiofluorination of dopamine:  $^{18}\text{F}$ -labeled 6-fluorodopamine for imaging cardiac sympathetic innervation in humans using positron emission tomography. *Nucl Med Biol* 1996;23:41-5.
- [19] Tjuvajev JG, Stockhammer G, Desai R, Uehara H, Watanabe K, Gansbacher B, et al. Imaging the Expression of Transfected Genes in Vivo. *Canc Res* 1995;55:6126-32.
- [20] Michael R, Lewis MR and Jia F. Antisense Imaging: And Miles to go Before we Sleep? *J Cel Biochem* 2003;90:464-72.
- [21] Min J-J and Gambhir SS. Molecular Imaging of PET Reporter Gene Expression. In: W Semmler and M Schwaiger editors. *Molecular Imaging II*: Springer Berlin Heidelberg; 2008, p. 277-303.
- [22] Banerjee D. Technology evaluation: gene therapy (mesothelioma), NCI. *Curr Opin Mol Ther* 1999;1:517-20.
- [23] Wang L, Saada A, and Eriksson S. Kinetic Properties of Mutant Human Thymidine Kinase 2 Suggest a Mechanism for Mitochondrial DNA Depletion Myopathy. *J Biol Chem* 2003;278:6963-8.
- [24] Tjuvajev JG, Avril N, Oku T, Sasajima T, Miyagawa T, Joshi R, et al. Imaging Herpes Virus Thymidine Kinase Gene Transfer and Expression by Positron Emission Tomography. *Canc Res* 1998;58:4333-41.
- [25] Gambhir SS, Bauer E, Black ME, Liang Q, Kokoris MS, Barrio JR, et al. A mutant herpes simplex virus type 1 thymidine kinase reporter gene shows improved sensitivity for imaging reporter gene expression with positron emission tomography. *Proc Nat Acad Sci* 2000;97:2785-90.
- [26] Sun H, Mangner TJ, Collins JM, Muzik O, Douglas K, and Shields AF. Imaging DNA Synthesis In Vivo with  $^{18}\text{F}$ -FMAU and PET. *J Nucl Med* 2005;46:292-6.
- [27] Cobben DCP, Jager PL, Elsinga PH, Maas B, Suurmeijer AJH, and Hoekstra HJ. 3'- $^{18}\text{F}$ -Fluoro-3'-Deoxy-l-Thymidine: A New Tracer for Staging Metastatic Melanoma? *J Nucl Med* 2003;44:1927-32.
- [28] Alauddin MM, Conti PS, and Fissekis JD. Synthesis of [ $^{18}\text{F}$ ]-labeled 2'-deoxy-2'-fluoro-5-methyl-1- $\beta$ -D-arabinofuranosyluracil ([ $^{18}\text{F}$ ]-FMAU). *J Label Comp Radiopharm* 2002;45:583-90.
- [29] Elion GB. Acyclovir: Discovery, mechanism of action, and selectivity. *J Med Virol* 1993;41:2-6.

- [30] Jacobs A, Voges J, Reszka R, Lercher M, Gossmann A, Kracht L, et al. Positron-emission tomography of vector-mediated gene expression in gene therapy for gliomas. *Lancet* 2001;358:727-9.
- [31] Alauddin MM and Gelovani JG. Radiolabeled Nucleoside Analogues for PET Imaging of HSV1-tk Gene Expression. *Cur Top Med Chem* 2010;10:1617-32.
- [32] Alauddin M, Shahinian A, Park R, Tohme M, Fissekis J, and Conti P. In vivo evaluation of 2'-deoxy-2'-[<sup>18</sup>F]fluoro-5-iodo-1-β-d-arabinofuranosyluracil ([<sup>18</sup>F]FIAU) and 2'-deoxy-2'-[<sup>18</sup>F]fluoro-5-ethyl-1-β-d-arabinofuranosyluracil ([<sup>18</sup>F]FEAU) as markers for suicide gene expression. *Europ J Nucl Med Mol Imag* 2007;34:822-9.
- [33] Buursma AR, Rutgers V, Hospers GAP, Mulder NH, Vaalburg W, and de Vries EFJ. <sup>18</sup>F-FEAU as a radiotracer for herpes simplex virus thymidine kinase gene expression: in-vitro comparison with other PET tracers. *Nucl Med Com* 2006;27:25-30.
- [34] Tseng J-C, Zanzonico PB, Levin B, Finn R, Larson SM, and Meruelo D. Tumor-Specific In Vivo Transfection with HSV-1 Thymidine Kinase Gene Using a Sindbis Viral Vector as a Basis for Prodrug Ganciclovir Activation and PET. *J Nucl Med* 2006;47:1136-43.
- [35] Tjuvajev JG, Doubrovin M, Akhurst T, Cai S, Balatoni J, Alauddin MM, et al. Comparison of Radiolabeled Nucleoside Probes (FIAU, FHBG, and FHPG) for PET Imaging of HSV1-tk Gene Expression. *J Nucl Med* 2002;43:1072-83.
- [36] Boyd MR, Bacon TH, Sutton D, and Cole M. Antiherpesvirus activity of 9-(4-hydroxy-3-hydroxy-methylbut-1-yl)guanine (BRL 39123) in cell culture. *Antimicrob Agents Chemother* 1987;31:1238-42.
- [37] Alauddin MM, Shahinian A, Gordon EM, Bading JR, and Conti PS. Preclinical Evaluation of the Penciclovir Analog 9-(4-[<sup>18</sup>F]Fluoro-3-Hydroxymethylbutyl)Guanine for In Vivo Measurement of Suicide Gene Expression with PET. *J Nucl Med* 2001;42:1682-90.
- [38] Yaghoubi S, Barrio JR, Dahlbom M, Iyer M, Namavari M, Satyamurthy N, et al. Human Pharmacokinetic and Dosimetry Studies of [<sup>18</sup>F]FHBG: A Reporter Probe for Imaging Herpes Simplex Virus Type-1 Thymidine Kinase Reporter Gene Expression. *J Nucl Med* 2001;42:1225-34.
- [39] Peñuelas I, Mazzolini G, Boán JF, Sangro B, Martí-Climent J, Ruiz M, et al. Positron Emission Tomography Imaging of Adenoviral-Mediated Transgene Expression in Liver Cancer Patients. *Gastroenterology* 2005;128:1787-95.
- [40] Yaghoubi SS, Jensen MC, Satyamurthy N, Budhiraja S, Paik D, Czernin J, et al. Noninvasive detection of therapeutic cytolytic T cells with <sup>18</sup>F-FHBG PET in a patient with glioma. *Nat Clin Prac Oncol* 2009;6:53-8.
- [41] Yaghoubi SS, Couto MA, Chen C-C, Polavaram L, Cui G, Sen L, et al. Preclinical Safety Evaluation of <sup>18</sup>F-FHBG: A PET Reporter Probe for Imaging Herpes Simplex Virus Type 1 Thymidine Kinase (HSV1-tk) or Mutant HSV1-sr39tk's Expression. *J Nucl Med* 2006;47:706-15.
- [42] McKenzie R, Fried MW, Sallie R, Conjeevaram H, Di Bisceglie AM, Park Y, et al. Hepatic Failure and Lactic Acidosis Due to Fialuridine (FIAU), an Investigational Nucleoside Analogue for Chronic Hepatitis B. *New Engl J of Med* 1995;333:1099-105.
- [43] Gambhir SS, Barrio JR, Phelps ME, Iyer M, Namavari M, Satyamurthy N, et al. Imaging adenoviral-directed reporter gene expression in living animals with positron emission tomography. *Proc Nat Acad Sci* 1999;96:2333-8.
- [44] Kessler U. Random Synthesis and Biological Characterization of Nucleoside Analogs New Perspectives for Drug Discovery. Dissertation ETH 2000;13592.
- [45] Johayem A, Raić-Malić S, Lazzati K, Schubiger PA, Scapozza L, and Ametamey SM. Synthesis and Characterization of a C(6) Nucleoside Analogue for the in vivo Imaging of the Gene Expression of Herpes Simplex Virus Type-1 Thymidine Kinase (HSV1 TK). *Chem Biodiv* 2006;3:274-83.
- [46] Johayem A. Development of novel nucleoside analogues for the PET imaging of herpes simplex virus type 1 thymidine kinase gene expression. Dissertation ETH 2004;15450.
- [47] Martić M. Development of new nucleoside analogues as PET imaging agents for monitoring gene expression. Dissertation ETH 2008;17632.
- [48] Cass CE, Young JD, and Baldwin SA. Recent advances in the molecular biology of nucleoside transporters of mammalian cells. *Biochem Cell Biol* 1998;76:761-70.
- [49] Baldwin S, Beal P, Yao SM, King A, Cass C, and Young J. The equilibrative nucleoside transporter family, SLC29. *Pflügers Archiv Europ J Physiol* 2004;447:735-43.
- [50] Gray J, Owen R, and Giacomini K. The concentrative nucleoside transporter family, SLC28. *Pflügers Archiv Europ J Physiol* 2004;447:728-34.
- [51] Molina-Arcas M, Casado FJ, and Pastor-Anglada M. Nucleoside Transporter Proteins. *Cur Vasc Pharm* 2009;7:426-34.

- [52] Sundaram M, Yao SYM, Ng AML, Cass CE, Baldwin SA, and Young JD. Equilibrative Nucleoside Transporters: Mapping Regions of Interaction for the Substrate Analogue Nitrobenzylthioinosine (NBMPR) Using Rat Chimeric Proteins. *Biochem* 2001;40:8146-51.
- [53] Pennycooke M, Chaudary N, Shuralyova I, Zhang Y, and Coe IR. Differential Expression of Human Nucleoside Transporters in Normal and Tumor Tissue. *Biochem Biophys Res Com* 2001;280:951-9.
- [54] Anderson CM, Baldwin SA, Young JD, Cass CE, and Parkinson FE. Distribution of mRNA encoding a nitrobenzylthioinosine-insensitive nucleoside transporter (ENT2) in rat brain. *Molecular Brain Res* 1999;70:293-7.
- [55] Anderson CM, Xiong W, Geiger JD, Young JD, Cass CE, Baldwin SA, et al. Distribution of Equilibrative, Nitrobenzylthioinosine-Sensitive Nucleoside Transporters (ENT1) in Brain. *J Neurochem* 1999;73:867-73.
- [56] Lu H, Chen C, and Klaassen C. Tissue distribution of concentrative and equilibrative nucleoside transporters in male and female rats and mice. *Drug Met Disp* 2004;32:1455-61.
- [57] Crawford CR, Patel DH, Naeve C, and Belt JA. Cloning of the Human Equilibrative, Nitrobenzylmercaptapurine Riboside (NBMPR)-insensitive Nucleoside Transporter ei by Functional Expression in a Transport-deficient Cell Line. *J Biol Chem* 1998;273:5288-93.
- [58] Griffiths M, Yao SY, Abidi F, Phillips SE, Cass CE, Young JD, et al. Molecular cloning and characterization of a nitrobenzylthioinosine-insensitive (ei) equilibrative nucleoside transporter from human placenta. *Biochem J* 1997;328:739-43.
- [59] Hyde R, Cass CE, Young JD, and Baldwin SA. The ENT family of eukaryote nucleoside and nucleobase transporters: recent advances in the investigation of structure/function relationships and the identification of novel isoforms. *Mol Membr Biol* 2001;18:53-63.
- [60] Baldwin SA, Yao SYM, Hyde RJ, Ng AML, Foppolo S, Barnes K, et al. Functional Characterization of Novel Human and Mouse Equilibrative Nucleoside Transporters (hENT3 and mENT3) Located in Intracellular Membranes. *J Biol Chem* 2005;280:15880-7.
- [61] Barnes K, Dobrzynski H, Foppolo S, Beal PR, Ismat F, Scullion ER, et al. Distribution and Functional Characterization of Equilibrative Nucleoside Transporter-4, a Novel Cardiac Adenosine Transporter Activated at Acidic pH. *Circ Res* 2006;99:510-9.
- [62] Baldwin SA. Image from homepage of Professor Stephen Baldwin. [http://www.fbs.leeds.ac.uk/staff/profile.php?tag=Baldwin\\_SA](http://www.fbs.leeds.ac.uk/staff/profile.php?tag=Baldwin_SA).
- [63] Wang J and Giacomini KM. Characterization of a Bioengineered Chimeric Na<sup>+</sup>-Nucleoside Transporter. *Mol Pharm* 1999;55:234-40.
- [64] Ritzel MWL, Ng AML, Yao SYM, Graham K, Loewen SK, Smith KM, et al. Molecular Identification and Characterization of Novel Human and Mouse Concentrative Na<sup>+</sup>-Nucleoside Cotransporter Proteins (hCNT3 and mCNT3) Broadly Selective for Purine and Pyrimidine Nucleosides (System cib). *J Biol Chem* 2001;276:2914-27.
- [65] Anderson CM, Xiong W, Young JD, Cass CE, and Parkinson FE. Demonstration of the existence of mRNAs encoding N1/cif and N2/cit sodium/nucleoside cotransporters in rat brain. *Mol Brain Res* 1996;42:358-61.
- [66] Guillén-Gómez E, Calbet M, Casado J, De Lecea L, Soriano E, Pastor-Anglada M, et al. Distribution of CNT2 and ENT1 transcripts in rat brain: selective decrease of CNT2 mRNA in the cerebral cortex of sleep-deprived rats. *J Neurochem* 2004;90:883-93.
- [67] Fernández-veledo S, Huber-ruano I, Aymerich I, Duflo S, Casado FJ, and Pastor-anglada M. Bile acids alter the subcellular localization of CNT2 (concentrative nucleoside cotransporter) and increase CNT2-related transport activity in liver parenchymal cells. *Biochem J* 2006;395:337-44.
- [68] Pastor-Anglada M, Errasti-Murugarren E, Aymerich I, and Casado F. Concentrative nucleoside transporters (CNTs) in epithelia: from absorption to cell signaling. *J Physiol Biochem* 2007;63:97-110.
- [69] Lee G, Dallas S, Hong M, and Bendayan R. Drug Transporters in the Central Nervous System: Brain Barriers and Brain Parenchyma Considerations. *Pharmacol Rev* 2001;53:569-96.
- [70] Wurth C, Kessler U, Vogt J, Schulz GE, Folkers G, and Scapozza L. The effect of substrate binding on the conformation and structural stability of Herpes simplex virus type 1 thymidine kinase. *Prot Sci* 2001;10:63-73.
- [71] Haberkorn U, Altmann A, Morr I, Knopf K-W, Germann C, Haeckel R, et al. Monitoring Gene Therapy with Herpes Simplex Virus Thymidine Kinase in Hepatoma Cells: Uptake of Specific Substrates. *J Nucl Med* 1997;38:287-94.
- [72] Yaghoubi SS, Barrio JR, Namavari M, Satyamurthy N, Phelps ME, Herschman HR, et al. Imaging progress of herpes simplex virus type 1 thymidine kinase suicide gene therapy in living subjects with positron emission tomography. *Cancer Gene Ther* 2004;12:329-39.
- [73] Sangro B, Mazzolini G, Ruiz M, Ruiz J, Quiroga J, Herrero I, et al. A phase I clinical trial of thymidine kinase-based gene therapy in advanced hepatocellular carcinoma. *Cancer Gene Ther* 2010;17:837-43.

- [74] Koehne G, Doubrovin M, Doubrovina E, Zanzonico P, Gallardo HF, Ivanova A, et al. Serial in vivo imaging of the targeted migration of human HSV-TK-transduced antigen-specific lymphocytes. *Nat Biotech* 2003;21:405-13.
- [75] Ponomarev V. Nuclear Imaging of Cancer Cell Therapies. *J Nucl Med* 2009;50:1013-6.
- [76] Doubrovin M, Ponomarev V, Beresten T, Balatoni J, Bornmann W, Finn R, et al. Imaging transcriptional regulation of p53-dependent genes with positron emission tomography in vivo. *Proc Nat Acad Sci U S A* 2001;98:9300-5.
- [77] Ponomarev V, Doubrovin M, Lyddane C, Beresten T, Balatoni J, Bornman W, et al. Imaging TCR-Dependent NFAT-Mediated T-Cell Activation with Positron Emission Tomography In Vivo. *Neoplasia* 2001;3:480-8.
- [78] Alauddin MM and Tjuvajev JG. Radiolabeled nucleoside analogues for PET imaging of HSV1-tk gene expression. *Curr Top Med Chem* 2010;10:1617-32.
- [79] Yaghoubi SS and Gambhir SS. PET imaging of herpes simplex virus type 1 thymidine kinase (HSV1-tk) or mutant HSV1-sr39tk reporter gene expression in mice and humans using [<sup>18</sup>F]FHBG. *Nat Protoc* 2007;1:3069-74.
- [80] Tjuvajev JG, Doubrovin M, Akhurst T, Cai S, Balatoni J, Alauddin MM, et al. Comparison of Radiolabeled Nucleoside Probes (FIAU, FHBG, and FHPG) for PET Imaging of HSV1-tk Gene Expression. *J Nucl Med* 2002;43:1072-83.
- [81] MacLaren DC, Toyokuni T, Cherry SR, Barrio JR, Phelps ME, Herschman HR, et al. PET imaging of transgene expression. *Biol Psy* 2000;48:337-48.
- [82] Yaghoubi S, Barrio JR, Dahlbom M, Iyer M, Namavari M, Satyamurthy N, et al. Human Pharmacokinetic and Dosimetry Studies of [<sup>18</sup>F]FHBG: A Reporter Probe for Imaging Herpes Simplex Virus Type-1 Thymidine Kinase Reporter Gene Expression. *J Nucl Med* 2001;42:1225-34.
- [83] Soghomonyan S, Hajitou A, Rangel R, Trepel M, Pasqualini R, Arap W, et al. Molecular PET imaging of HSV1-tk reporter gene expression using [<sup>18</sup>F]FEAU. *Nat Protoc* 2007;2:416-23.
- [84] Raić-Malić S, Johayem A, Ametamey SM, Batinac S, De Clercq E, Folkers G, et al. Synthesis, <sup>18</sup>F-Radiolabelling and Biological Evaluations of C-6 Alkylated Pyrimidine Nucleoside Analogues. *Nucl Nucleot Nuclei Acids* 2004;23:1707 - 21.
- [85] Alauddin MM and Conti PS. Synthesis and Preliminary Evaluation of 9-(4-[<sup>18</sup>F]-Fluoro-3-Hydroxymethylbutyl)Guanine ([<sup>18</sup>F]FHBG): A New Potential Imaging Agent for Viral Infection and Gene Therapy Using PET. *Nucl Med Biol* 1998;25:175-80.
- [86] Pilger BD, Perozzo R, Alber F, Wurth C, Folkers G, and Scapozza L. Substrate Diversity of Herpes Simplex Virus Thymidine Kinase. *J Biol Chem* 1999;274:31967-73.
- [87] Birringer MS, Perozzo R, Kut E, Stillhart C, Surber W, Scapozza L, et al. High-level expression and purification of human thymidine kinase 1: Quaternary structure, stability, and kinetics. *Prot Exp Purif* 2006;47:506-15.
- [88] Wilson AA, Jin L, Garcia A, DaSilva JN, and Houle S. An admonition when measuring the lipophilicity of radiotracers using counting techniques. *Appl Rad Isot* 2001;54:203-8.
- [89] Issa W, Tochon-Danguy HJ, Lambert J, Sachinidis JI, Ackermann U, Liu Z, et al. Synthesis and evaluation of a thymidine analog for positron emission tomography study of tumor DNA proliferation in vivo. *Nucl Med Biol* 2004;31:839-49.
- [90] Yaghoubi SS and Gambhir SS. Measuring herpes simplex virus thymidine kinase reporter gene expression in vitro. *Nat Protoc* 2006;1:2137-42.
- [91] Honer M, Bruhlmeier M, Missimer J, Schubiger AP, and Ametamey SM. Dynamic Imaging of Striatal D2 Receptors in Mice Using Quad-HIDAC PET. *J Nucl Med* 2004;45:464-70.
- [92] Wang Y, Seidel J, Tsui BMW, Vaquero JJ, and Pomper MG. Performance Evaluation of the GE Healthcare eXplore VISTA Dual-Ring Small-Animal PET Scanner. *J Nucl Med* 2006;47:1891-900.
- [93] Martin JC, McGee DPC, Jeffrey GA, Hobbs DW, Smee DF, Matthews TR, et al. Synthesis and anti-herpes virus activity of acyclic 2'-deoxyguanosine analogs related to 9-[(1,3-dihydroxy-2-propoxy)methyl]guanine. *J Med Chem* 1986;29:1384-9.
- [94] Alauddin MM, Shahinian A, Gordon EM, Bading JR, and Conti PS. Preclinical Evaluation of the Penciclovir Analog 9-(4-[<sup>18</sup>F]Fluoro-3-Hydroxymethylbutyl)Guanine for In Vivo Measurement of Suicide Gene Expression with PET. *J Nucl Med* 2001;42:1682-90.
- [95] Alauddin MM, Shahinian A, Park R, Tohme M, Fissekis J, and Conti P. Synthesis and Evaluation of 2'-Deoxy-2'-<sup>18</sup>F-Fluoro-5-Fluoro-1--D-Arabinofuranosyluracil as a Potential PET Imaging Agent for Suicide Gene Expression. *J Nucl Med* 2004;45:2063-9.
- [96] Griffith DA and Jarvis SM. Nucleoside and nucleobase transport systems of mammalian cells. *Biochimica et Biophysica Acta (BBA). Rev Biomembr* 1996;1286:153-81.
- [97] Baldwin SA, Mackey JR, Cass CE, and Young JD. Nucleoside transporters: molecular biology and implications for therapeutic development. *Mol Med Tod* 1999;5:216-24.

- [98] Damaraju VL, Damaraju S, Young JD, Baldwin SA, Mackey J, Sawyer MB, et al. Nucleoside anticancer drugs: the role of nucleoside transporters in resistance to cancer chemotherapy. *Oncogene* 2003;22:7524-36.
- [99] Paproski RJ, Wuest M, Jans H-S, Graham K, Gati WP, McQuarrie S, et al. Biodistribution and Uptake of 3'-Deoxy-3'-Fluorothymidine in ENT1-Knockout Mice and in an ENT1-Knockdown Tumor Model. *J Nucl Med* 2010;51:1447-55.
- [100] Griffiths M, Beaumont N, Yao SM, Sundaram M, Boumah CE, Davies A, et al. Cloning of a human nucleoside transporter implicated in the cellular uptake of adenosine and chemotherapeutic drugs. *Nat Med* 1997;3:89-93.
- [101] Handa M, Choi D-S, Caldeiro RM, Messing RO, Gordon AS, and Diamond I. Cloning of a novel isoform of the mouse NBMPR-sensitive equilibrative nucleoside transporter (ENT1) lacking a putative phosphorylation site. *Gene* 2001;262:301-7.
- [102] Murray PE, McNally VA, Lockyer SD, Williams KJ, Stratford IJ, Jaffar M, et al. Synthesis and enzymatic evaluation of pyridinium-Substituted uracil derivatives as novel inhibitors of thymidine phosphorylase. *Bioorg Med Chem* 2002;10:525-30.
- [103] Lipshutz BH, Moretti R, and Crow R. Mixed higher-order cyanocuprate-induced epoxide openings: 1-benzyloxy-4-penten-2-ol. *Org Synth Coll Vol* 1993;8:33.
- [104] Akiama Y, Fukuhara T, and Hara S. Regioselective synthesis of fluorohydrines via S[N]2-type ring-opening of epoxides with TBABF-KHF[2], Stuttgart, ALLEMAGNE: Thieme,2003.
- [105] Müller U, Martić M, Gazivoda Kraljević T, Krištafor S, Ross TL, Ranadheera C, et al. Synthesis and evaluation of a C-6 alkylated pyrimidine derivative for in vivo imaging of HSV1-TK gene expression. *J Nucl Med Biol* 2011 (in press)
- [106] Gati WP and Paterson ARP. Measurement of nitrobenzylthioinosine in plasma and erythrocytes: a pharmacokinetic study in mice. *Canc Chem Pharm* 1997;40:342-6.
- [107] Heintzelman G, Fang W-K, Keen SP, Wallace GA, and Weinreb SM. Stereoselective Total Synthesis of the Cyanobacterial Hepatotoxin 7-Epicylindrospermopsin: Revision of the Stereochemistry of Cylindrospermopsin. *J Am Chem Soc* 2001;123:8851-3.
- [108] Martin JC, Jeffrey GA, McGee DPC, Tippie MA, Smee DF, Matthews TR, et al. Acyclic analogs of 2'-deoxynucleosides related to 9-[(1,3-dihydroxy-2-propoxy)methyl]guanine as potential antiviral agents. *J Med Chem* 1985;28:358-62.
- [109] Alauddin MM, Shahinian A, Park R, Tohme M, Fissekis JD, and Conti PS. Synthesis and Evaluation of 2'-Deoxy-2'-<sup>18</sup>F-Fluoro-5-Fluoro-1-β-d-Arabinofuranosyluracil as a Potential PET Imaging Agent for Suicide Gene Expression. *J Nucl Med* 2004;45:2063-9.
- [110] Cass CE, Young JD, and Baldwin SA. Recent advances in the molecular biology of nucleoside transporters of mammalian cells. *Biochem Cell Biol* 1998;76:761-70.





## Curriculum Vitae

Ursina Müller  
Born 16<sup>th</sup> February 1980

### Education

- 2008 – 2011 **ETH Zürich, Institute of Radiopharmaceutical Sciences**  
PhD thesis: *C-6 Pyrimidine Analogs for the PET Imaging of HSV1-Thymidine Kinase Expression*
- 2000 – 2006 **ETH Zürich, Institute of Pharmaceutical Sciences**  
Master of Science in Pharmaceutical Sciences, Licensed Pharmacist
- 2005 – 2006 Pharmaceutical trainee as a part of the master program, Tödi-Apotheke (pharmacy) Zürich
- 2005 **Karolinska Institutet Stockholm Sweden, Department of Clinical Neuroscience**, Master thesis
- 2004 **Paul Scherrer Institut (PSI) Villigen**, Semester thesis
- 2000 **Alte Kantonsschule Aarau**  
Matura Typ C (graduation from secondary school)
- 1998 **Sacred Heart College Lower Hutt, New Zealand**  
Senior year of high school spent as an exchange-student

### Employment

- 2008 – 2011 PhD student at ETH Zürich, under the supervision of Professor Simon Mensa Ametamey in the group of Professor Pius August Schubiger and Professor Roger Schibli
- 2007 – 2011 Pharmacist, working night- and weekend-shifts, Bellevue Apotheke Zürich
- 2006 – 2008 Pharmacist and representative of the management, Coop Vitality Apotheke Zürich
- 2005 – 2006 Internship in a pharmacy as a part of the master program, Tödi Apotheke Zürich

### Qualifications

- 2010 Presentation Skills Course for Scientists, ETH Zürich
- 2010 Training Course on Essentials of Clinical Study Management (DIA), Wien
- 2010 Animal Handling Course (LTK1), ETH Zürich
- 2010 Basic (Course 1) and advanced (Course 2) knowledge in humanitarian affairs for pharmacists, pharmacists without borders (AoG), Germany
- 2009 Radiation Safety Course, PSI Villigen

## Publications

### **Synthesis and preclinical evaluation of a new C-6 alkylated pyrimidine derivative as a PET imaging agent for HSV1-*tk* gene expression**

Ursina Müller, Tobias L. Ross, Charlene Ranadheera, Adrienne Müller, Mariana Born, Evelyn Trauffer, Stefanie D. Krämer, Simon M. Ametamey  
*Nuclear Medicine and Biology*, 2011 (submitted)

### **Synthesis and evaluation of a C-6 alkylated pyrimidine derivative for *in vivo* imaging of HSV1-TK gene expression**

Ursina Müller, Miljen Martić, Tatjana Gazivoda Kraljević, Svjetlana Krištafor, Tobias L. Ross, Charlene Ranadheera, Adrienne Müller, Mariana Born, Stefanie D. Krämer, Silvana Raić-Malić, Simon M. Ametamey  
*Nuclear Medicine and Biology*, 2011 (in press)

### **Synthesis and Preclinical Evaluation of a Folic Acid Derivative Labeled with <sup>18</sup>F for PET Imaging of Folate Receptor-Positive Tumors**

Andrea Bettio, Michael Honer, Cristina Müller, Matthias Brühlmeier, Ursina Müller, Roger Schibli, Viola Groehn, August P. Schubiger and Simon M. Ametamey  
*Journal of Nuclear Medicine*, 2006; 47(7): 1153-1160

## Presentations

- Oral
- Syntheses and evaluation of C-6 pyrimidine derivatives for the *in vivo* imaging of the HSV1-TK gene expression**  
IPW Doktorandentag, ETH Zürich, 16<sup>th</sup> February 2011
  - C-6 Pyrimidine Analogues for the *in vivo* Imaging of Herpes Simplex Virus Type 1 Thymidine Kinase (HSV1-TK) Expression**  
18. Jahrestagung der Arbeitsgemeinschaft Radiochemie / Radiopharmazie der DGN in Bad Boll Germany, 16 - 18<sup>th</sup> September 2010
- Poster
- C-6 pyrimidine analogues for the PET imaging of HSV1-thymidine kinase expression**  
19th International Symposium on Radiopharmaceutical Sciences (ISRS), Amsterdam, 28<sup>th</sup> August - 2<sup>nd</sup> September 2011
  - C-6 pyrimidine analogues for the PET imaging of HSV1-thymidine kinase expression**  
Pharmacology Poster Day, Institute of Pharmacology and Toxicology, University of Zürich, 6<sup>th</sup> June 2011

## Grants

- 2011 Travel grant from International Symposium on Radiopharmaceutical Sciences (ISRS)
- 2011 Travel grant from Schweizerische Gesellschaft für Radiopharmazie / Radiopharmazeutische Chemie (SGRRC)